

Examining changes in intradiscal pressure during intervertebral disc herniation

by

Mamiko Noguchi

A thesis

presented to the University of Waterloo

in fulfillment of the

thesis requirement for the degree of

Master of Science

in

Kinesiology

Waterloo, Ontario, Canada, 2013

© Mamiko Noguchi 2013

Author's Declaration

I hereby declare that I am the sole author of this thesis. This is a true copy of the thesis, including any required final revisions, as accepted by my examiners.

I understand that my thesis may be made electronically available to the public.

Mamiko Noguchi

Abstract

Background: Low back pain is experienced by 80% of the population at some point in their lives. Approximately 40% of these cases are attributed to internal disc disruption, which is characterized by damage to the internal structure of the intervertebral disc (IVD) and is a precursor to herniation. Since mechanical loading directly affects intradiscal pressure and the stresses that the inner annulus fibrosus experiences, the mechanism that leads to disruption of the inner annulus fibrosus may be linked to changes in intradiscal pressure. Hence, there is a need to examine how intradiscal pressure changes over time during a flexion extension cyclic (FEC) loading protocol known to induce internal disc disruption.

Purpose: 1) To determine whether a bore-screw pressure sensor system could be used as an alternative sensor to the needle pressure sensor for measuring intradiscal pressure over time, and 2) to characterize changes in intradiscal pressure, moments, and axial deformation using a FEC loading protocol.

Study 1 summary: In the first study, technical specifications of the bore-screw pressure sensor system were compared to the needle pressure sensor, which has been used in previous spine *in vitro* studies. The error projected at a static compressive load of 1500 N was approximately eight percent and the bore-screw pressure sensor had an excellent dynamic response (no lag and good correlation) compared to the needle pressure sensor. Several factors have been identified for consideration when conducting *in vitro* tests using this bore-screw pressure sensor: baseline pressure, test duration, hydration, loading protocol, specimen choice, and ambient temperature.

Study 2 methods: The bore-screw pressure sensor system was successfully instrumented in 14 porcine specimens (C34 and C56). The FEC loading protocol consisted of 3600 cycles of 1 Hz flexion-extension movement (one hour) while applying a 1500 N compressive load. The four dependent variables collected were intradiscal pressure, moment, axial deformation (specimen height loss), and angular displacement. In each flexion-extension cycle, average, maximum, minimum, and difference between maximum and minimum values were identified.

Study 2 results: Intradiscal pressure and specimen height decreased by 45 % and 62 %, respectively, and the peak moment and axial deformation increased by 102 % following the FEC loading protocol. There was a strong negative correlation between average intradiscal pressure and peak moment and a strong positive correlation between average intradiscal pressure and average axial deformation. All variables exhibited significant initial changes, except the angle at maximum pressure, which demonstrated a significant difference after 2700 cycles ($p < 0.01$). There were no sequential changes in pressure difference after 2100 cycles ($p > 0.05$), whereas moments and axial deformation were significantly different throughout the protocol. Of the 14 specimens, 12 specimens showed partial herniation (85.7%); however, the injury type was not correlated to any of the pre-post dependent variable changes.

Conclusions: Changes in intradiscal pressure were successfully characterized over time, in conjunction with previously studied measures such as moments and axial deformation. Average intradiscal pressure decreased and the difference between maximum and minimum pressure in each cycle increased over time during a FEC loading protocol. Although the pre-post change in the pressure difference was not predictive of an injury type, its increasing trend over time suggested that the inner annulus fibrosus failure mechanism may be related to fatigue. Another measure to be examined further in future studies is the angle where maximum pressure occurred, which shifted significantly towards the end of the protocol, indicating that substantial structural change in passive tissues may have occurred.

Keywords: low back pain; intradiscal pressure; internal disc disruption; pressure sensor; injury mechanics; fatigue

Acknowledgements

I would like to begin my acknowledgement by thanking my supervisor, Dr. Jack Callaghan for being an exceptional mentor. His professional and personal guidance has been the key to not losing sight of what is important in research and life outside of school. Thank you for believing in my ability to complete this thesis. I would also like to thank my committee members Dr. Richard Wells and Dr. Andrew Laing for their expertise and guidance.

I would like to thank my colleagues and friends who have contributed to various aspects of this process. It has been a privilege to work with the members of the Callaghan Spine Lab, and the expertise and advice from Thomas Karakolis and Chad Gooyers were eminent in developing a new device. In particular, I would like to acknowledge Chad Gooyers for his tireless dedication to research and teaching. So many of the days, nights, and weekends spent in the lab were more enjoyable because of the conversations we had. To all of my fellow graduate students who have become dear friends to me – these past two years would not have been the same without you being there to share laughs, struggles, and thoughts about the “bigger picture” – so thank you.

Finally, I would like to thank my family for always being my number one supporters. Special thanks to my brother, Dr. Kimihiro Noguchi, whose expert knowledge in statistics was instrumental in the completion of this thesis. My younger brother, Masahiro, has always brought joy and excitement in research. Last but not least, to my parents, Keiko and Toshifumi, thank you for being so patient with me this year. I know I don't express it enough, but I love you and I'm sorry that I don't come home enough!

Table of Contents

Author's Declaration.....	ii
Abstract.....	iii
Acknowledgements.....	v
List of Tables.....	viii
List of Figures.....	ix
List of Equations.....	xii
List of Acronyms.....	xiii
Chapter 1 Introduction.....	1
1.1 General introduction.....	1
1.2 Purposes.....	1
1.3 Expected outcomes and hypotheses.....	2
Chapter 2 Literature Review.....	4
2.1 Prevalence of low back pain related to intervertebral disc damage.....	4
2.2 Intervertebral disc anatomy and physiology - The evidence of why it is vulnerable.....	6
2.2.1 Nucleus pulposus.....	6
2.2.2 Annulus fibrosus.....	7
2.2.3 Endplate.....	8
2.2.4 Nutrition.....	9
2.2.5 Nerve supply and potential source of pain.....	9
2.3 Degeneration associated with intradiscal pressure.....	10
2.3.1 Degeneration occurring in everyday life.....	10
2.3.2 Degeneration associated with kinematic changes.....	13
2.3.3 Association of abnormal intradiscal stress/pressure profile and low back pain.....	13
2.3.4 Counterarguments for abnormal intradiscal stress/pressure profile associated with low back pain.....	16
2.4 Incomplete evidence in the current literature.....	18
2.5 Consideration for <i>in-vitro</i> testing protocol.....	19
2.5.1 Specimen choice.....	19
2.5.2 Loading protocol.....	21
2.6 Research purposes.....	23
Chapter 3 Part I: Bore-Screw Pressure Sensor Validation Study.....	24
3.1 Introduction.....	24
3.1.1 Background.....	24
3.1.2 Purposes and expected outcomes.....	26
3.2 Rationale behind the final design.....	26
3.2.1 Factors affecting the pressure system.....	26
3.2.2 Factors affecting the system with specimen.....	32
3.3 Methodology considerations.....	35
3.3.1 Pressure estimation at 300 N (P ₃₀₀) and 1500 N (P ₁₅₀₀).....	35
3.3.2 Duration, hydration, and dynamic (vs. static) load during a trial.....	37
3.3.3 Range of motion.....	40
3.3.4 Size and level of specimen.....	40
3.3.5 Pressure change during flexion extension cyclic (FEC) loading protocol.....	41
3.4 Comparison to the gold standard.....	43
3.4.1 Stepwise response.....	43

3.4.2 Dynamic response	45
3.5 Validation study summary	47
3.6 Successful trial / FEC loading protocol criteria.....	48
3.6.1 Preparation	48
3.6.2 Duration	50
3.6.3 Post-test inspection	50
Chapter 4 Part II: Intradiscal Pressure Study	51
4.1 Introduction.....	51
4.1.1 Background	51
4.1.2 Purposes and hypotheses.....	52
4.1.3 Importance and implications	54
4.2 Methods	55
4.2.1 Bore-screw pressure sensor system preparation	55
4.2.2 Specimen preparation and bore-screw insertion	55
4.2.3 Baseline pressure setting.....	59
4.2.4 Specimen conditioning procedures	59
4.2.5 Flexion extension cyclic (FEC) loading protocol	61
4.2.6 Post FEC loading protocol procedures	62
4.2.7 Morphology observations	62
4.2.8 Data analysis	63
4.2.9 Statistical analysis	65
4.3 Results.....	67
4.3.1 Correlation between pressure, moments, and axial deformation	67
4.3.2 Intradiscal pressure, moments, axial deformation, and angular displacement change over time	68
4.3.3 Pressure at flexion limit, extension limit, and neutral angle change over time	75
4.3.4 Angles at maximum pressure change over time	77
4.3.5 Correlation between injury type and other dependent variables.....	78
4.4 Discussion.....	81
4.4.1 Correlation between pressure, moments, and axial deformation	81
4.4.2 Changes in pressure, moments, axial deformation, and angular displacement over time	82
4.4.3 Correlation between injury type and other dependent variables.....	88
4.4.4 Limitations	89
4.4.5 Conclusions and future directions.....	90
Chapter 5 Summary of Contributions	93
References.....	95

List of Tables

Table 1: Intradiscal pressure values for frequently experienced loading types	17
Table 2: Peak stress values obtained from tissue and FSU in-vitro tests.....	18
Table 3: A list of herniation protocols used in the past studies	22
Table 4: Specifications of the Fluke pressure sensor.....	27
Table 5: Neutral zone range compared with and without the bore-screw pressure sensor system	34
Table 6: Specimen height loss and peak moment compared with and without bore-screw pressure sensor system	35
Table 7: Specifications of the Gaeltec needle pressure sensor	43
Table 8: Step-wise test results comparing pressure values from bore-screw and needle pressure sensors.....	45
Table 9: Dependent variables used for Pearson correlation.....	65
Table 10: Dependent variables used for multiple contrast testing procedures	66
Table 11: Dependent variables used for Spearman's rank correlation.....	67

List of Figures

Figure 1: Midsagittal section of the intervertebral disc (Male 42, L23) after endplate fracture (indicated by a star) and cyclic loading shows inward buckling of the inner annulus fibrosus (indicated by an arrow) (Adams et al., 2000).	15
Figure 2: Apparatus for nuclear pressurization: The piston cylinder device (in the red box) containing the contrast gel connected to the injection line consisted of a hydraulic hose, pressure sensor, ball valve, and bore-screw (right to left in the foreground) (Veres, 2009)	26
Figure 3: A bore-screw pressure system consisted of Fluke pressure sensor, bore-screw, and high- pressure valve (left to right)	27
Figure 4: Temperature (grey) and pressure (black) change over nine hours without temperature correction	28
Figure 5: System pressure change over nine hours without temperature correction (black) and with temperature correction (grey)	29
Figure 6: Prototype I: The piston cylinder device (in between the c-clamp) containing the gel connected to the injection line consisted of a hydraulic hose, bore-screw, and pressure sensor (left to right).....	31
Figure 7: Final design of the bore-screw pressure sensor: before (top) and after (bottom) the system was instrumented with the specimen	31
Figure 8: Unsuccessful trial: a) Leaking gel during priming (no load); b) Tip of bore-screw touching the superior endplate; c) Indent on the superior endplate (left) and inferior endplate stellate fracture (right)	33
Figure 9: Successful trial: a) No leak under load (1500N); b) Tip of bore-screw well below the superior endplate; c) No indent on the superior endplate (left) and no inferior endplate stellate fracture (right).....	33
Figure 10: Needle pressure sensor insertion point (left, white dot) and the sensor inserted (right)	36
Figure 11: Pressure projection at 1500 N from various compressive loads below 600 N.....	36
Figure 12: Example of an unsuccessful trial: black arrows indicate where the pressure dropped (bottom). Notice that there was no visible change in the moment plot where the pressure drop occurred	39
Figure 13: Pressure decline due to static loading (grey) and cyclic loading (black): there was a greater decline due to cyclic loading than static loading in one hour	39
Figure 14: Pressure change associated with temperature change in one hour during a FEC loading protocol (secondary axis on the left is scaled to the conversion factor of 0.145 MPa/°C).....	42
Figure 15: Static step-wise tests for determining accuracy and reliability of the bore-screw pressure sensor compared to the needle pressure sensor	44
Figure 16: Dynamic test for determining accuracy and dynamic response of the bore-screw pressure sensor compared to the needle pressure sensor	46
Figure 17: A flowchart indicating the decisions made during this validation study	47

Figure 18: Potted specimen with the bore-screw pressure sensor system when the baseline pressure was set with a grease gun filled with gel (top) and when the high pressure valve was closed to create a closed system for testing (bottom)	57
Figure 19: Specimen with the bore-screw pressure sensor system in the material testing system (top). Each specimen was mounted on a raised platform to provide clearance for the pressure sensor system at the bottom (bottom two pictures)	58
Figure 20: Partial herniation grading system: Level 1. Minimal Disruption: no sign of herniation initiation; Level 2. Partial Herniation (Posterior): herniation initiated but breached nucleus contained only in the posterior region; Level 3. Partial Herniation (Ring): herniation initiated and the nucleus had reached anterior annulus.	63
Figure 21: Dependent variables associated with intradiscal pressure: average, maximum, minimum, and the difference between maximum and minimum	64
Figure 22: Confidence intervals for the sequential comparisons of the intradiscal pressure: on the x-axis, one represents the comparison between the baseline (0 min) and the 5 th min, two represents the comparison between the 5 th and 10 th minutes, and so on up to the 55 th min. An asterisk represents significance ($p < 0.05$).	69
Figure 23: Averages and standard deviations of intradiscal pressure over time: on the x-axis, zero represents the baseline (0 min), and it goes up in an increment of five min	70
Figure 24: Confidence intervals for the sequential comparisons of the moments: on the x-axis, one represents the comparison between the baseline (0 min) and the 5 th min, two represents the comparison between the 5 th and 10 th minutes, and so on up to the 55 th min. An asterisk represents significance ($p < 0.05$).	71
Figure 25: Averages and standard deviations of moments over time: on the x-axis, zero represents the baseline (0 min), and it goes up in an increment of five min	72
Figure 26: Confidence intervals for the sequential comparisons of the axial deformation (specimen height): on the x-axis, one represents the comparison between the baseline (0 min) and the 5 th min, two represents the comparison between the 5 th and 10 th minutes, and so on up to the 55 th min. An asterisk represents significance ($p < 0.05$).	73
Figure 27: Averages and standard deviations of axial deformation over time: on the x-axis, zero represents the baseline (0 min), and it goes up in an increment of five min	74
Figure 28: Confidence intervals for the sequential comparisons of the intradiscal pressure at specific angles: on the x-axis, one represents the comparison between the baseline (0 min) and the 5 th min, two represents the comparison between the 5 th and 10 th minutes, and so on up to the 55 th min. An asterisk represents significance ($p < 0.05$).	75
Figure 29: Averages and standard deviations of intradiscal pressure at specific angles over time: on the x-axis, zero represents the baseline (0 min), and it goes up in an increment of five min	76
Figure 30: Confidence intervals for the sequential comparisons of the angles at maximum pressure: on the x-axis, one represents the comparison between the baseline (0 min) and the 5 th min, two represents the comparison between the 5 th and 10 th minutes, and so on up to the 55 th min. An asterisk represents significance ($p < 0.05$).	77

Figure 31: Averages and standard deviations of angles at maximum pressure over time: on the x-axis, zero represents the baseline (0 min), and it goes up in an increment of five min, up to 55 min 78

Figure 32: Scatter plots of six dependent variables examined using Spearman’s rank correlation - each specimen was classified into one of the three injury classifications 79

Figure 33: Injury morphology of 14 specimens classified into one of the three injury levels 80

Figure 34: Radiographs of the specimens before (A) and after (B) endplate damage and cyclic loading (Male 61yrs old; L23). Younger specimen (Male 21yrs old; L23) after endplate fracture and cyclic loading (C) did not show noticeable radiographic signs of damage (Adams et al., 1996b)..... 82

Figure 35: H&E staining of control (top) and FEC loading protocol (bottom) specimens. Posterior region of annulus fibrosus was dissected following each protocol and immediately fixed in the OCT (optimal cutting temperature). The fixed annulus was cut horizontally (along the layers of lamellae) into 10µm slices using a cycrotome. Following the H&E staining procedure, above images were taken using a PixeLINK PL-B623CU microscope camera (B700; magnification 10x/0.03; PixeLINK, Ottawa, ON). Specimens that underwent FEC loading protocol showed multiple clefts along the orientation of fibres, whereas the control group showed minimal gap between fibres. 92

List of Equations

Equation 1: Temperature correction	29
Equation 2: Calculating pressure change due to temperature	41
Equation 3: Cross-correlation	43
Equation 4: Root-mean square error	45
Equation 5: Range of motion for the flexion extension cyclic loading protocol	61
Equation 6: Paris' law	85

List of Acronyms

IVD: Intervertebral Disc
FEC: Flexion Extension Cyclic (loading protocol)
LBP: Low Back Pain
FSU: Functional Spine Unit
PFE: Passive Flexion Extension
ROM: Range of Motion
NIAD: National Instruments Analog to Digital
RMSE: Root Mean Square Error

Chapter 1

Introduction

1.1 General introduction

Low back pain is experienced by 80% of the population at some point in their lives.

Approximately 40% of these cases are attributed to internal disc disruption (Schwarzer et al. 1995; Dammers et al., 2002; DePalma et al., 2011), which is characterized by damage to the internal structure of the intervertebral disc (IVD) and is the precursor to herniation. The mechanism of injury initiation in healthy discs that are exposed to normal, yet repetitive physiological loading has not been identified, partly because it is difficult to identify a measurable variable that is sensitive enough to detect the initiation of internal disc disruption. Mechanical loading directly affects the intradiscal pressure, and therefore, the stresses that the inner annulus fibrosus experiences. Several cross-sectional studies have demonstrated that patients with low back pain show abnormal disc stress profiles on discography, indicating that the initial changes may be observed in the intradiscal pressure (McNally et al., 1996; Ito et al. 1998). Hence, there is a need to examine how the intradiscal pressure changes over a prolonged period of time during a flexion extension cyclic (FEC) loading protocol known to induce internal disc disruption.

1.2 Purposes

This thesis consisted of two studies: [Study 1] the instrument validation study and [Study 2] the intradiscal pressure study. The purposes of this thesis were:

- To determine whether a bore-screw pressure sensor system can be used as an alternative pressure sensor, to enable time-varying continuous intradiscal pressure measurement without damage induced to the annulus fibrosus, and
- To characterize intradiscal pressure change as well as moments and axial deformation changes that occur during the generation of internal disc disruption.

The results could impact preventative strategies for occupational exposures as well as guide diagnostic or treatment options that are available to LBP patients.

1.3 Expected outcomes and hypotheses

The expected outcomes for the validation study were:

1. The bore-screw pressure sensor system performance would be comparable to the current gold standard or method of current practice (needle pressure sensor).
2. The time varying pressure responses in the IVD nucleus would be related to internal disc disruption.

The hypotheses for the pressure study were:

1. Intradiscal pressure change would be correlated to moments and axial deformation (Adams et al., 1996a; Tanaka et al., 1993; Sato et al., 1999; Wilke et al., 1999, Adams et al., 2000; Nachemson, 1981).
2. There would be significant changes in intradiscal pressure, moments, and axial deformation over time, specifically from the baseline and sequential time points (Pflaster et al., 1997; Adams and Hutton, 1983; Adams et al., 1990; Adams et al., 1996a; Sato et

al., 1999; Adams et al., 1993; Gordon et al., 1991; Callaghan and McGill, 2001; Drake et al., 2005; Zhao et al., 2005).

3. The primary mode of failure was expected to be partial disruption of the inner annulus fibrosus in the posterior or posterolateral region (Callaghan and McGill, 2001; Aultman et al., 2005; Tampier et al., 2007; Drake et al., 2005; Yates, 2009), and the injury type would be correlated to the intradiscal pressure change.

Chapter 2

Literature Review

2.1 Prevalence of low back pain related to intervertebral disc damage

Discogenic low back pain (LBP), defined as pain originating from the intervertebral disc, is one of the most common, yet difficult, conditions to diagnose, since contributions from external (i.e. mechanical exposure), internal (i.e. biologic cell-mediated exposure), and intrinsic (e.g. age, anatomical structures) factors are often intertwined. It is suggested that 80% of the population will experience LBP at least once in their lifetime (Hadler et al. 1986). LBP falls under an umbrella of musculoskeletal disorders, which account for more than 40% of lost time claims. From 2003 to 2007, there were 187,000 musculoskeletal claims that resulted in lost time, which equates to a direct cost of \$314 million (Ministry of Labor, 2009). Lost time claims by bodily reaction and exertion (44.7 – 46.6%) was the leading category of event in the workplace from 2000 to 2009, and the body part most affected was the lower back (19.0 – 21.3%) (WSIB Annual Report, 2009). Epidemiological evidence suggests that there is “strong evidence” or “evidence” of a causal relationship between exposure to ergonomic risk factors such as force, posture, and repetition/duration and musculoskeletal disorders (National Institute for Occupational Safety and Health, 1997). In addition, there is a direct correlation between age and the level and severity of herniated discs (Kormano et al. 1997), indicating that the aging population in the workplace may further increase the prevalence of LBP. In 2011 in Canada, 42.2% of the working population were aged between 45 and 64, and this number is expected to grow. For instance, in 2011, there was a greater proportion of older population (age group between 55 and 64 who typically leave the workforce) compared to the younger population (age group between 15 and 24 who typically

enter the workforce) for the first time since 1921 (Stats Canada, 2011). However, specific signs of discogenic pain do not appear on traditional medical examinations such as CT or MRI (Endean et al., 2010). Furthermore, the diagnostic confidence following the positive provocative tests for discogenic pain such as disc stimulation and discography is only 57% (Adams et al., 2003). Therefore, there is a need to identify the etiology of discogenic degenerative cascade leading to pain occurrence.

Previous studies have shown that approximately 40% of LBP cases may be related to internal disc disruption (Schwarzer et al. 1995; Dammers et al., 2002; DePalma et al., 2011), which suggests that understanding the initiation of disc disruption may be able to address a large proportion of the lost time claims. Internal disc disruption is characterized by damage to the internal structure of the intervertebral disc and is the precursor of herniation and other degenerative disc diseases (Adams et al., 2003; Bogduk and Twomey, 1997). In a cross-sectional study conducted by Dammers et al. (2002), 50% of patients of 2838 patients suffering from back and sciatic pain, showed signs of disc disruption, with the site of disruption occurring at L4/L5 in approximately 50% of the cases (Schwarzer et al., 1995). Both Schwarzer et al. (1995) and DePalma et al. (2011) showed the prevalence of internal disc disruption in LBP patients to be approximately 40%, whereas LBP patients with facet joint pain and sacroiliac joint pain varied from 15 to 40% and from 18% to 30%, respectively. It should be noted that degenerated discs are seen in 85 to 95% of adults by the age of 50 at autopsy (Quinet et al., 1979), and approximately 50 to 60% of asymptomatic middle aged adults (45 to 50 years old) have degenerative disc disease or disc pathology (Jensen et al., 1994; Greenberg et al., Jarvik et al., 2001). However, LBP due to internal disc disruption is significantly more prevalent in a younger population (aged between 41 and 46 year olds), where the majority of the workforce population lies (Human

Resources and Skills Development Canada, 2013), as opposed to the prevalence of LBP originating from facet joint or sacroiliac joint pain, which was seen in an older population (mean age 60 and 61, respectively) (DePalma et al., 2011). Therefore, understanding the mechanism that initiates internal disc disruption may be the key to characterize how discogenic pain develops, and early detection of those signs would be important in minimizing the risk of developing chronic LBP. To understand the function and mechanism of the intervertebral disc, detailed anatomy and physiology of the nucleus pulposus, annulus fibrosus, and endplate will be described in the next section.

2.2 Intervertebral disc anatomy and physiology - The evidence of why it is vulnerable

An intervertebral disc, located in between adjacent vertebra, is the largest avascular system in the body, and allows dissipation and transmission of force transmitted through the vertebral column (Adams et al., 2003) while enabling multiple degrees of freedom at each joint. An intervertebral disc consists of hydrated gel called the nucleus pulposus located between sheets of collagen called the annulus fibrosus. These structures are enclosed superiorly and inferiorly by cartilaginous endplates that attach to the vertebral body.

2.2.1 Nucleus pulposus

The nucleus pulposus consists mainly of proteoglycan, and functions as a hydrodynamic system, which attracts and retains a large amount of water. A recent study conducted by Canella et al. (2008) demonstrated that the nucleus pulposus is majorly responsible for tensioning the inner annulus fibrosus under compressive load up to 400 N in order to prevent disc collapse. It is

composed of 70 – 85% water, proteoglycans (50% dry weight), and collagen (less than 20% dry weight). Proteoglycan is a complex molecule consisting of a protein core with side chains of glycosaminoglycan molecules (chondroitin sulphate and keratin sulphate) (Adams et al., 2003). The glycosaminoglycan molecule is a negatively charged hydrophilic molecule. The nucleus cells found in adult humans are chondrocyte-like cells, which are differentiated from notochordal cells. Notochordal cells are considered the remnants of the embryonic tissue that are responsible for spinal column and brain formation. Some notochordal cells remain in the nucleus pulposus after birth, and they have the ability to synthesize new extracellular matrix material and to regulate proteoglycan synthesis (Hunter et al., 2003). In humans, notochordal cells may eventually disappear (usually by the age of 10) by either terminal differentiation or through apoptotic or other biochemical processes (Hunter et al., 2003).

2.2.2 Annulus fibrosus

In humans, the annulus fibrosus consists of 15 to 25 layers of collagen called lamella, and plays a major role in bearing the load and determining the range of motion (Merchand and Ahmed, 1990; Ayturk et al., 2010). The composition is similar to nucleus pulposus as it contains water (50%), proteoglycan, and collagen; however, it has a substantially higher amount of collagen (up to 70% dry weight) and less proteoglycan (10% dry weight). In each lamella, collagen fibres are arranged in parallel, passing obliquely from superior endplate to the inferior endplate at an approximate angle of 65 degrees with respect to the sagittal plane (Adams et al., 2003). The fibre orientation of each successive layer runs in an opposite direction. There are two collagen types, Type I and Type II, predominantly present in the annulus fibrosus. Type I collagen is usually found in tensile structures such as tendons. Type II collagen is found in compressive structures

such as articular cartilage. Since the outer annulus bears mostly tension under loading (Canella et al., 2008), the collagen type in the outer annulus is mainly Type I collagen and subsidiary Type II collagen. The outer region of the annulus fibrosus attaches to the ring apophysis constituting ligamentous portion. The inner region of the annulus fibrosus attaches to the fibrocartilaginous endplate constituting capsular portion, further emphasizing the role of supporting load while allowing flexibility. Further, there are extensive networks of elastin within the translamellar network; however, it only plays an aiding role in restoring the collagen fibre crimp at low stress levels (Schollum et al., 2008). The hydrated proteoglycan between the lamella acts to adhere adjacent layers, and a recent study using the ovine model demonstrated the presence of Type I and IV collagens forming extensive intra- and inter-lamellar bridging networks (Melrose et al., 2008). These properties allow discs to undergo complex deformation including compression, tension, torsion, and shear (Ayturk et al., 2010).

2.2.3 Endplate

The surface adjacent to the nucleus pulposus consists of fibrocartilage, and the deeper region of the endplate consists of hyaline cartilage enabling deformation when loaded. Most surfaces of the vertebral body are covered by the subchondral bone, except the ring apophysis which is located around the perimeter of the vertebral body. Instead, there are pockets of marrow cavity allowing diffusion of nutrients from the highly vascularized vertebral body (Bogduk, 1991). A recent study examining the morphology of the intervertebral disc found that there is a nodal anchorage mechanism between nucleus and endplate, which is suggested to resist tension (i.e. bending and/or twisting) between superior and inferior endplates (Wade et al., 2012).

2.2.4 Nutrition

The metabolic rate of the intervertebral disc is very low since only the small vessels from arteries enter the outer annulus fibrosus. There are three main transport pathways: 1) through the outer annulus, 2) through cyclic loading allowing blood flow from the vertebral body, and 3) through diffusion of solutes down the concentration gradients from the vertebral body. As mentioned, glycosaminoglycan molecules in the nucleus pulposus are negatively charged. Therefore, positively charged molecules enter the disc primarily via the annulus pathway. Cyclic axial loading allows transportation of larger solutes (>40kD) into the disc and diffusion transports smaller solutes (<1kD) and essential nutrients (Ferguson et al., 2004; Urban et al., 2004). However, because these systems cannot transport large amounts of oxygen and nutrients, tissue healing is limited once it is damaged. This indicates that certain types of mechanical exposure may impose risks for degenerative changes (Urban et al., 2004).

2.2.5 Nerve supply and potential source of pain

Anterior and lateral annulus are supplied by fine nerves from sympathetic trunks and its grey rami communicantes and posterior annulus is supplied by branches of sinuvertebral nerves. The outer third of the annulus fibrosus contains a large amount of nerve endings. Most of them are free nerve endings, which are considered to have a nociceptive function, while the remaining ones have capsulated and complex encapsulated endings. Complex encapsulated endings are considered to have proprioceptive function.

Though there are no free nerve endings in the nucleus pulposus or inner annulus fibrosus, internal disc disruption can be painful. One potential cause is the displaced nucleus pulposus triggering the release of pain-sensitizing chemicals. The nucleus can cause an inflammation

reaction, releasing chemicals such as tumor necrosis factor alpha (TNF- α), and stimulating free nerve endings in the periphery (Olmarker et al., 1998), producing neuropathic pain (Tobinick and Britschgi-Davoodifar, 2003). This process has also been shown to cause neural damage (Iragashi et al., 2000). Furthermore, several studies have shown increased levels of other proinflammatory mediators such as interferon gamma (INF- γ), interleukin-1, 6, and 8 (IL-1, 6, 8), and prostaglandin E₂ (PGE₂) in symptomatic patients (Cuellar et al., 2010; Burke et al., 2002). In rats, TNF inhibitors have been demonstrated to reduce nucleus pulposus-induced pain and neuropathy (Olmarker and Rydevik, 2000). A recent study by Olmarker (2011) demonstrated that in a porcine model, using two cytokine inhibitors (TNF and IL-1) could efficiently reduce nucleus pulposus-induced nerve conduction velocity. Therefore, degeneration causing nucleus pulposus to leak out of the enclosed system can trigger pain. So how does the degeneration occur?

2.3 Degeneration associated with intradiscal pressure

It is difficult to define “degeneration” of intervertebral discs as there is no consistent degenerative cause or pathway. In this section, degeneration is defined as a process that weakens or damages the structure, which may negatively affect its functional integrity and may eventually cause pain.

2.3.1 Degeneration occurring in everyday life

Degeneration of the intervertebral disc involves mechanical exposure and biochemical changes. With aging, the level of oxidative stress and the occurrence of cell apoptosis increase. As mentioned, intervertebral discs lack a major metabolite transportation system. A lack of oxygen may cause nucleus cells to turn quiescent and will encourage non-enzymatic glycation (Horner

and Urban, 2001). Since there will be fewer active cells, the matrix turnover rate may be slowed. Non-enzymatic glycation involves reducing sugars to form a bridge between parallel collagen molecules. This process can reduce the availability of nutrition (e.g. glucose), which can destroy the nucleus cells, and, with low matrix turnover rate, form advanced glycation end products (Bank et al., 1998). The advanced glycation end products can inhibit the proteoglycan turnover, which reduce water content, increase stiffness, and eventually lead to reduced tissue strength (DeGroot et al., 2004). With an increase in cross-linking of adjacent collagens, matrix turnover and repair would be further compromised. These changes give rise to the fibrous and discoloured (brownish yellow) tissues seen in aged discs (Bank et al., 1998).

Although age-related changes occur, disc degeneration is seen mostly at L4/L5 (Schwarzer et al. et al., 1995), indicating that mechanical exposure can also alter the degenerative pathway leading to LBP. For instance, moderate manual material handling or a few hours of sitting, which occur in everyday life, can induce degenerative changes. Light to moderate manual labour (approximately 2000 – 3000 N compression) can increase the intradiscal pressure to 2 – 3 MPa (Nachemson, 1966; Nachemson, 1981). Handa et al., (1997) demonstrated that pressures exceeding 3 MPa can increase the synthesis of matrix metalloproteinase-3 (MMP3), which is an enzyme that degrades nucleus pulposus. In addition, cyclic and prolonged compressive loading may occur during repetitive material handling and sitting, respectively. A sustained creep loading (50% of body weight) as short as 1.5 hours led to reduced transportation of small solutes ($p < 0.331$) compared to the unloaded condition (Arun et al., 2009). The reduction in transportation was particularly lower in the center of the disc ($p < 0.04$). From the discussion above, reduced oxygen and nutrients would contribute to triggering the degenerative changes. A study conducted by Hutton et al. (1998) showed that a static compressive load applied to a

canine model stimulated Type I collagen synthesis and inhibited proteoglycan synthesis in the nucleus pulposus. A study conducted by Walsh and Lotz (2004) used the murine model to test the effect of biological response after dynamic loading at a 50% duty cycle between 0 MPa and one of two peak stresses (0.9 or 1.3 MPa) at one of two frequencies (0.1 or 0.01 Hz) for 6 hours per day for 7 days. The results demonstrated that at lower frequency and/or higher stress, there was an increase in proteoglycan content, matrix gene expression, and cell death, indicating that the repair process has increased due to mechanical exposure (Walsh and Lotz, 2004). Therefore, changes in pressure due to mechanical loading may accelerate the degenerative changes.

It should be noted that mechanical exposure may be altered by intrinsic factors such as genetics, psychosocial factors, and individual factors other than age. Several studies examining twins demonstrated that genetic heredity explained over 70% of the variance in disc degeneration, and therefore has a dominant role in determining the degenerative path (Battie et al., 2004; Sambrook et al., 1999). Although it may not directly trigger degeneration, weaker tissue structures formed due to specific gene expression may impose higher risk for disc degeneration. Gene expression can also influence individual factors (e.g. anthropometry and gender) and psychosocial profile (e.g. character). On the other hand, Sambrook et al. (1999) in their twin study noted that there was no significant effect of genetic influence on disc signal intensity (e.g. hydration level). This evidence highlights the fact that environmental factors including working culture, nutrition, and fitness level can influence the process of degeneration. Therefore, it is important to keep in mind that low back pain associated with disc degeneration may involve multiple interacting and compounding factors.

2.3.2 Degeneration associated with kinematic changes

One way to assess the level of degeneration is by observing kinematic changes. Compression causes axial creep, in which the magnitude of creep increases with increasing compressive load. Following a nine hour herniation protocol, specimen height decreased by 11.18 (SD 2.17) mm (Callaghan and McGill, 2001). This axial creep caused radial bulging of the annulus fibrosus, significantly increasing the average stiffness ($p < 0.001$) and extension moments ($p < 0.014$) of porcine functional spine units (Callaghan and McGill, 2001). Though the stiffness increased with cyclic loading, the range between the peak flexion and extension angles significantly increased following the herniation protocol ($p < 0.003$), suggesting that mechanical instability may occur when the structure is damaged (Callaghan and McGill, 2001). Previous epidemiological studies demonstrated that low back pain patients can be subdivided into individuals with increased lumbar segmental instability (i.e., increased range of motion and/or neutral zone), which is linked to disc degeneration (Alqarni et al., 2011; Panjabi, 1992). However, all of these kinematic variables failed to detect the initiation of herniation event since no acute changes were observed. Furthermore, there was no correlation between the extrusion pattern of the disc and the biomechanical parameters in terms of stiffness and energy loss (Gordon et al., 1991). Therefore, there may be a more sensitive parameter – such as the intradiscal pressure – that is better able to detect the initiation of the mechanical instability associated with disc degeneration.

2.3.3 Association of abnormal intradiscal stress/pressure profile and low back pain

Patients with low back pain have demonstrated higher annular stress and lower nucleus pressure profiles on discography, indicating that the initial changes may be observed in the intradiscal pressure (McNally et al., 1996; Ito et al. 1998). Mechanical loading directly affects the

intradiscal pressure, and therefore, the stress that the inner annulus fibrosus experiences. To clarify the terminology, stress (circumferential, radial, or longitudinal) in the inner annulus occurs as a result of intradiscal pressure. There are two proposed pathways that abnormal pressure can arise: 1) degeneration or pre-existing endplate damage causing a decrease in intradiscal pressure, and 2) mechanical loading causing an increase in static pressure inside the intervertebral disc.

The first phenomenon, a decrease in intradiscal pressure in the degenerated discs or discs with pre-existing endplate damage, has been thought to relate to inward collapse or buckling of the inner annulus (Figure 1), leading to increased radial strain on the outer annulus. Several cross sectional studies reported that inward collapse of lamella was a common feature in elderly discs on post-mortem dissection (Tanaka et al., 1993; Gunzburg et al., 1992). Adams et al. (1996) examined human discs at different degenerative stages and compared horizontal and vertical stress values along the anterior-posterior diameter using a needle pressure sensor. They found that Grade 3 and 4 discs had a 30% reduction in hydrostatic pressure, and higher stress peaks were seen in the posterior annulus (Adams et al., 1996b). Several studies in which they induced endplate damage have also exhibited a reduction in intradiscal pressure (Adams et al., 1993; Adams et al., 2000; Holm et al., 2004). The endplates can be damaged due to fatigue, even under normal loads occurring in everyday life (Adams and Hutton, 1983). Following endplate fracture, the nuclear pressure decreased by 25 – 30%, and the cyclic loading after fracture caused further pressure reduction (Adams et al., 1993; Adams et al., 2000). Stress peaks in the inner posterior annulus also increased from 0.45 MPa to 1.13 MPa (Adams et al., 2000).

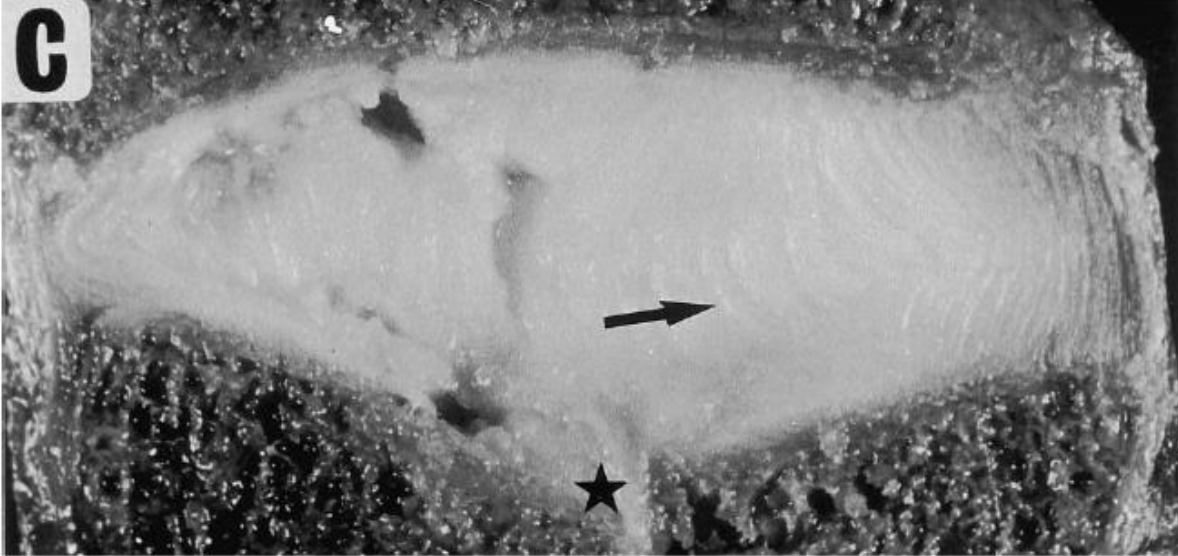


Figure 1: Midsagittal section of the intervertebral disc (Male 42, L23) after endplate fracture (indicated by a star) and cyclic loading shows inward buckling of the inner annulus fibrosus (indicated by an arrow) (Adams et al., 2000).

The second phenomenon, an increase in hydrostatic pressure occurring during combined mechanical loading, such as during manual material handling, has been linked to the development of herniation (Kelsey et al., 1984; Wilke et al., 1999; Gordon et al., 1991). Increases in hydrostatic pressure may exceed the stress tolerance in the disc, leading to internal disc disruption. Veres et al. (2008 and 2009) examined the mode of failure due to elevated intradiscal pressure using an ovine model and found that failure occurred predominantly in the posterior region. This failure may be attributed to the posterior annular wall being thinner and located adjacent to a higher number of incomplete lamellae. The mean failure pressure and the direction of radial fissure were also dependent on the posture (Veres et al., 2008; Veres et al., 2009). The mean failure pressure in the neutral posture was 14.1 ± 3.9 MPa, whereas in 10 degree flexion, it was 9.8 MPa ($p = 0.02$). Further, specimens showed increased annular failure at a 7 degree flexion posture (65%) compared to a 10 degree flexion posture (41%), although the amount of nucleus displaced was greater at 10 degrees (Veres et al., 2009). Furthermore, it was

noted that flexed postures increased the occurrence of endplate-annulus junction failure as well as radial fissure instead of circumferential disruption (Veres et al., 2009).

2.3.4 Counterarguments for abnormal intradiscal stress/pressure profile associated with low back pain

So far it has been presented that a decrease in intradiscal pressure may lead to inward collapse of the annulus; however, there is no evidence for how much pressure is required to maintain sufficient radial tension in the annulus (Table 1) to prevent this buckling. Canella et al. (2008) demonstrated that the nucleus pulposus contributes to maintaining tension under 400 N of compression. This finding is interesting because the annulus fibrosus can be assumed to be in tension under compression beyond 400 N. From the observations stated in previous literature (Adams et al., 1996b; Wilke et al., 1999), 400 N equates to approximately 0.4 – 0.72 MPa of intradiscal pressure, assuming that the compressive load and intradiscal pressure have a linear relationship. During standing, a healthy individual may experience 0.50 – 0.97 MPa of intradiscal pressure (Wilke et al., 1999), and in a degenerated disc, approximately 1.0 – 1.5 MPa can be built up under 2000 N compression (Adams et al., 2003). Therefore, it seems sufficient to hold the inner annulus in tension even in a degenerated disc; however, cyclic loading may promote continuous leakage of the nucleus, causing further reduction in the intradiscal pressure. In addition, Fujita et al. (1997) has shown that the inter-lamellar strength is weaker than the intra-lamellar strength, but with recent findings demonstrating substantial trans-lamellar connections that span over a few lamellae (Schollum et al., 2008), the strength may have been underestimated in their experiment. As evidenced, Gregory et al. (2011) has shown that inter-lamellae bone was able to withstand 0.30 (SD 0.05) N/mm based on a 0.18mm thick lamella (equivalent of 6.06 MPa), using the novel lap test protocol. Further, the stress profile

demonstrated by Adams et al. (1993 and 1996) in degenerated discs and discs with endplate fracture have been the dominant explanation for this theory. However, there is no apparent pressure gradient in the stress profile of the degenerated nucleus, and the fact that annulus failure can occur without endplate failure (Gordon et al., 1991; McNally et al., 1993; Callaghan and McGill, 2001) could weaken their argument for the genesis of inward collapse in healthy discs.

Table 1: Intradiscal pressure values for frequently experienced loading types

Condition	Intradiscal Pressure (MPa)
Unloaded	0.05 ^a
Pre-tension in ligamentum flavum (intact; unloaded)	0.05 – 0.12 ^{b,c}
Pre-tension in ligamentum flavum (degenerated; unloaded)	0.05 – 0.06 ^{b,c}
Prone or supine (intact; low muscle activity)	0.08 – 0.15 ^{d,e}
Standing (500 N)	0.50 – 0.97 ^e
Light manual labor (Grade 1; 2000 N)	2.00 – 3.60 ^{e,f}
Light manual labor (Grade 4; 2000 N)	1.50 – 1.60 ^c

^aNachemson (1966); ^bPanjabi et al. (1988); ^cAdams et al. (1996); ^dSchendel et al. (1993); ^eWilke et al. (1999); ^fNachemson and Elfstrom (1970)

An increase in intradiscal pressure is also a plausible injury initiation mechanism; however, how the pressure is related to the stress experienced in the annulus fibrosus remains unclear. The morphology of annular failure resembled protrusion or extrusion herniation that is clinically observed in studies conducted by Veres et al. (2008, 2009). The mean failure pressure in the neutral posture shown by Schectman et al. (2006) was 18 (SD 3) MPa, which was calculated to exert 45 (SD 7) MPa hoop stress, assuming linear elastic isotropic properties and neglecting the end point beyond the elastic region. Taking into account the fibre orientation, which was angled at 52 degrees (caudal), the tensile failure stress of 62 MPa in the fibre direction was derived. Although there are differences between bovine caudal and human models, this failure stress falls within the spectrum of what has been observed in humans (Table 2). The failure pressure of 18 MPa is 3 to 4 times greater than the intradiscal pressure observed during light manual labor,

which indicates that physiologically relevant mechanical loading may not build enough pressure to exceed the tissue tolerance. The failure pressure decreases to half (9.8 MPa) in the flexed posture (Veres et al., 2008; Veres et al., 2009), but the margin of safety is still large. Therefore, although the morphology of annular failure resembled clinically observed protrusion or extrusion herniation, the pressure may not build to this extent within the expected range of physiological loading.

Table 2: Peak stress values obtained from tissue and FSU in-vitro tests

Authors (Year)	Type of load and model	Stress
Marchand & Ahmed (1989)	Human (tissue; L4/5)	110 MPa (circumferential direction)
Galante (1967)	Human (tissue; anterior)	10 MPa (fibre direction)
Green et al. (1993)	Human (tissue; anterior and posterior)	3.9 and 8.6 MPa (axial direction)
Skaggs et al. (1994)	Human (tissue; various location)	3.6 – 10.3 MPa (depends on location and direction)
Schechtman et al. (2006)	Caudal (FSU)	62 MPa (fibre direction - estimated)
Gregory (2009)	Porcine (tissue; single layer in various location)	0.69 – 1.81 MPa (initial failure) and 1.17 – 2.16 MPa (ultimate failure) (circumferential direction)

2.4 Incomplete evidence in the current literature

It is evident that there are substantial amounts of mechanical connections between the passive structures; however, the “weak link” among those has not been identified (Wade et al., 2012; Schollum et al., 2008), partly because identifying a measurable variable that is sensitive enough to detect the initiation of internal disc disruption is difficult. In addition, the correlation between intradiscal pressure and moments and axial deformation (specimen height) has not been examined over time. Hence, there is a need to examine how the intradiscal pressure changes over time during a protocol known to induce internal disc disruption.

2.5 Consideration for *in-vitro* testing protocol

2.5.1 Specimen choice

Porcine cervical functional spine units (FSUs) have been adopted as a surrogate of the human lumbar spine since they have similar anatomical and functional structures while providing better control over age, gender, and activity level (Yingling et al., 1999). Anatomically, porcine cervical vertebrae are similar to those of humans, including ligamentous structures and facet joint orientation, except they have non-load bearing anterior processes (Oxland et al., 1991; Yingling et al., 1999). Geometrically, the porcine vertebrae are approximately one third smaller in all dimensions (Yingling et al., 1999); therefore, the components making up the intervertebral disc also fall in the lower range of human discs (Tampier, 2006). The number of lamellae in the porcine discs is approximately 18 to 30 layers (width 0.062 – 0.192mm) as opposed to 20 to 40 layers (width 0.059 – 0.260mm) in human discs. The porcine disc has a fibre angle of 39 to 48 degrees while the human disc has an angle of 47 to 62 degrees. Although there are minor differences, both discs have similar orientation of the lamellae: inner lamellae are thicker than outer lamellae; posterior annulus is thinner and has fewer numbers of lamellae than the anterior annulus; the inclination of the fibre angle decreases in the inner annulus; and there is predominantly Type I collagen in the outer annulus (Tampier, 2006).

The age of the porcine specimens that has typically been used is approximately 6 month old, simulating the young human population with healthy discs. Notochordal cells in pigs remain in the nucleus throughout their lives, indicating that degeneration that occurs naturally in humans due to aging may not be seen in porcine specimens (Butler, 1988). Mechanically, the porcine cervical spine demonstrates similar range of neutral zone and stiffness values in compression and shear compared to the human lumbar spine (Yingling et al., 1999; Wilke et al., 2011). The pig

cervical region is designed to bear a large compressive load, generated by muscle activity required to align the spine horizontally against gravity, which in turn mimics the compressive load experienced in the human lumbar spine. In addition, mechanical loading has been shown to cause internal disc disruption similarly observed in human (Callaghan and McGill, 2001; Park et al., 2005; Tampier, 2006) though its failure moments may be lower in pigs (61 Nm vs. 156 Nm in human) (Osvalder et al., 1990). Therefore, porcine cervical functional spine units are deemed a suitable animal model for the human lumbar spine in mechanical testing.

Another consideration includes the effect of freezing and hydration on the material and mechanical properties of the porcine spine. Freezing has been shown to cause permanent changes to the porcine spine (Bass et al., 1997; Callaghan and McGill, 1995). For instance, following freezing, the swelling pressure of the discs decreased by 25%, the ultimate compressive load increased by 24%, and the energy absorption increased by 33% (Bass et al., 1997; Callaghan and McGill, 1995). However, there was no change in stiffness and angular displacement at failure. The pressure difference may be of concern; however, since the purpose of the study is to examine the changes in pressure over time, the difference will not affect the dependent variable. Hydration normally varies post-mortem and throughout the testing protocol. According to the study conducted by McMillan et al. (1996), 6 hours of prolonged loading in a flexed posture experienced 18% hydration variation, which has been shown to occur naturally in humans during the course of the day (Adams et al., 1990).

2.5.2 Loading protocol

A flexion extension cyclic loading protocol (FEC loading protocol), or previously known as a herniation generating protocol, has been used to induce internal disc disruption in healthy intervertebral discs. It has been reported that complex loading including compression, bending, and/or rotation can produce internal disc disruption (Table 3). The nucleus tracking through the annulus fibrosus occurs along the plane of motion (Aultman et al., 2005). The range of motion was within physiological limits to simulate the exposure that occurs frequently in everyday life. In addition, position control (instead of load control) was used since it has been shown to increase the occurrence of internal disc disruption (Callaghan and McGill, 2001). Therefore, the motion range was determined using the neutral zone obtained from the passive flexion extension (PFE) test under 300 N of compressive load (Noguchi et al., In Press). Furthermore, a compressive load of 1500 N was used in the protocol since 1000 to 2000 N of compressive load is experienced during light manual labour (Nachemson et al., 1966; Nachemson et al., 1981) and a higher compressive load (>2000 N) has been associated with an increased occurrence of endplate fracture (McNally et al., 1993; Adams and Hutton, 1982; Veres et al., 2009). The maximum number of cycles was 3600 cycles, since disruption has been shown to occur within 4,000 cycles (Tampier et al., 2007, Drake et al., 2005). Specific details of this cyclic loading protocol will be outlined in Section 4.2.5 Flexion Extension Cyclic Loading Protocol.

Table 3: A list of herniation protocols used in the past studies

Authors (Year)	Outline of protocol	Type of damage induced
Adams & Hutton (1982)	<i>Intact disc (human)</i> Increasing compression (up to 8000 N) in anterolaterally-flexed (8-15°) position	35/61 endplate/vertebral body failure 26/61 disc failure (posterior disc prolapsed)
McNally et al. (1993)	<i>Intact disc (human)</i> Compression at around 2000 N with a flexion angle of elastic limit + 2deg until failure	12/22 vertebral body fracture 10/22 disc failure (8 prolapse and 2 major tears posterolaterally)
Adams and Hutton (1985)	<i>Intact disc (human)</i> Cyclic compression in (1500-4000 N) anterolaterally-flexed posture	Most failed by endplate fracture and most showed disc disruption (6/29 disc prolapsed)
Gordon et al. (1991)	<i>Intact disc (human)</i> 1.5 Hz complex loading (flexion 7°, rotation up to 3°, and compression 1334 N) for an average of 6.9 hrs (3 – 13 hrs)	14/14 disc failure (10/14 annular protrusion and 4/14 nuclear extrusion through annular tears)
Callaghan & McGill (2001) Aultman et al., 2005 and Drake et al., 2005 adopted similar protocol	<i>Intact disc (pig)</i> Cyclic flexion and extension (within neutral zone) with light compression (260, 867, and 1472N)	260N: 1/2 damage 867N: 4/4 damaged (4 stage4) 1472N: 4/4 damaged (3 stage 4) *no report of whether endplate was intact
Tampier et al. (2007)	<i>Intact disc (pig)</i> Cyclic flexion and extension (within neutral zone) with 1472 N compression under varying cycle number	8/16 complete herniation 4/16 partial herniation 4/16 no apparent damage *2/16 reported endplate damage; however, no indication of which specimen
Kuga & Kawabuchi (2001)	<i>Intact disc (mouse)</i> 400 repetitions (1-2 Hz) of flexion (30°) and axial rotation (6°) (Cyclic flexion/extension with light or no compression)	1/10 extrusion with endplate fracture 3/10 posterior protrusion with annular-endplate rupture 6/10 no sign of protrusion or rupture
Veres et al. (2009)	<i>Intact disc (sheep)</i> Flexion (7 and 10°) with increasing intradiscal pressure at 0.04-0.10 MPa/s	16/34 vertebral body failure 18/34 disc failure (11 in 7° and 7 in 10°; 4 diffuse rupture, 4 radial mid-axial annular ruptures, and 10 radial annular-endplate ruptures)
Simunic et al. (2004)	<i>Intact disc (ox tail)</i> Increasing compression in different conditions (postures, hydration, loading rates, and test sequence)	0 vertebral body fracture 96 disc failure *no report on the type of failure
Adams et al. (2000)	<i>EP fractured (human)</i> Cyclic compressive load (2.2 kN) applied in flexed (4-10° flexion) or lordotic (2° extension) posture	8/15 anterior annulus inward bulging; 9/15 posterior annulus inward bulging; 8/15 anterior annulus outward bulging; 14/15 posterior annulus outward bulging; bell-shaped deformation *no report of whether endplate was intact

2.6 Research purposes

The purpose of this thesis research was to characterize pressure changes during a FEC loading protocol known to induce internal disc disruption. The thesis was broken down into two parts: [Study 1] to determine the validity of the bore-screw pressure sensor system and [Study 2] to examine the changes in intradiscal pressure, moments, and axial deformation (specimen height) during a FEC loading protocol and to examine morphology of the discs. In the first study, the rationale behind the design of the pressure sensor and methodology was described, and the bore-screw pressure sensor was compared to the gold standard (needle pressure sensor) to determine accuracy and reliability. The second study characterized the change in intradiscal pressure, moments, and axial deformation during a one-hour FEC loading protocol. It was hypothesized that [Study 1] results from the bore-screw pressure sensor would be comparable to those from the needle pressure sensor and [Study 2] i) intradiscal pressure change would be correlated to moments and axial deformation, ii) pressure would significantly decrease and moments and axial deformation would significantly increase over time, and iii) partial herniation would be seen in the posterolateral region following the FEC loading protocol, and the injury type would be correlated to the pressure change.

Chapter 3

Part I: Bore-Screw Pressure Sensor Validation Study

3.1 Introduction

3.1.1 Background

In previous intervertebral disc (IVD) *in vitro* studies, a needle pressure sensor has been the only transducer capable of measuring the intradiscal pressure (McNally et al., 1993; Nachemson 1981; Adams et al., 1996a; Adams et al., 1996b; McNally et al., 1996; Tanaka et al., 1993; Sato et al., 1999; Adams et al., 1993; Wilke et al., 1999). In order to insert a needle pressure sensor in an IVD, the annulus fibrosus must be punctured, which directly damages the structure of the lamellae and creates a path that nucleus pulposus can travel through to induce herniation (Carragee et al., 2009; Ryan and Hsieh, 2006; Kim et al., 2004). In a prospective, match-cohort study examining the progression of IVD degeneration in subjects who have and have not been exposed to discography has shown a significantly higher prevalence of disc degeneration, herniation, and height loss in subjects who have undergone the procedure 10 years ago (Carragee et al., 2009). In an *in vitro* study examining the relationship between gauge size and the viscoelastic behaviour of rodent annulus fibrosus, it was reported that even an 18 gauge (1.2 mm diameter) needle could cause significant change in IVD mechanics in rodents (Ryan and Hsieh, 2006). The same size needle has shown to effectively induce disc degeneration in a rabbit model as well (Kim et al., 2004). This evidence demonstrates that needle pressure sensors are particularly problematic when examining the precursors of herniation, such as inner annulus fibrosus disruption. In addition, a needle pressure sensor can be expensive and easily broken during a repetitive dynamic range of motion loading protocol frequently used for *in vitro* studies

(Callaghan and McGill, 2001; Aultman et al., 2005; Drake et al., 2005; Tampier et al., 2007; Kuga and Kawabuchi, 2001; Gordon et al., 1991). Typically, a needle pressure is inserted during a static loading (Adams and Hutton, 1982; McNally et al., 1993; Adams et al., 1996a), a cyclic compressive loading (Adams and Hutton, 1985; Adams et al., 2000) or a slow dynamic movement (Wilke et al., 1999). However, these loading protocols would not be able to capture a range of motion time-varying response, which has been shown to initiate herniation in a healthy disc. Therefore, there is a need to examine an alternative transducer that does not induce annular damage during instrumentation.

A bore-screw pressure system was originally developed at the University of Auckland for examining the morphology of annular damage due to rapidly induced intradiscal pressure increases (Simunic et al., 2004; Schechtman et al., 2006; Schollum et al., 2008; Veres et al., 2008; Veres et al., 2009). The device consisted of a bore-screw, which was inserted into the inferior vertebra and through the endplate, and was connected to a hydraulic jack via a high pressure tube for controlling the pressure (Figure 2). Although instrumentation damages the endplate, it does not cause any puncture or disruption to the annulus fibrosus. The system has been used as a pathway to artificially increase the pressure within the IVD nucleus, however, not as a means to measure intradiscal pressure. It is a challenge to implement the sensor system without causing a catastrophic damage to the endplate while maintaining accuracy and reliability for measuring the intradiscal pressure. Therefore, the objective of this study was to outline the rationale behind the final design of the bore-screw pressure sensor system and demonstrate its performance characteristics for an *in vitro* study using a porcine model.

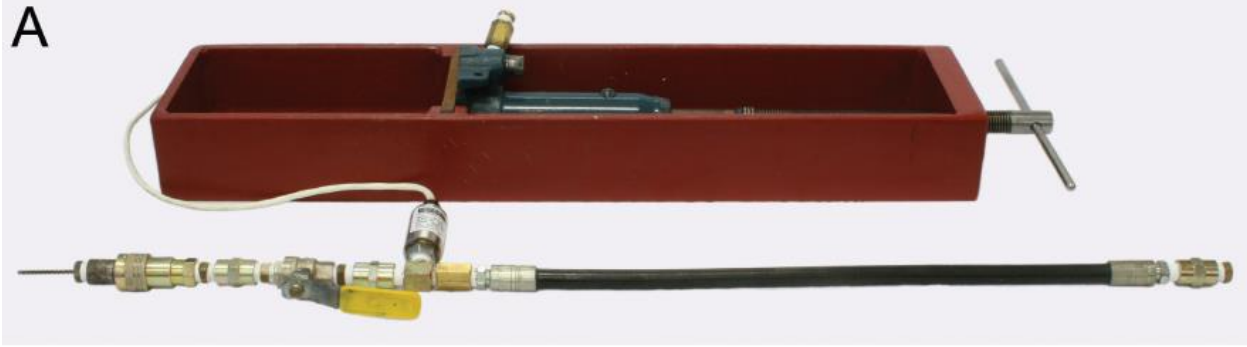


Figure 2: Apparatus for nuclear pressurization: The piston cylinder device (in the red box) containing the contrast gel connected to the injection line consisted of a hydraulic hose, pressure sensor, ball valve, and bore-screw (right to left in the foreground) (Veres, 2009)

3.1.2 Purposes and expected outcomes

Specific purposes of the validation study were 1) to identify factors affecting the bore-screw pressure sensor system only and for the system inserted into a specimen in order to optimize the sensor design and implementation method, 2) to identify methodology considerations when conducting a porcine *in vitro* study using a bore-screw pressure sensor system, and 3) to test its accuracy, reliability, and dynamic response compared to the gold standard (needle pressure sensor). The final design of the bore-screw pressure sensor system was expected to have comparable accuracy and reliability to those of the gold standard.

3.2 Rationale behind the final design

3.2.1 Factors affecting the pressure system

The objective for testing the bore-screw pressure sensor system without a specimen was to design a reliable pressure system that could maintain pressure for a prolonged period of time so as not to introduce error in the instrumentation that would confound IVD pressure measures. The pressure system consisted of a high pressure valve (1/4 inch NPT 2-Way High Pressure Ball

Valve), a steel bore-screw (1/4 inch diameter x 6 inch length with an internal bore of 1/8 inch, 94624A220, McMaster-Carr, Elmhurst, IL, USA), and the pressure sensor (Fluke PV350, Fluke, Everett, WA, USA) (Figure 3, Table 4) The bore-screw was sealed with a metal cap for the purpose of this test. The two factors identified that could affect the reliability of the pressure sensor were: 1) pressure leaks and 2) temperature.

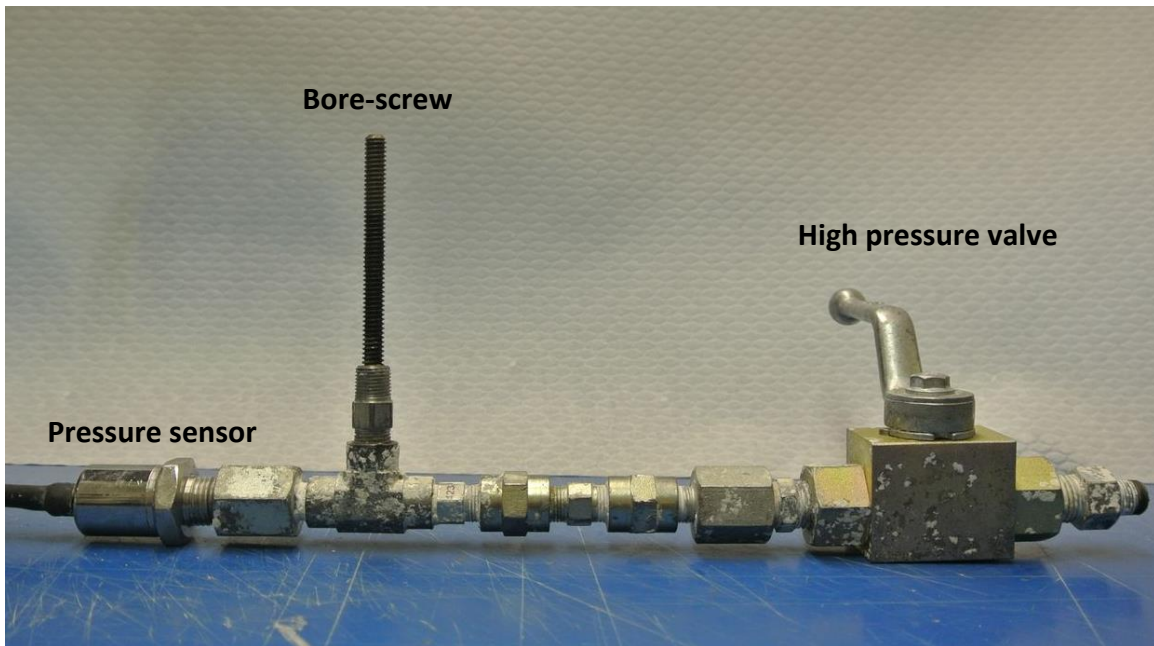


Figure 3: A bore-screw pressure system consisted of Fluke pressure sensor, bore-screw, and high-pressure valve (left to right)

Table 4: Specifications of the Fluke pressure sensor

Specification	Range	Accuracy
Range	0 to 2.4 MPa	$\pm 1\% \pm 0.0021$ MPa
	2.4 to 3.5 MPa (Max 6.0 MPa)	$\pm 5\% \pm 0.0070$ MPa
Temperature Range	18 and 28°C	No correction necessary

3.2.1.1 Pressure leaks

In industrial settings, leak tests are typically done using either air or a specific test gas as the medium to measure changes in pressure over time (Geiger, 2008). To test whether a closed-system could be established without a specimen, an air compressor (maximum pressure = 120psi/

0.8 MPa) was used to build pressure to 0.76 (SD 0.009) MPa, and a high-pressure valve was closed to simulate testing condition. Pressure measurements were collected using the National Instruments Analog to Digital (NIAD) program (University of Waterloo) at 32 Hz for 9 hours. After 9 hours of static loading, the pressure was 0.70 MPa (SD 0.00028), a decrease of 0.053 MPa (7.02%).

3.2.1.2 Temperature

The pressure sensor used for this study was temperature sensitive as shown by the high correlation coefficient ($r > 0.95$) between pressure and the temperature (Figure 4). The temperature sensor (Electro-numeric dual T Thermometer) was attached to the pressure sensor and the data were collected at 32 Hz using the NIAD program.

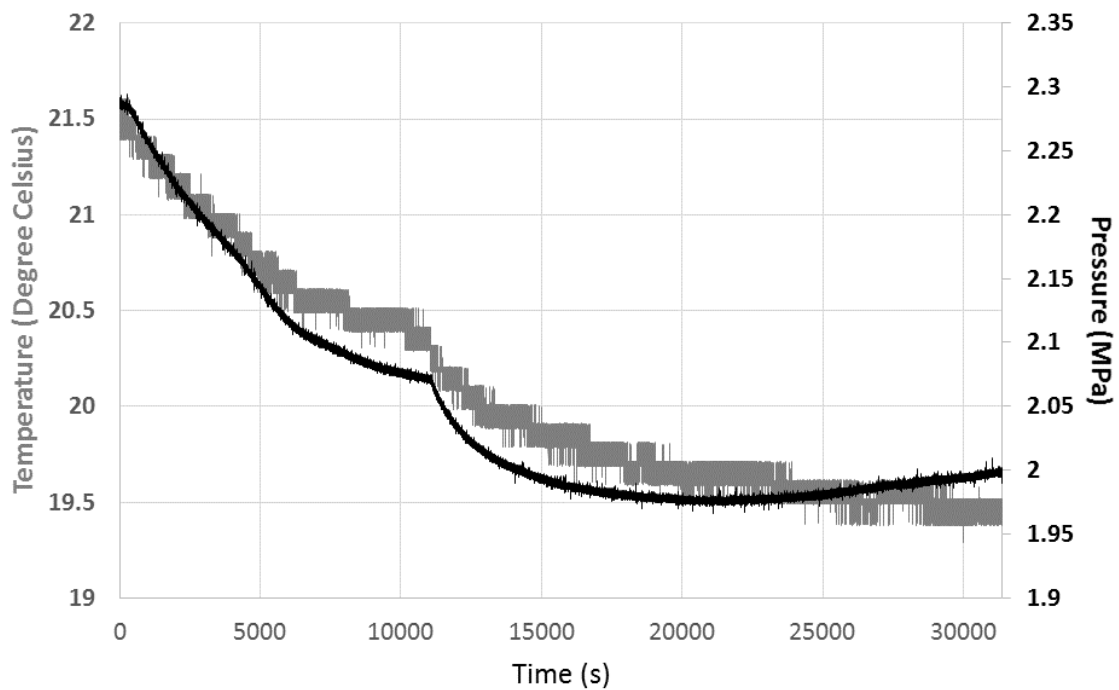


Figure 4: Temperature (grey) and pressure (black) change over nine hours without temperature correction

The following correction equation was developed and used to take into account the temperature effect on pressure:

$$P_{corrected} = P_{measured} - P_{temperature}$$

$$P_{temperature} = ({}^{\circ}\text{C}_n - {}^{\circ}\text{C}_i) \times P/{}^{\circ}\text{C}$$

Equation 1: Temperature correction

where $P_{temperature}$ was the pressure change due to temperature, $P_{measured}$ was the pressure measured from the sensor, and $P_{corrected}$ was the pressure corrected. $P_{temperature}$ was defined by the difference between ${}^{\circ}\text{C}_n$, temperature at a given point and ${}^{\circ}\text{C}_i$, temperature at an initial point multiplied by a change in pressure per degree Celsius, $P/{}^{\circ}\text{C}$.

In the second leak test, hydrated silica gel was injected by a grease gun in order to build pressure to over 2.0 MPa to simulate a testing condition. The pressure data were collected at 32 Hz and monitored for 9 hours using the NIAD program (University of Waterloo). The pressure decreased from 2.30 (SD 0.0068) MPa to 2.29 (SD 0.00083) MPa, indicating that the change was only 0.0034 MPa (0.15%) with temperature correction (Figure 5).

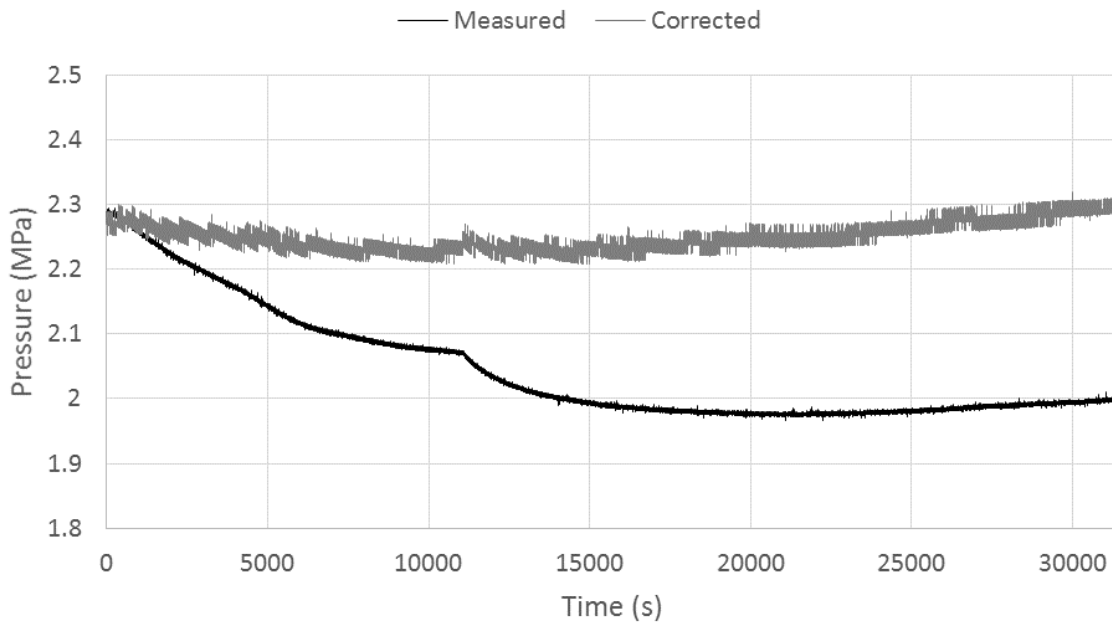


Figure 5: System pressure change over nine hours without temperature correction (black) and with temperature correction (grey)

3.2.1.3 Other considerations

There were several changes made to the design of the pressure system throughout the validation stage in order to minimize instrumentation errors. The first prototype consisted of a hydraulic jack (filled with ultrasound gel) and a hydraulic hose connected to a bore-screw and a pressure sensor with a T-joint (Figure 6). This original design was adopted from a series of studies conducted at the University of Auckland (Simunic et al., 2004; Schechtman et al., 2006; Schollum et al., 2008; Veres et al., 2008; Veres et al., 2009) in which they had examined IVD failure mechanisms due to elevated intradiscal pressure. A hydraulic jack was able to build enough pressure for the purpose of this study; however, it was impossible to sustain over a period of time due to leakage through an O-ring in the pump. Since the piston needed to be taken out repeatedly to refill the gel, the O-rings quickly wore out, and therefore, using a hydraulic jack was deemed not practical. In addition, pressure was affected by a small change in volume, for example, bending a high pressure tube, tightening each connection, and having air bubbles in the gel. Because the total volume was small to begin with, any change in volume was proportionally seen in the change in pressure. Therefore, the tube was also eliminated from the design, each connection was properly tightened and sealed prior to every collection, and hydrated silica gel was used instead of ultrasound gel to minimize errors caused by inconsistencies within the gel composition (especially the presence of air pockets). The bore-screw was primed with harvested nucleus pulposus from the adjacent IVDs (not used for tests) in order to minimize the hydrated silica gel from going into the IVD and reacting with water. Finally, as mentioned in the previous section, temperature was a major factor that could greatly affect the pressure reading, independent of the construction of this pressure system. In order to ensure that temperature change was not contributing to the overall trend, the temperature sensor was attached to the pressure sensor to monitor temperature throughout each collection.

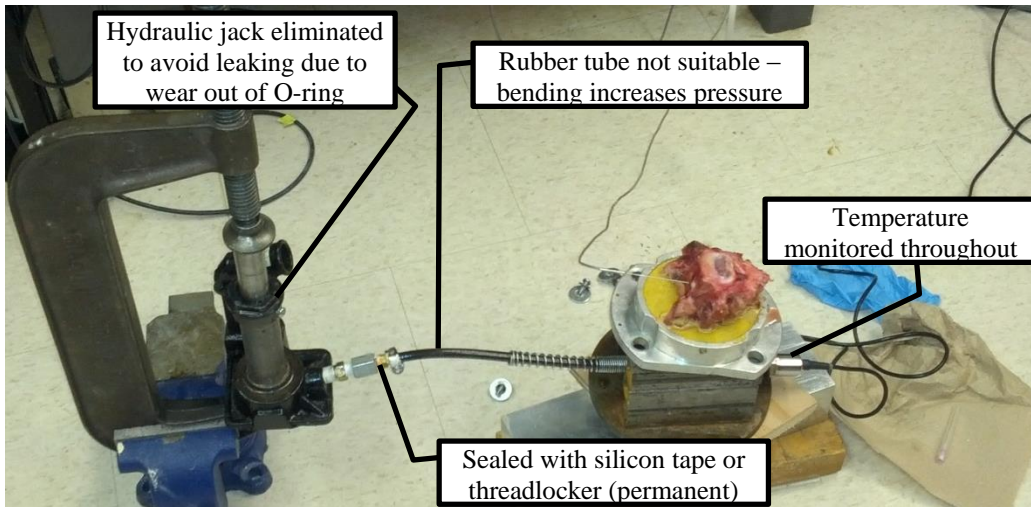


Figure 6: Prototype I: The piston cylinder device (in between the c-clamp) containing the gel connected to the injection line consisted of a hydraulic hose, bore-screw, and pressure sensor (left to right)

The most reliable design was to use a high pressure valve to isolate the volume of gel used for testing. This approach also allowed for a target pressure to be built easily with a detachable grease gun prior to mounting the specimen on the material testing system. With this design, the only possible leak site was the valve, and less than 5% difference from the baseline was seen after nine hours (Figure 7).

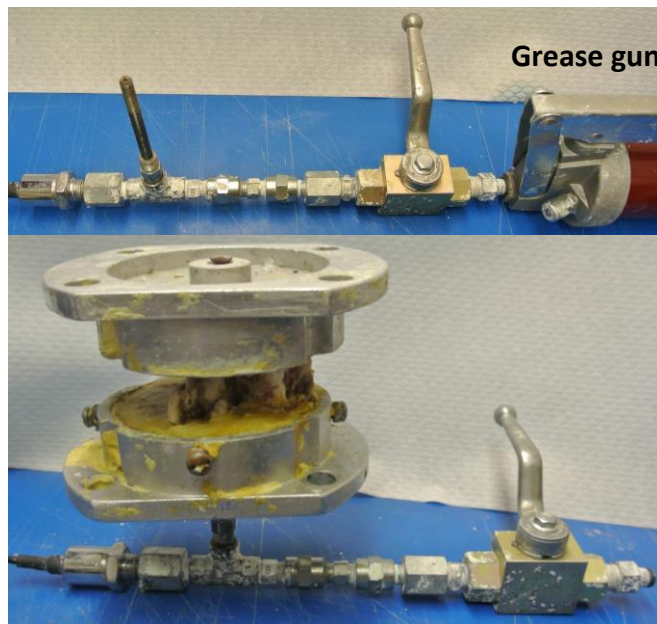


Figure 7: Final design of the bore-screw pressure sensor: before (top) and after (bottom) the system was instrumented with the specimen

3.2.2 Factors affecting the system with specimen

Unlike testing the pressure system only, the system with a specimen would not be a closed-system due to its inherent biological properties (e.g. capillaries and porous structures). The objectives for testing the bore-screw pressure sensor system inserted in a specimen were to determine whether the system with specimen could maintain pressure and its passive tissue properties, similar to that of an intact IVD. To test whether the insertion of bore-screw would compromise tissue integrity, damage to the endplate was visually examined and the passive tissue properties were tested by performing PFE tests.

3.2.2.1 Tissue integrity

Stellate endplate fracture was found to be the major cause of pressure leakage. As was shown in previous studies examining the effect of endplate fracture on intradiscal pressure (Adams et al., 1993; Adams et al., 2000), this type of fracture has caused de-pressurization in the nucleus, and this was observed within 30 minutes of the initiation of a FEC loading protocol. Drilling into the endplate did damage the semi-closed structure of the IVD; however it did not necessarily cause a stellate fracture. A stellate fracture of the endplate was typically indicated by a leakage of gel (mixture of nucleus pulposus and hydrated silica gel) from the anterior IVD (Figure 8a). A two-stage drilling method was developed, using a 1/8 inch (Dremel; Robert Bosch Tool Corporation, Mount Prospect, IL, USA) followed by a 3/16 inch (Makita, Whitby, ON) drill bits. This approach was found to be the most effective in reducing the likelihood of fracturing the endplate, with a success rate of 50%. In addition, an x-ray (Mercury Modulator X-Ray; Line adjustment 240mV; 100S; 64kV; MAV 0.05) was taken and viewed using a Kodak Direct View CR 500 (Carestream, Toronto, ON) prior to and following each collection to ensure that the tip of bore-screw was not touching the endplate of superior vertebra (Figure 8b, Figure 9b).

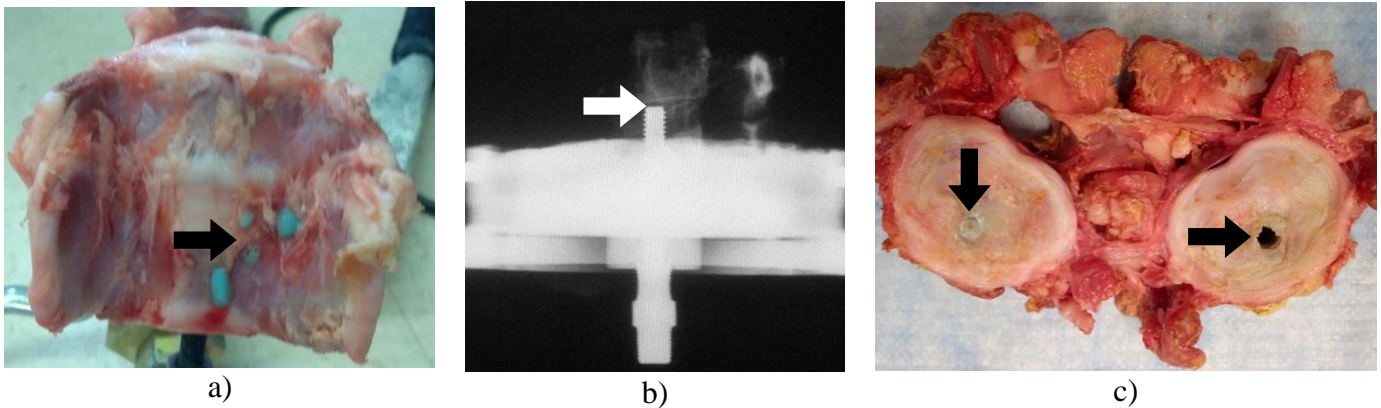


Figure 8: Unsuccessful trial: a) Leaking gel during priming (no load); b) Tip of bore-screw touching the superior endplate; c) Indent on the superior endplate (left) and inferior endplate stellate fracture (right)

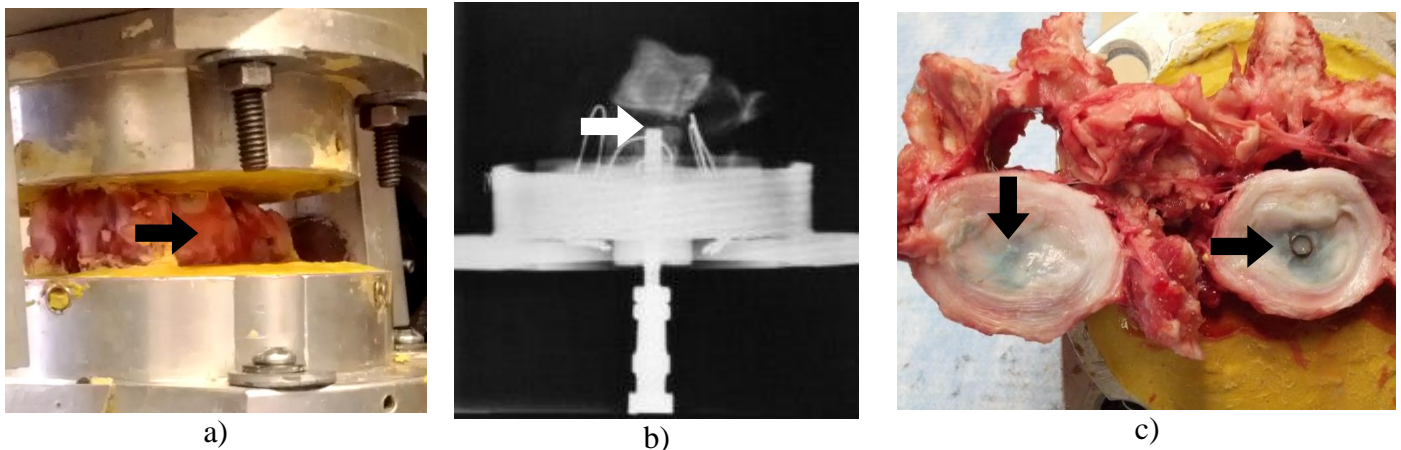


Figure 9: Successful trial: a) No leak under load (1500N); b) Tip of bore-screw well below the superior endplate; c) No indent on the superior endplate (left) and no inferior endplate stellate fracture (right)

3.2.2.2 Passive tissue properties

To ensure that passive tissue properties did not change with bore-screw insertion, PFE tests were performed as described in Section 4.2.4.2 (Table 5). The average neutral zone range without the bore-screw pressure system was 4.70 (SD 0.29) degrees and with the bore-screw pressure system inserted was 4.89 (SD 1.10) degrees, resulting in a difference of 4.04%. The FEC loading protocol as described in Section 4.2.5 was also conducted without and with the bore-screw. The change in neutral zone range was again similar in both conditions, 1.58 degrees

(without bore-screw) and 1.96 (with bore-screw) degrees. A two-way mixed ANOVA was conducted (R Development Core Team, 2013) to assess the effect of bore-screw pressure sensor instrumentation (with or without) and a repeated measure of time (pre and post). A p-value of 0.05 was used to indicate significance. No significant effect of interaction effect [$F = 0.57$, $p = 0.46$] and bore-screw pressure sensor implementation on the neutral zone range was observed [$F = 0.00$, $p = 0.96$]. There was a significant effect of time, and a post hoc analysis (Tukey HSD) revealed that a pre/post change in neutral zone with bore-screw [$F = 69.74$, $p < 0.001$] was significant. It should be noted that having small sample size may have precluded achieving significance due to variability. However, both groups (with and without the bore-screw pressure sensor system) demonstrated ranges in agreement with prior work (Noguchi et al., In press) and a similar reduction in range following the FEC loading protocol. Therefore, the passive tissue property indicated by a change in neutral zone range was not altered by the pressure sensor instrumentation.

Table 5: Neutral zone range compared with and without the bore-screw pressure sensor system

Mean (SD)	NZ range without screw N = 3	NZ range with screw N = 13
Pre (degrees)	4.57 (0.15)	4.74 (0.97)
Post (degrees)	3.16 (1.29)	2.93 (1.29)

A decrease in specimen height and an increase in peak moment were also compared between the specimens with and without bore-screw pressure sensor system. The same FEC loading protocol (Section 4.2.5) was conducted on three specimens in order to examine whether the pressure sensor interfered with changes in specimen height and moments. The results showed that there was more specimen height loss and less moment increase with specimens without the pressure sensor implemented (Table 6). However, the difference was minimal as the height loss and moment increase differed only by 0.38 mm and 0.63 Nm, respectively. Welch two-sample t-

tests were conducted (R Development Core Team, 2013) to test whether there was a significant difference between specimens with or without bore-screw. No significance was observed for both specimen height loss [$t(5.90) = 1.83, p = 0.12$] and peak moment increase [$t(6.03) = 0.61, p = 0.56$], indicating that implementation of the bore-screw pressure sensor system did not cause different passive tissue responses within the functional spinal unit.

Table 6: Specimen height loss and peak moment compared with and without bore-screw pressure sensor system

Mean (SD)	Specimens without screw N = 3	Specimens with screw N = 14
Specimen height loss (mm)	1.98 (0.27)	2.36 (0.53)
Peak moment increase (Nm)	8.13 (1.32)	8.76 (2.58)

3.3 Methodology considerations

3.3.1 Pressure estimation at 300 N (P_{300}) and 1500 N (P_{1500})

Intradiscal pressure was measured by a needle pressure sensor using intact porcine specimens. The pressure was measured at compressive loads from 0 N to 600 N. Each specimen was prepared (Section 4.2.2) and the preload was applied (Section 4.2.4.1). Under no load, a Gaeltec needle pressure sensor (8CTssh; Medical Measurements Inc., Hackensack, NJ, USA) was inserted in the mid-sagittal and transverse location from the anterior IVD towards the center of the nucleus pulposus (Figure 10). Since healthy animal and human discs have shown hydrostatic pressure in neutral posture, intradiscal pressure was expected to be the same regardless of direction (Ishihara et al., 1996; Adams et al., 1996b). The needle remained in the specimen between compressive load adjustments. A linear regression model fit to these data points ($y = 0.0016x + 0.049$) was used as a guide to set the starting pressure in each specimen (approximately 0.05 – 0.1 MPa) (Figure 11). Since all specimens came from the same source, age, gender, nutrition, and exercise level were controlled and therefore considered homogeneous.

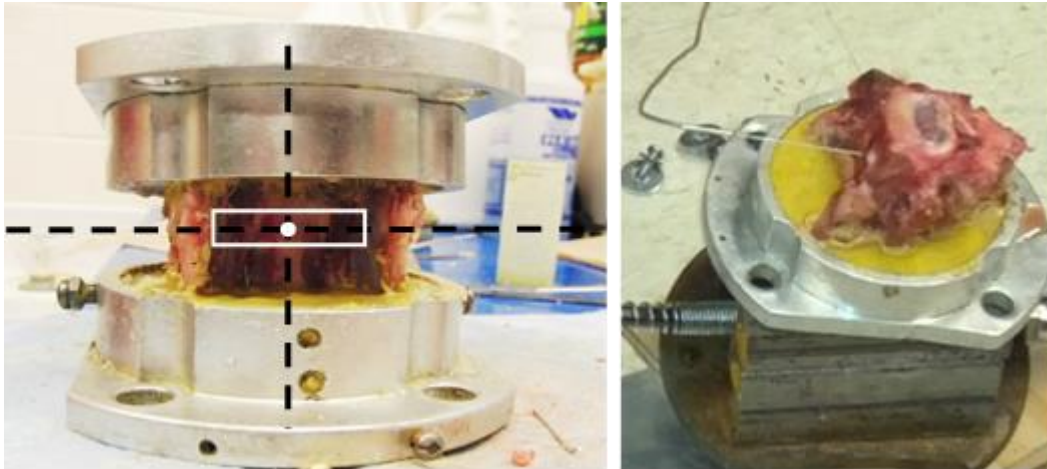


Figure 10: Needle pressure sensor insertion point (left, white dot) and the sensor inserted (right)

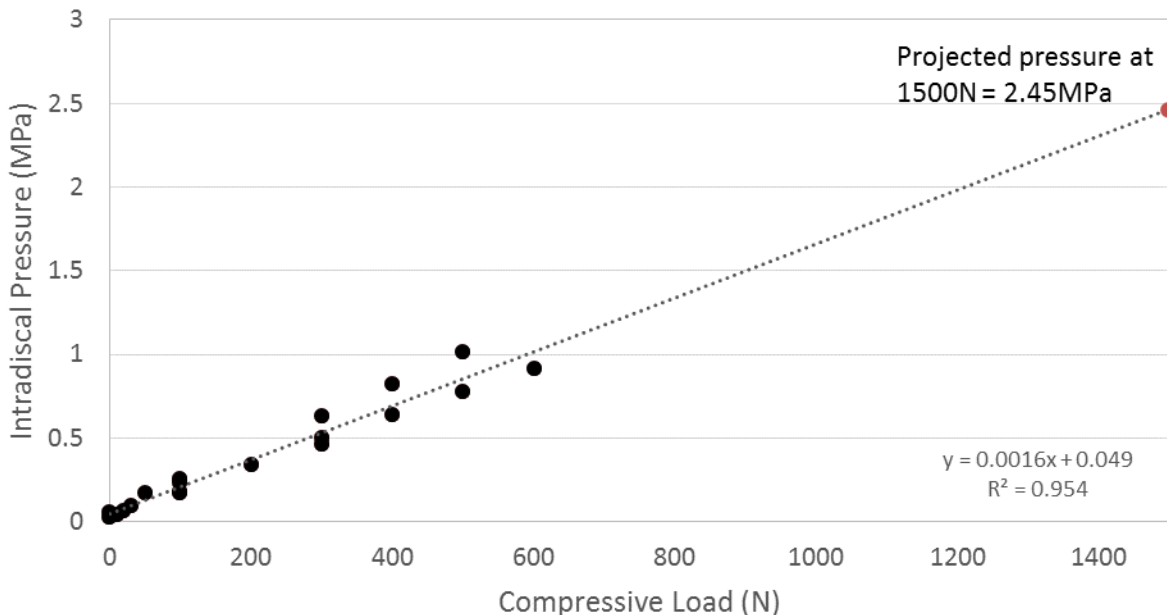


Figure 11: Pressure projection at 1500 N from various compressive loads below 600 N

The measured and projected pressure values were similar to previously reported in-vivo intradiscal pressures (Wilke et al., 1999; Sato et al., 1999; Nachemson, 1966; Nachemson and Elfstrom, 1970; Nachemson, 1981). At 300 N, the pressure was 0.53 (SD 0.09) MPa, while Wilke et al. (1999) reported that the intradiscal pressure of their participant (70kg = According to Drillis et al.'s body segment parameters, it approximately equals to 365 N H.A.T.) during quiet standing was 0.5 MPa (also similar in Sato et al., 1999). Based on the developed compression to

pressure relationship equation, at 1500 N, the intradiscal pressure was projected to reach 2.45 MPa, similarly seen in a person lifting 20 kg, bent over with round back (Wilke et al., 1999).

Average pressure values at 300 N and 1500 N prior to a FEC loading protocol were within 0.5 MPa (<20%) of the expected values. At 300 N and 1500 N, the pressure was at 0.86 (SD 0.21) MPa and 2.76 (SD 0.54) MPa, respectively. Although the pressure was higher than expected, the slope of the linear line generated from the experimental results was as expected (slope = 0.0016 MPa/N), similar to the reported value in the literature ($y = 0.081N + 0.00125$ MPa/N) (Ekstrom et al., 2004). Therefore, it was concluded that a condition similar to an intact IVD was achieved with an implementation of bore-screw pressure sensor system.

3.3.2 Duration, hydration, and dynamic (vs. static) load during a trial

According to previous studies, partial IVD herniation can occur within 3600 cycles (one hour in duration) (Drake et al., 2005; Aultman et al., 2005; Tampier et al., 2007; Yates et al., 2010). Drake et al. (2005) demonstrated that within 4000 cycles, all specimens partially herniated and approximately 55% of the porcine specimens herniated using sagittal bending motions at a frequency of 1 movement per second. Similarly, Tampier (2006) showed that partial herniation in 25% of the porcine specimens was seen after 5650 cycles (1.57 hours) on average. In addition, Yates et al. (2010) reported that noticeable disruption was seen in 82% of the porcine specimens following 7000 cycles of herniation protocol under 1472 N compressive load, and 94% of them were partially herniated. Since the purpose of the study was to observe changes in pressure until the initiation of herniation, 3600 cycles (one hour) was deemed acceptable, and it was hypothesized to cause noticeable disruption in all specimens.

The amount of dehydration during a FEC loading protocol may be difficult to monitor since it is influenced by the humidity in the testing environment (Pflaster et al., 1997) as well as the repetitive dynamic motion of the specimen, which would accelerate the fluid loss. In order to understand the effect of load-induced dehydration, tissue creep, and other potential sources of fluid loss (e.g. bore-screw insertion), a static load trial at 1500 N was conducted for an hour. There have been many studies conducted for well over one hour (Callaghan and McGill, 2001; Drake et al., 2005; Aultman et al., 2005; Tampier et al., 2007; Yates et al., 2010) and a 33% decrease in fluid weight within 30 minutes has been shown to naturally occur in intact specimen in response to a 445 N compressive load (Pflaster et al., 1997). Age-related degenerative changes that reduce water content by 20% (Adams and Hutton, 1983) cause a decrease in intradiscal pressure of 30% (Nachemson, 1981). Since 20% diurnal variation *in vivo* occurs normally within a day (Adams et al., 1990), it was assumed that pressure change of 30% during a static load trial is within an expected range due to dehydration. The results demonstrated that a loss in pressure following an hour of static compressive load at 1500 N in a neutral posture was 26.78% (N = 1), which was within the acceptable limit (Figure 13). It should be noted that when the bore-screw was not inserted properly, there was an immediate drop in pressure (Figure 12), which was easily distinguished from a successful trial.

Comparing pressure loss during a static trial to a dynamic (FEC) loading trial was another way to ensure that the motion of a specimen was causing a different response in pressure. A dynamic loading protocol consisted of applying a 1 Hz flexion-extension cycle under a 1500 N compressive load for an hour (Section 4.2.5). The mean pressure drop following a FEC loading protocol was 47.58 (SD 18.92) % (N = 14) while it was 26.78% (N = 1) for the static trial (Figure 13). FEC loading caused a much greater decrease in pressure, indicating that various

types of movement can induce different responses in pressure, which highlights the importance of my thesis work.

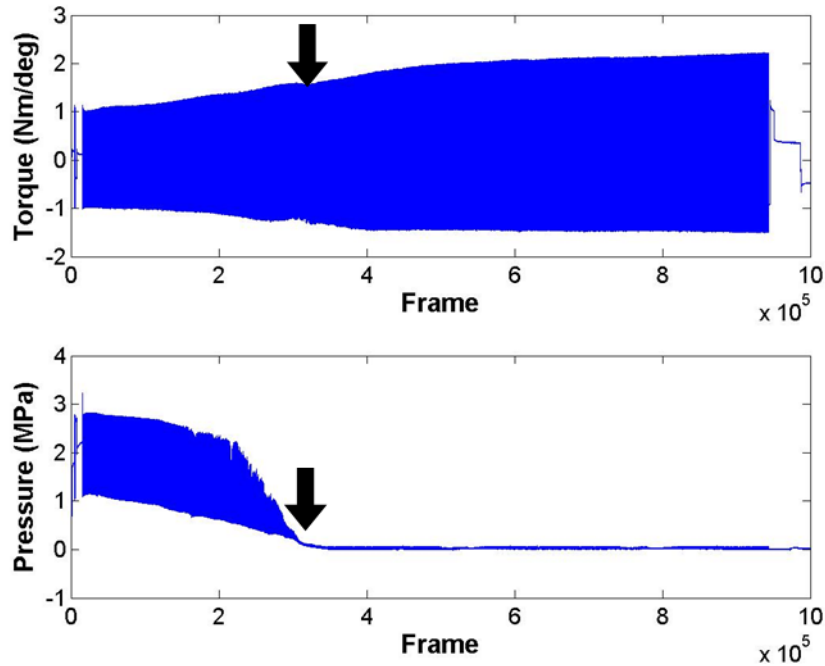


Figure 12: Example of an unsuccessful trial: black arrows indicate where the pressure dropped (bottom). Notice that there was no visible change in the moment plot where the pressure drop occurred

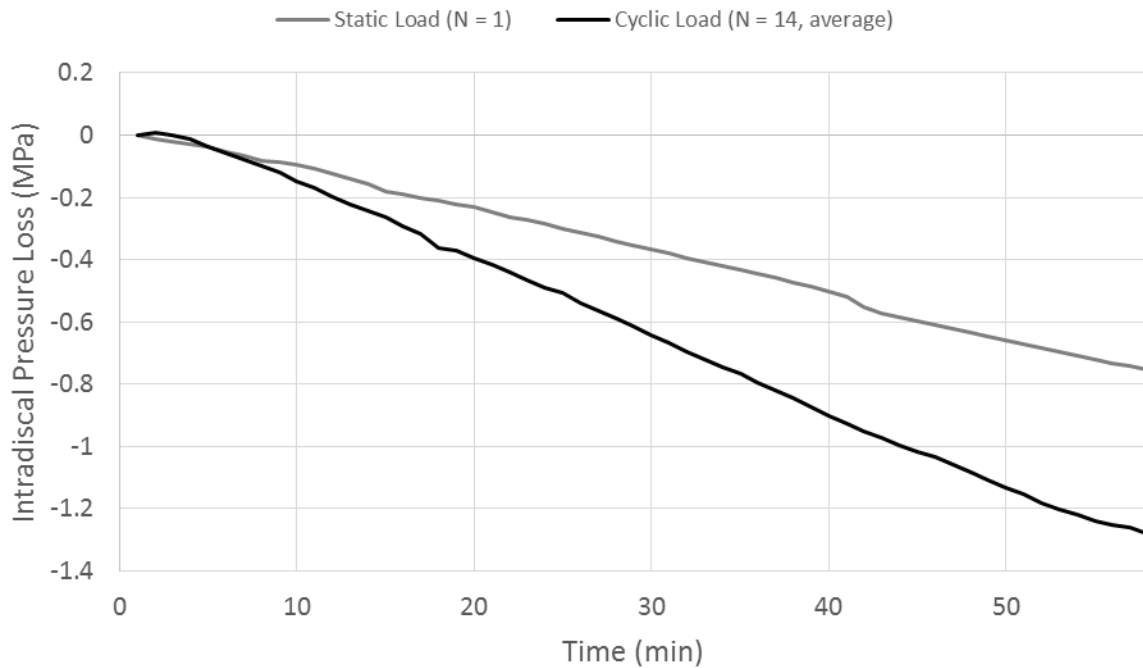


Figure 13: Pressure decline due to static loading (grey) and cyclic loading (black): there was a greater decline due to cyclic loading than static loading in one hour

3.3.3 Range of motion

The range of motion (flexion and extension limits) used in the FEC loading protocol was 400% of the neutral zone range (mean 18.30 (SD 3.76) degrees), which was comparable to the range used in previous studies (Tampier, 2006; Callaghan and McGill, 2001; Drake et al., 2005; Parkinson and Callaghan, 2009) and physiological ROM at L4/L5 joint (approximately 15 degrees) (Adams et al., 2003). The neutral zone was defined as a region of minimal passive stiffness (Section 4.2.4.3). To initiate internal disc disruption, it required specimens to go through their end range of motion (Callaghan and McGill, 2001). Some studies have used a set range of motion for every specimen (Tampier, 2006; Adams and Hutton, 1982; McNally et al., 1993; Gordon et al., 1991; Kuga and Kawabuchi, 2001; Veres et al., 2009); however, in this study, a range of motion was experimentally determined in order to account for any specimen variability. The method was deemed suitable since partial herniation was induced in 86% of the specimens using this method following the FEC loading protocol.

3.3.4 Size and level of specimen

Fourteen specimens (C34 = 5; C56 = 9) successfully completed the FEC loading protocol. In order to implement a bore-screw through an endplate, specimens needed to be skeletally matured and relatively large in size. The width and depth of the superior endplate of the inferior vertebra were 32.52 (SD 1.66) mm and 24.44 (SD 1.07) mm, respectively, indicating that they were all similar in size and therefore, the volume of IVD was assumed to be similar. It was decided *a priori* that dependent measures considered for analysis in the next chapter were collapsed across cervical levels, similar to previous *in vitro* studies using the same animal model employed in this study (Parkinson and Callaghan, 2009; Gooyers et al., 2012; Howarth et al., 2013). There was

no apparent difference observed when all plots were visually inspected, and no significance was observed [$t(10.23) = -1.32, p = 0.21$] when a Welch two-sample t-test was conducted (R Development Core Team, 2013) for an average pressure change comparison between C34 (Mean = 1.09, SD = 0.42) and C56 (Mean = 1.32, SD = 0.53).

3.3.5 Pressure change during flexion extension cyclic (FEC) loading protocol

Although the temperature was shown to have an effect on the pressure measurements (Section 3.2.1.2), there were several challenges associated with temperature correction. First, even though there was a high correlation ($r > 0.95$) between temperature and pressure, it was not a perfect correlation in order to confidently use the correction equation for the duration of the FEC loading protocol. In addition, there was a time lag between the temperature and the pressure changes, indicating that simple linear correction would potentially create a greater error. Therefore, to avoid over-correction of the pressure data, temperature correction was not performed on the intradiscal pressure data collected during a FEC loading protocol. However, the temperature was monitored throughout each protocol in order to characterize the error value that may have occurred in the pressure measurements due to temperature change. The data were averaged over five minutes (Figure 14), and the difference between maximum and minimum temperature was identified for each trial. The difference between maximum (V_{max}) and minimum (V_{min}) temperature was then used to estimate the largest error that could have occurred in pressure measurement:

$$\Delta P_{temp} = (V_{max} - V_{min}) \times 5^{\circ}\text{C}/V \times 0.145\text{MPa}/^{\circ}\text{C}$$

Equation 2: Calculating pressure change due to temperature

where $5^{\circ}\text{C}/\text{V}$ was a conversion factor used by the temperature sensor and another conversion factor, $0.145 \text{ MPa}/^{\circ}\text{C}$ was experimentally derived in the previous section (Section 3.2.1.2).

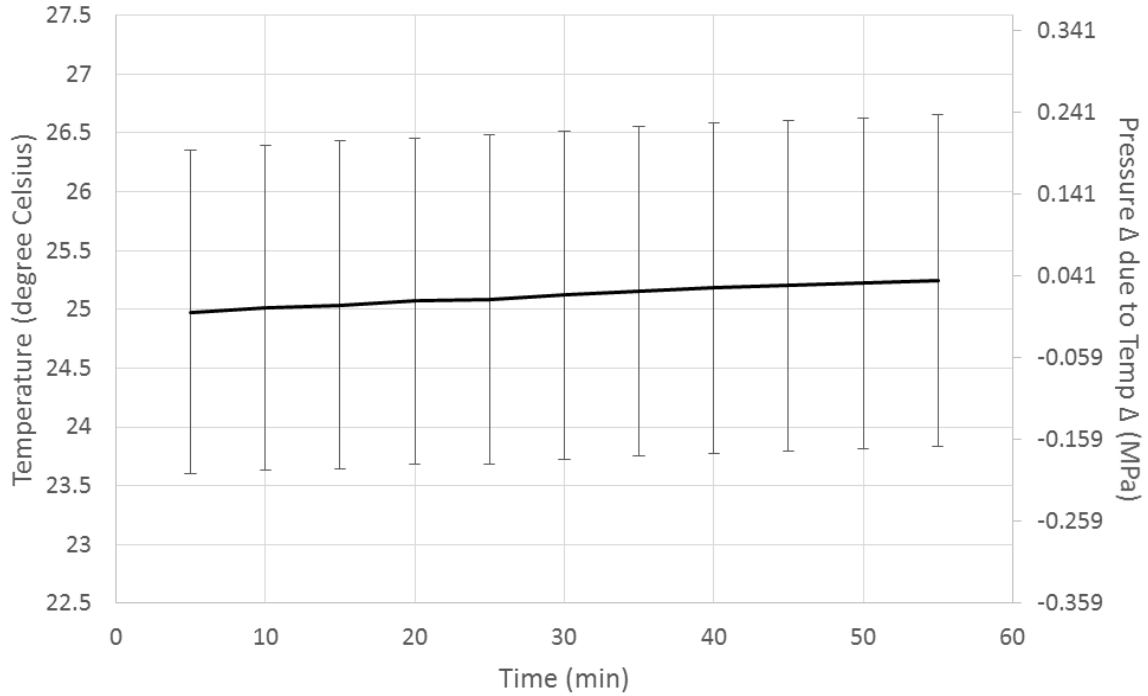


Figure 14: Pressure change associated with temperature change in one hour during a FEC loading protocol (secondary axis on the left is scaled to the conversion factor of $0.145 \text{ MPa}/^{\circ}\text{C}$)

The results showed that the maximum and minimum pressure difference during a loading protocol was 0.05 (SD 0.04) MPa on average. Since the mean pressure at 1500 N was 2.76 (SD 0.54) MPa, a fluctuation in pressure due to temperature was only 1.81% . The largest temperature difference observed among 14 specimens was 0.99°C , which was equivalent of 5.22% (0.14 MPa) error. Therefore, the effect of temperature on pressure was deemed minimal, and hence no correction was made to the pressure data in the next chapter.

3.4 Comparison to the gold standard

The goal of the validation study was to compare the pressure readings from the bore-screw pressure sensor to the gold standard (needle pressure sensor) in order to characterize its accuracy and reliability. In this study, a specimen was prepared with the bore-screw pressure system (Section 4.2.1 – 4.2.4) and the Gaeltec needle pressure sensor (8CTssh; Medical Measurements Inc., Hackensack, NJ, USA) was inserted from the anterior IVD (Table 7, Figure 10) in order to collect data simultaneously.

Table 7: Specifications of the Gaeltec needle pressure sensor

	Specifications
Range	0 to 2.0 MPa
Sensitivity	0.0036 MPa/mV

3.4.1 Stepwise response

In this test, the specimen was mounted on a servo-hydraulic materials testing system (8872, Instron, Canton, MA), and compressive loads of 0, 100, 200, 300, 400, and 500 N were applied in increasing order. A 100 N trial was repeated following the 500 N compressive load trial, in order to determine its repeatability. During each trial, pressure was collected from both sensors at 32Hz using the NIAD program. Collected data were low-pass filtered at 3 Hz using a Butterworth filter (dual pass; 4th order) and averaged over 5 seconds at each compressive load. The difference between the bore-screw and the needle pressure sensor was expressed as absolute and relative differences. Cross-correlation was conducted to determine a lag time and a correlation coefficient (r_{xy} in Equation 3).

$$r_{xy}(\tau) = \frac{1}{n} \int_0^n x(t)y(t + \tau)dt$$

Equation 3: Cross-correlation

where τ denotes time lag, t is the frame number or time, n is the total frame number, x is the bore-screw pressure values, and y is the needle pressure values.

The results of static trials demonstrated that at each compressive load, differences between the bore-screw and needle pressure sensor readings were less than 0.10 MPa (Figure 15, Table 8). Both sensors demonstrated linear increases in pressure and therefore the difference also increased as the compressive load increased. At lower compressive load (< 400 N), the difference was less than 5%; however, when extrapolated to a 1500N compressive load, it was estimated to be 8.60%. A repeated measurement taken at 100 N showed a difference of 6.14% (0.03 MPa). Cross-correlation demonstrated that there was no lag time between needle and bore-screw pressure sensor measurements ($\tau = 0$). Correlation between these two sensors was also excellent as it demonstrated $r > 0.99$.

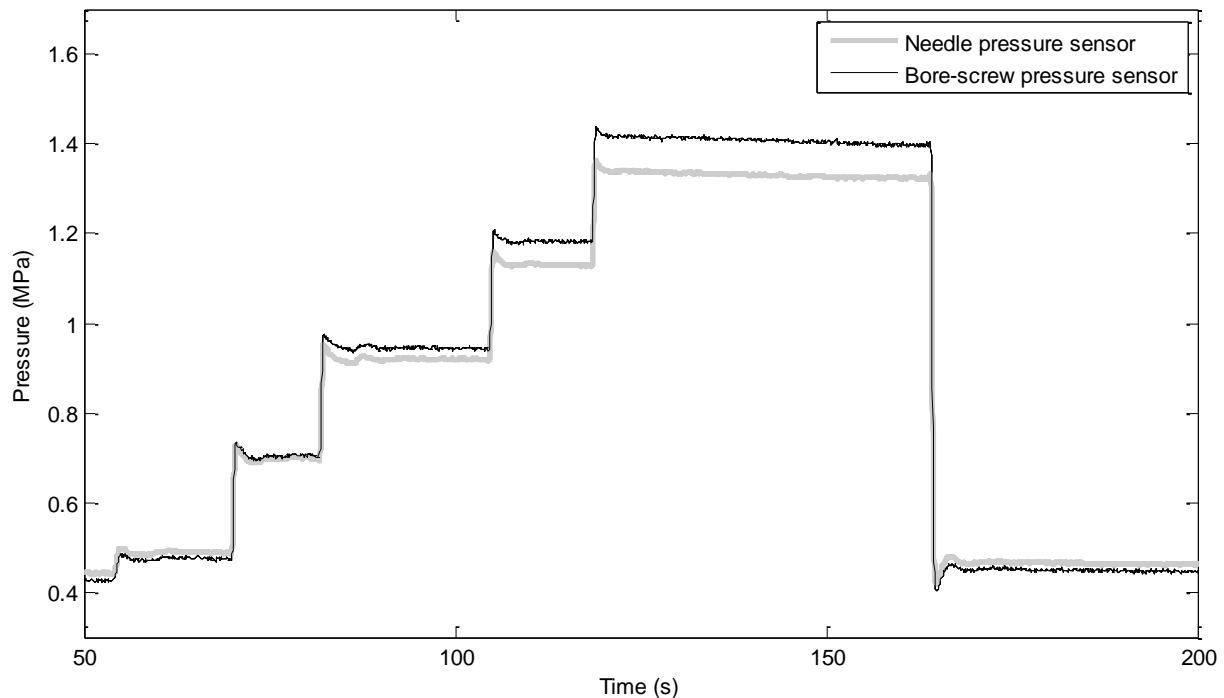


Figure 15: Static step-wise tests for determining accuracy and reliability of the bore-screw pressure sensor compared to the needle pressure sensor

Table 8: Step-wise test results comparing pressure values from bore-screw and needle pressure sensors

Compressive load (N)	100	200	300	400	500	100 Repeated	1500 Projected
Needle mean pressure (MPa) (SD)	0.49 (0.0011)	0.70 (0.0012)	0.92 (0.0011)	1.13 (0.0011)	1.32 (0.0012)	0.47 (0.012)	3.43
Bore-screw mean pressure (MPa) (SD)	0.48 (0.0023)	0.70 (0.0028)	0.94 (0.0022)	1.18 (0.0022)	1.40 (0.0026)	0.45 (0.013)	3.73
Absolute difference (MPa)	-0.01	0.01	0.02	0.05	0.07	-0.02	0.30
Relative difference (%)	-2.82	0.84	2.58	4.66	5.55	-3.77	8.60

3.4.2 Dynamic response

To evaluate a higher frequency response simulating a 1 Hz testing protocol, the specimen was flexed and extended manually. The compressive load during a dynamic trial was not conducted using a material testing system in order to avoid mechanical failure of the needle pressure sensor. During the trial, pressure was collected from both sensors at 32Hz using the NIAD program. Collected data were low pass filtered at 3 Hz using a Butterworth filter (dual pass; 4th order). Cross-correlation was conducted to determine a lag time and a correlation coefficient (Equation 3). Root-mean square error (RMSE) (Equation 4) and maximum absolute difference were also calculated to estimate the magnitude of the error.

$$RMSE \text{ (MPa)} = \sqrt{\frac{1}{n} \sum_{t=1}^n (x_t - y_t)^2}$$

Equation 4: Root-mean square error

where x_t is the bore-screw pressure values (observed), y_t is the needle pressure values (predicted), t is the frame number or time, and n is the number of frames used to compare observed and predicted values.

The dynamic test results demonstrated that pressure measurements from the needle and bore-screw pressure sensors were highly correlated ($r > 0.99$) without any lag time ($\tau = 0$) (Figure 16). The maximum difference seen at a peak (+0.023 MPa) and the RMSE (0.007 MPa) were both minimal. Therefore, the bore-screw pressure sensor system has a good dynamic response and was deemed acceptable to use as a replacement of needle pressure sensor.

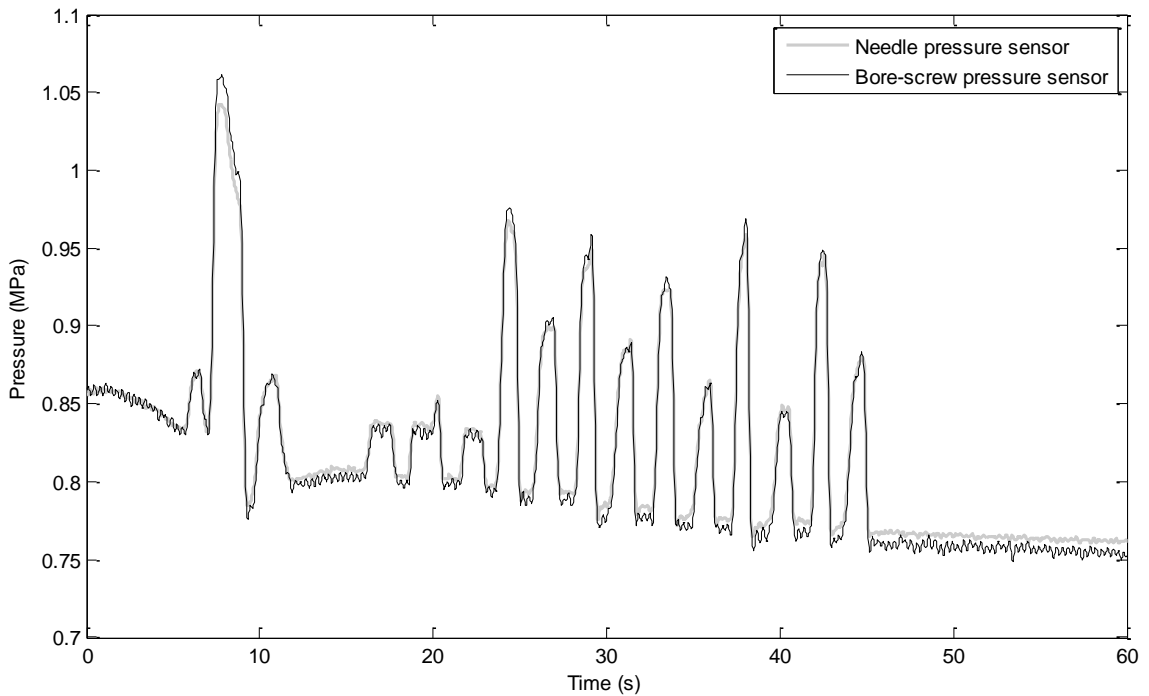


Figure 16: Dynamic test for determining accuracy and dynamic response of the bore-screw pressure sensor compared to the needle pressure sensor

3.5 Validation study summary

The following figure (Figure 17) indicates the steps taken to ensure that instrumentation error was minimized and characterized for interpreting the pressure measurements from the bore-screw pressure sensor system appropriately:

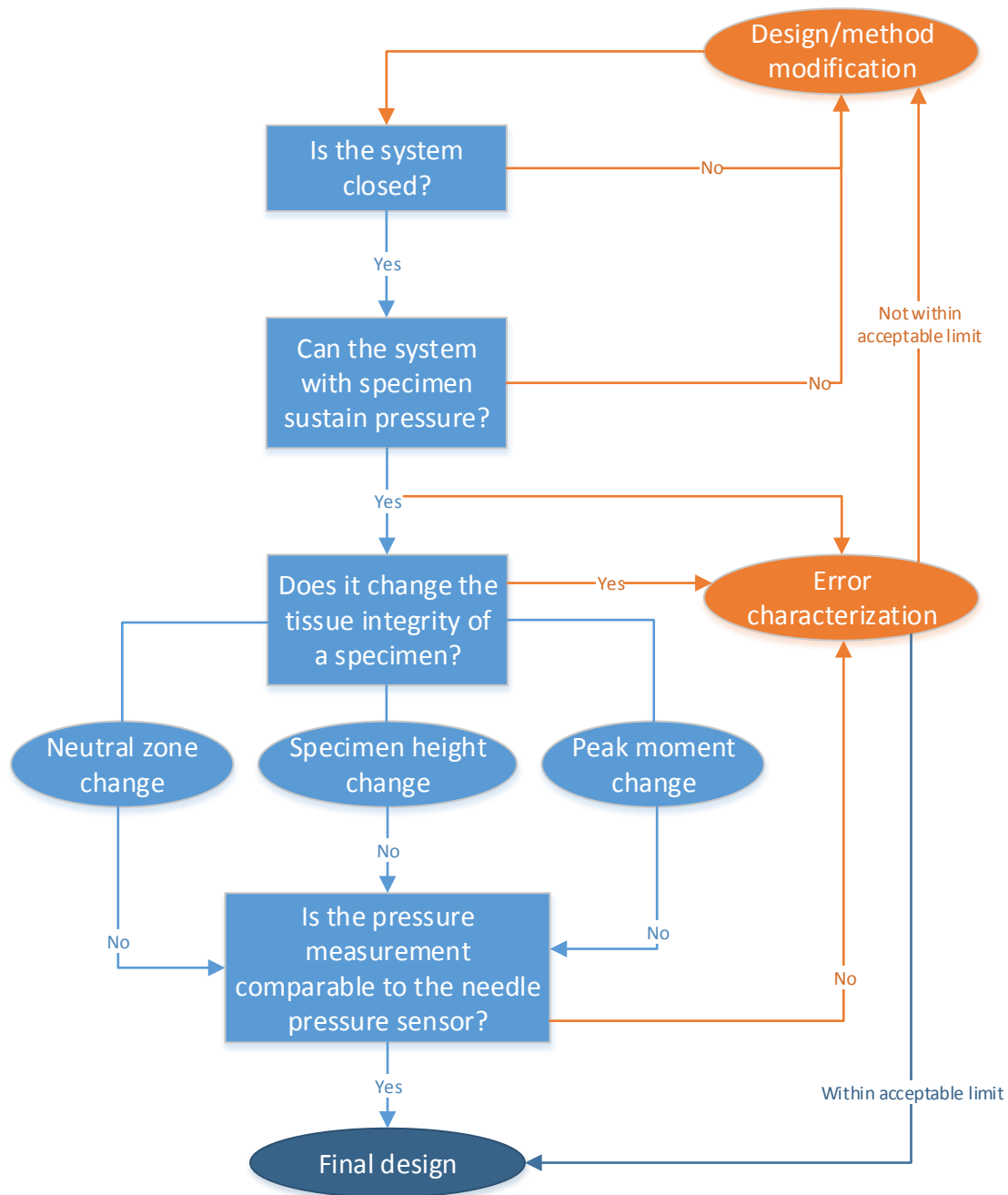


Figure 17: A flowchart indicating the decisions made during this validation study

- A leak test simulating the testing condition demonstrated a 0.15% decrease in pressure over nine hours.
- Temperature should be controlled and monitored closely during a trial in order to avoid temperature induced pressure change.
- Implementing the bore-screw pressure sensor system did not change specimen's neutral zone range (pre and post), height loss, and peak moment increase following the FEC loading protocol compared to those results of intact specimens.
- Step-wise and dynamic responses of the bore-screw pressure sensor system were comparable to the needle pressure sensor, as the maximum error projected at 1500 N was 0.30 MPa (< 10% error).
- Bore-screw pressure sensor system can be used as a replacement of needle pressure sensor when implemented successfully.

3.6 Successful trial / FEC loading protocol criteria

FEC loading protocol parameters such as duration, hydration, cyclic motion used, pressure at specific compressive loads, range of motion, and specimen choice were justifiable (Section 3.3).

Based on the validation study, the following criteria were set for conducting a FEC loading protocol:

3.6.1 Preparation

Pressure was checked at three key points during instrumentation to ensure that the bore-screw pressure sensor system was implemented successfully:

a. Initial pressure

Initial pressure, prior to mounting the specimen on to the material testing system, was set to approximately 0.15 MPa. Although it was slightly higher than the resting (0 N) pressure value, it was raised above 0.10 MPa to test whether the bore-screw pressure sensor was implemented properly. When there was a stellate fracture, the pressure either declined rapidly past 0.10 MPa or the hydrated silica gel (blue colour) was visibly seen to leak out from an anterior disc and vertebrae (Figure 8a). If the specimen was unable to maintain the pressure at this initial stage, it was considered a failed trial.

b. Pressure during preload and PFE

In a successful trial, the intradiscal pressure was above 0.50 MPa during preload and PFE tests (300 N compressive load applied). When the bore-screw pressure sensor was not implemented properly, a rapid drop in pressure occurred, and there was no fluctuation in pressure when a specimen went through a range of flexion/extension postures during PFE tests. When the pressure remained constant during the PFE test, with no pressure fluctuations, it was typically due to vertebral bones clogging the tip of the bore-screw, and it was considered a failed trial.

c. Pressure at 1500 N

When the target dynamic test compression load of 1500N was applied, the pressure linearly increased from the pressure value at 300 N. When the bore-screw pressure sensor was not implemented properly, a rapid drop in pressure occurred, and a hydrated silica gel leak was visibly seen.

3.6.2 Duration

Pressure was monitored over time during a FEC loading protocol. The trial was terminated when pressure was not maintained for the duration of the protocol (one hour; 3600 cycles), for example when there was a sudden loss of pressure (Figure 12). This drop typically happened when there was a stellate fracture from inserting the bore-screw. In this case, leaking did not happen rapidly; however, it eventually led to a complete loss of pressure well before the end of the protocol. The data were not used for analysis if the pressure reached zero before the 3600th cycle.

3.6.3 Post-test inspection

Endplate fracture of the inferior vertebra was identified before the end of the protocol; however, a few specimens have shown damage to the endplate of the superior vertebra, which was discovered during post-protocol inspection (on x-ray or during dissection). If there was damage, or an indent, to the superior vertebra caused by the tip of bore-screw (Figure 8c), the data were not used for analysis.

Should any one of the criteria failed, a trial was terminated and the data were excluded from the analysis.

Chapter 4

Part II: Intradiscal Pressure Study

4.1 Introduction

4.1.1 Background

Discogenic low back pain (LBP), defined as pain originating from the intervertebral disc, is one of the most common, yet difficult, conditions to diagnose, since contributions from external (i.e. mechanical exposure), internal (i.e. biologic cell-mediated exposure), and intrinsic (e.g. age, anatomical structures) factors are often intertwined. It is suggested that 80% of the population will experience LBP at least once in their lifetime (Hadler et al. 1986), and approximately 40% of LBP cases may be related to internal disc disruption (Schwarzer et al. 1995; Dammers et al., 2002; DePalma et al., 2011). Internal disc disruption is characterized by damage to the internal structure of the intervertebral disc (IVD) and is the precursor to herniation and other degenerative disc diseases (Bogduk and Twomey, 1997; Adams et al., 2003). LBP due to internal disc disruption is significantly more prevalent in a younger population (aged between 41 and 46 year olds), where the majority of the workforce population lies (Human Resources and Skills Development Canada, 2013; DePalma et al., 2011). Therefore, understanding the mechanism that initiates internal disc disruption may be the key to minimizing the risk of chronic LBP through early detection and intervention.

Patients with LBP have demonstrated high annular stress profiles on discography, indicating that the initial degenerative change may be observed in the intradiscal pressure (McNally et al., 1996; Ito et al. 1998). This stress profile has been suggested to occur due to a

decrease in intradiscal pressure, which would lead to inward collapse or buckling of the inner annulus, causing increased radial strain on the outer annulus (Adams et al., 2003; McNally et al., 1996); Tanaka et al., 1993; Adams et al., 1993; Adams et al., 2000). A decrease in pressure may occur as a result of degenerated discs (Nachemson, 1981; Adams et al., 1996b) or discs with pre-existing endplate damage (Adams et al., 1996b; Adams et al., 1993; Adams et al., 2000; Holm et al., 2004). Inward collapse of lamella has been seen as a common feature in elderly discs on post-mortem dissection (Tanaka et al., 1993; Gunzburg et al., 1992); however, the mechanism that initiates this internal disc disruption has not been clearly identified. Hence, there is a need to characterize intradiscal pressure changes over time during a protocol known to induce internal disc disruption. The following dependent variables were monitored: intradiscal pressure, flexion/extension moments, axial deformation (specimen height loss), and angular displacement (flexion/extension).

4.1.2 Purposes and hypotheses

There were three specific purposes of this study: 1) to determine if previously examined variables such as moments and axial deformation were correlated to intradiscal pressure, 2) to characterize changes in intradiscal pressure, moments, axial deformation, and angular displacement over time, and 3) to examine if the injury types observed during morphology observation were correlated to the pre and post difference in neutral zone range and cycle average intradiscal pressure, moment, and axial deformation. The following hypotheses were made for each purpose:

1. The intradiscal pressure would negatively correlate to moments and positively correlate to axial deformation. There has been evidence demonstrating the relationship between

intradiscal pressure and disc height (Adams et al., 1996a; Tanaka et al., 1993) and postures (Sato et al., 1999; Wilke et al., 1999, Adams et al., 2000; Nachemson, 1981). Since a change in posture involves a change in the moment applied to the spine and deformation of the IVD, it was hypothesized that a correlation between pressure and those variables would exist over time.

2. There would be a significant change in the following variables over time:
 - a. Intradiscal pressure would decrease as the fluid content leaked out of the IVD and disruption initiated. The fluid content has been shown to decrease under compressive loading (Pflaster et al., 1997; Adams and Hutton, 1983; Adams et al., 1990; Adams et al., 1993; Adams et al., 1996a) and with degeneration (Sato et al., 1999; Adams et al., 1993).
 - b. Moments would increase over time. Moments at a given angular displacement have been shown to increase over time as the stiffness of the specimen increases (Gordon et al., 1991; Callaghan and McGill, 2001; Drake et al., 2005; Adams et al., 1990). Therefore, it was hypothesized that moments would increase significantly over time given a set range of motion.
 - c. Axial deformation would increase (specimen height would decrease) over time. The specimen height was expected to decrease due to loss of fluid content and tissue deformation (Callaghan and McGill, 2001; Adams et al., 1996a; Zhao et al., 2005).
 - d. Angular displacement at maximum pressure would change over time. Changes would occur in viscoelastic tissues as a result of cyclic loading on the specimen. Since there is evidence that increased compressive loading shifts the center of

rotation more towards flexion due to facet joint contact (Noguchi et al., In press), the angle where maximum pressure occurs was expected to change anteriorly.

3. The primary mode of failure was expected to be partial disruption of the inner annulus fibrosus in the posterior or posterolateral region (Callaghan and McGill, 2001; Aultman et al., 2005; Tampier et al., 2007; Drake et al., 2005; Yates et al., 2010; Adams et al., 2000; Tanaka et al., 1993). Injury types would be correlated to the intradiscal pressure change since painful discs (abnormal stress concentration in posterolateral annulus) have been shown to have a lower mean intradiscal pressure *in vivo* (McNally et al., 1996). Although neutral zone, moment, and axial deformation have been shown to change as the discs degenerate, those variables have not been able to predict the progression of tissue damage (Callaghan and McGill, 2001; Tampier, 2006). Therefore, those variables were not hypothesized to correlate with injury types.

4.1.3 Importance and implications

Intradiscal pressure change over time in healthy discs has never been reported in the published literature. These observed changes may narrow down the factors that may be contributing to the initiation of degenerative disruptions involved in IVD disruption and eventual herniation. In addition, they may provide additional evidence as to why it is difficult to detect the initiation of disc injury using medical images only. Utilizing the data from this study, we would be able to understand the direction for preventative (e.g. work guideline) and regenerative (e.g. restoring 'normal' pressure) strategies to reduce LBP prevalence.

4.2 Methods

Fourteen porcine cervical FSUs (mean age = 6 months; five C3-C4 and nine C5-C6), each consisting of two adjacent vertebrae and the intervening IVD, were used in this study.

4.2.1 Bore-screw pressure sensor system preparation

The pressure system consisted of a grease gun (395721; Grease Gun 3-Way Load) filled with hydrated silica gel (Veres et al., 2009), a high pressure valve (1/4 in. NPT 2-Way High Pressure Ball Valve), a steel screw (65 x 6.2mm with an internal bore of 3.0mm), and a pressure sensor (Fluke PV350, Fluke, Everett, WA, USA). A high pressure valve was connected to the pressure sensor using a T-joint, and these connections were sealed using a permanent threadlocker (Permatex, CT, USA). This portion was primed with hydrated silica gel using a grease gun.

However, a steel screw and a grease gun were not permanently affixed since the steel screw must be primed with nucleus pulposus and inserted into the specimen first and the grease gun must be detached from the pressure system prior to mounting the specimen on the material testing jig. A steel screw was filled with nucleus pulposus collected from adjacent IVDs (C23 and C67), using an 18 gauge syringe without a needle.

4.2.2 Specimen preparation and bore-screw insertion

The specimens were obtained immediately after death and stored at -20°C. Prior to testing, frozen specimens were thawed at room temperature for approximately 12 hours. All FSUs used in this investigation met a non-degenerated disc quality (Grade 1) as outlined by Galante (1967). Excess muscles and osteoligaments were removed from each specimen. The specimens were misted with a 0.9% saline solution in order to avoid dehydration during the experiment.

Prior to potting the specimen in the custom machined aluminum cups, a pilot hole was drilled longitudinally from the approximate center of the inferior vertebra. A two-stage drilling technique was used to minimize damage to the superior endplate of the inferior vertebra. Initially, the specimen was drilled using a 1/8 inch drill bit (Dremel; Robert Bosch Tool Corporation, Mount Prospect, IL, USA) followed by a 3/16 inch drill bit (Makita, Whitby, ON) using a battery operated hand drill (6281 DWPE; Makita, Whitby, ON). Drilling was stopped immediately after resistance from the endplate was perceived. A steel screw filled with nucleus pulposus was passed through one of the aluminum cups and was inserted along the same trajectory as the pilot hole until just above the endplate adjacent to the inferior vertebra. An x-ray (Mercury Modulator X-Ray; Line adjustment 240mV; 100S; 64kV; MAV 0.05) was taken and viewed using a Kodak Direct View CR 500 (Carestream, Toronto, ON) to ensure proper placement of the steel screw (Figure 18). The superior vertebra was fixed in the aluminum cups using a wood screw inserted into the centre of the cranial endplate of the superior vertebra. Non-exothermic dental stone (Denstone®, Miles, South Bend, IN, USA) was used to ensure fixation of the superior and inferior vertebrae in their respective aluminum cups. Once the dental stone set, the specimen in the aluminum cup was properly secured to the rest of bore-screw pressure sensor using a T-joint.

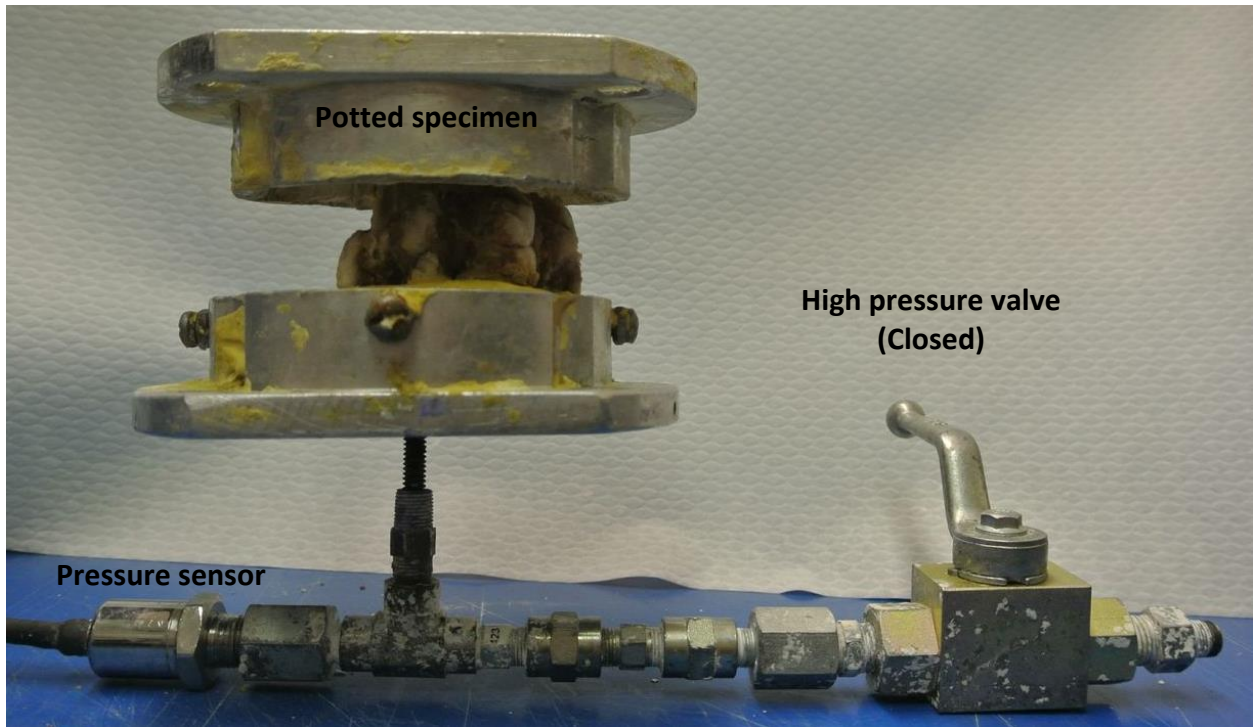
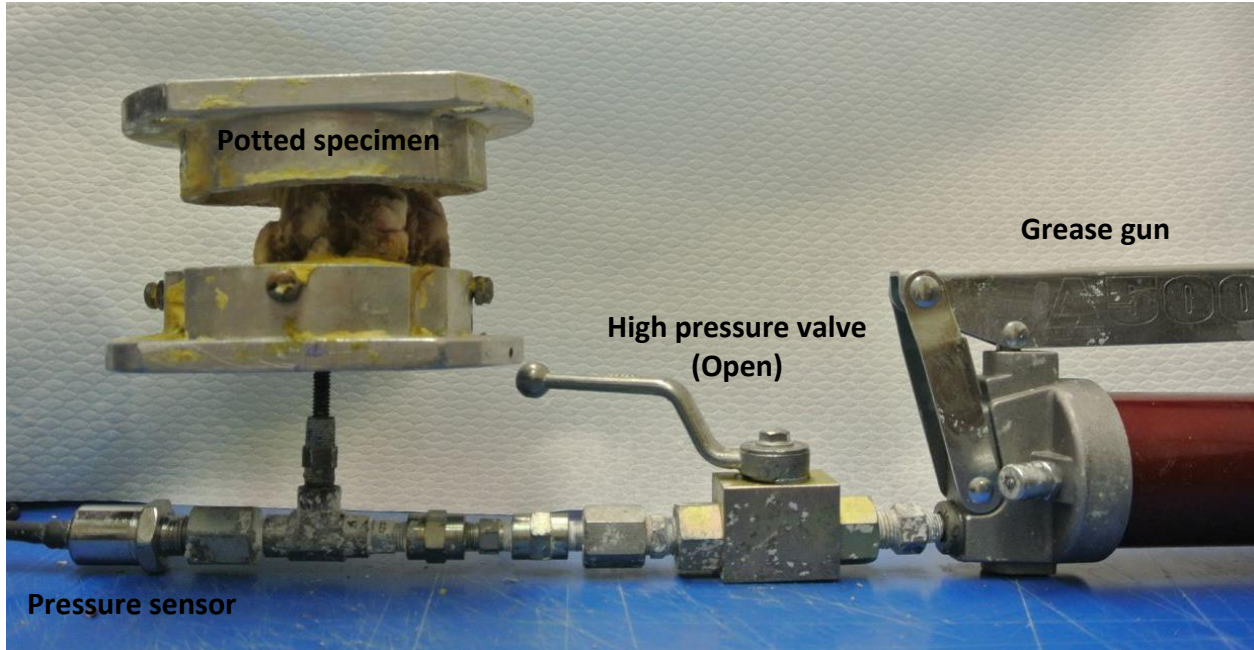


Figure 18: Potted specimen with the bore-screw pressure sensor system when the baseline pressure was set with a grease gun filled with gel (top) and when the high pressure valve was closed to create a closed system for testing (bottom)

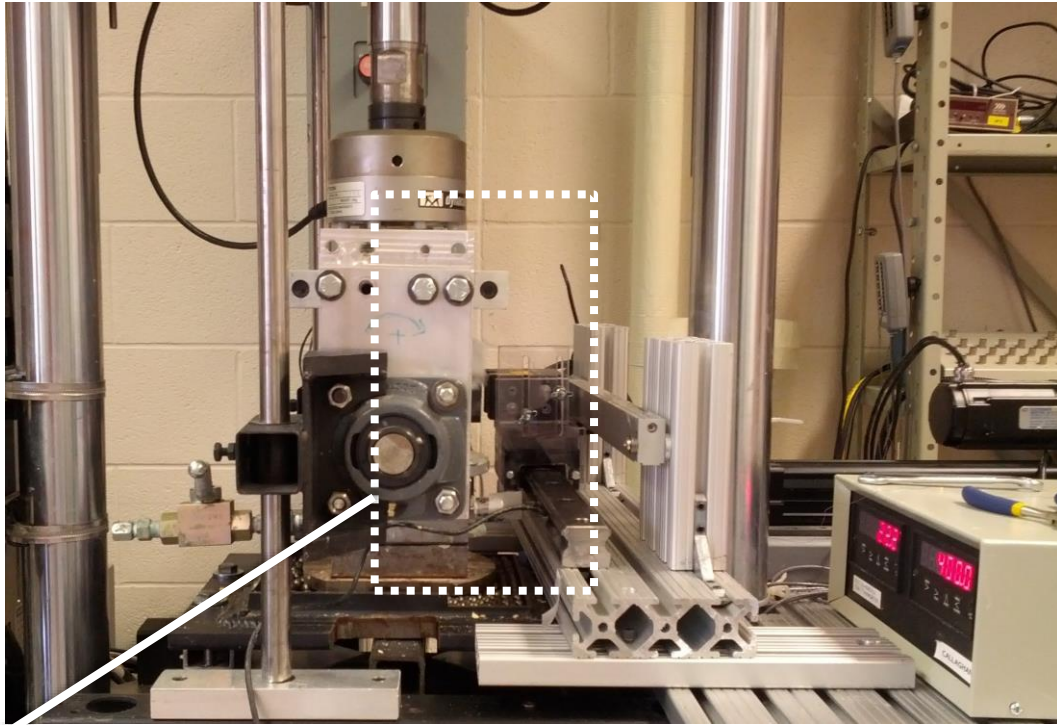


Figure 19: Specimen with the bore-screw pressure sensor system in the material testing system (top). Each specimen was mounted on a raised platform to provide clearance for the pressure sensor system at the bottom (bottom two pictures)

4.2.3 Baseline pressure setting

Prior to mounting the specimen onto the material testing jig, the pressure was set at approximately 0.15 MPa. The grease gun was used to increase the pressure, and once the desired pressure was reached, the high pressure valve was closed (Figure 18). The pressure was monitored throughout the protocol to ensure that damage to the endplate did not cause sudden pressure drop. The trial was deemed unsuccessful when a pressure drop was observed immediately after the valve was closed. The grease gun was detached from the pressure sensor system before the specimen conditioning procedures.

4.2.4 Specimen conditioning procedures

Specimen conditioning procedures consisted of applying a preload, performing a passive flexion extension test, and defining flexion and extension limits (Figure 19).

4.2.4.1 Preload

The purpose of the preload phase was to reduce the post-mortem swelling of the intervertebral disc. During this test, a 300 N static compressive load was applied for 15 minutes using a servo-hydraulic materials testing system (8872, Instron, Canton, MA), where the potted specimen was mounted to simulate physiological loading. During this preload phase, a zero-moment position (an angular position with minimal resistive moment) was established as the FSU's neutral position, using an independent servomotor (AKM23D; Danaher Motion, Radford, VA, USA) connected in series with a torque cell (T120-106-1K; SensorData Technologies Inc., Sterling Heights, MI, USA) (Callaghan and McGill, 2001; Tampier, 2006; Aultman et al., 2005; Drake et al., 2005).

4.2.4.2 Passive flexion extension (PFE) test

A range of motion (ROM) PFE test was performed to measure moment at given angular displacement. In each test, a 300 N compressive load was applied and three cycles of PFE tests were completed at a rate of 0.5 degrees per second (Callaghan and McGill, 2001; Tampier, 2006; Aultman et al., 2005; Drake et al., 2005; Adams et al., 1996a; Adams et al., 2000). The applied moment (Nm) and angular displacement (degrees) were sampled at 15 Hz using a custom software program (University of Waterloo). The direction of loading was reversed when the moment reached ± 6 Nm from the baseline value.

4.2.4.3 Determining flexion and extension limits from the neutral zone

From the graphs obtained from the PFE test, flexion and extension limits used for the subsequent protocol (flexion extension cyclic loading protocol) were determined. Neutral zone, defined as the region of minimal passive stiffness (Panjabi 1992), was used to standardize the testing posture of functional spinal units (FSU) for in-vitro biomechanical studies. Flexion and extension limits were defined using the 400% of neutral zone boundary angles. To determine the neutral zone, the last two cycles from the PFE test were used. A fourth order polynomial curve was fitted to the data points, and the neutral zone was defined using the range between ± 0.05 Nm per degree of the first derivative of the fitted curve (Thompson et al., 2003). The neutral angle was defined as the midpoint of the neutral zone range. The flexion and extension limits were calculated by multiplying the difference between the midpoint and each end of neutral zone range by four:

$$Limits \text{ (deg)} = Neutral \text{ angle} \pm \left[4 \times \frac{(NZ \text{ upper limit} - NZ \text{ lower limit})}{2} \right]$$

Equation 5: Range of motion for the flexion extension cyclic loading protocol

4.2.5 Flexion extension cyclic (FEC) loading protocol

The FEC loading protocol consisted of applying a 1500 N compressive load in conjunction with flexion extension movement in angular position control at a rate of 45 degrees per second. The specimen moved through the range of motion defined in the previous section (Section 4.2.4.3). The specimen was cyclically loaded at 1 Hz for an hour (3,600 cycles) using an independent servomotor (AKM23D; Danaher Motion, Radford, VA, USA) connected in series with a torque cell (T120-106-1K; SensorData Technologies Inc., Sterling Heights, MI, USA). The servomotor was controlled using custom software (University of Waterloo), which was interfaced with an ISA bus motion controller (DMC 1701, Galil Motion Control, Mountain View, CA, USA). The angular displacement was measured by an optical encoder attached to the motor shaft (LDA-048-1000, SUMTAK Corporations of America, Piscataway, NJ, USA). Intradiscal pressure, angular displacement, and moment data were collected at 32 Hz using the custom software and intradiscal pressure, moment, compressive load, and axial deformation data were collected at 32 Hz using the NIAD program (University of Waterloo) for the full duration of the protocol. During the pilot study, the data were oversampled at 256 Hz and a Fast Fourier Transform analysis was conducted to ensure that there was no prominent frequency component above 8 Hz. The NIAD program was used to collect data for all fourteen specimens, and the custom program was used to collect data for eleven specimens (of the fourteen specimens collected). Data from the two data collection programs for those eleven specimens were synchronized using a triggered custom designed external mouse that initiated both programs simultaneously. The protocol was

terminated and the trial was deemed unsuccessful if a sudden drop in pressure was observed, which typically indicated the presence of a stellate endplate fracture (See Chapter 3). Following the FEC loading protocol, a sagittal x-ray image of each specimen was taken. The trial was also deemed unsuccessful if the bore-screw had caused damage to the endplate of the superior vertebra.

4.2.6 Post FEC loading protocol procedures

A ROM PFE test was performed as described in Section 4.2.4.2, and an x-ray image was taken to ensure that the bore-screw did not damage the endplate of the superior vertebra. The trial was deemed unsuccessful if such a case was confirmed.

4.2.7 Morphology observations

Following the FEC loading protocol, a gross examination of tissue damage was performed. The intervertebral disc in each functional spine unit was dissected transversely to examine the inner annulus fibrosus. Since the goal of protocol was to induce partial herniation, Galante's guideline (1967) was not applicable to classify the extent of damage. Therefore, an original classification system was created according to the types of damage that were observed among specimens which successfully completed the FEC loading protocol (Figure 20).

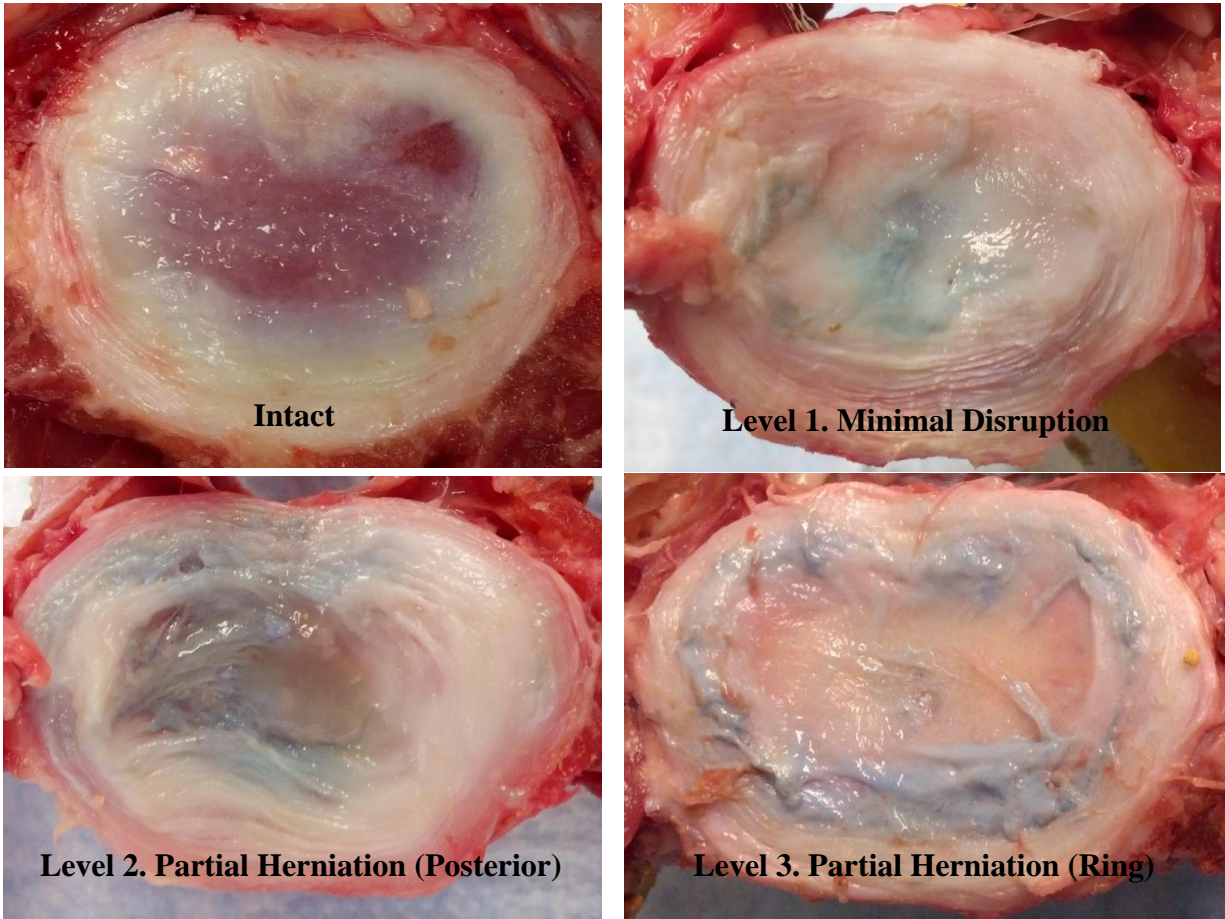


Figure 20: Partial herniation grading system: Level 1. Minimal Disruption: no sign of herniation initiation; Level 2. Partial Herniation (Posterior): herniation initiated but breached nucleus contained only in the posterior region; Level 3. Partial Herniation (Ring): herniation initiated and the nucleus had reached anterior annulus.

4.2.8 Data analysis

Intradiscal pressure (MPa), moment (Nm), axial deformation (mm), and angular displacement (degrees) data were segmented into each loading cycle to examine changes over time. Moment data were used to segment each cycle: the first cycle was used to determine the maximum and minimum moments, and the midpoint was used as the reference point to differentiate one cycle from another. Since the data were collected from two different sources, the number of cycles was compared for each specimen to ensure that segmentation was done correctly.

Four dependent variables, from a total of 16 variables (Table 10 in Section 4.2.9.2), were extracted from each data set collected. From the intradiscal pressure, moment, and axial deformation data, cycle average, maximum, minimum, and difference between maximum and minimum were identified (Figure 21). Maximum pressure was identified in each cycle, and the angular displacement that corresponded to that maximum pressure was used as a maximum pressure angle. In addition, flexion and extension limits and neutral angle were identified, and the intradiscal pressure that corresponds to those angles were extracted from the data. Each variable was averaged over 60 cycles (one minute) to produce a total of 58 data points over time (58 minutes). All 58 data points were used for Pearson correlation. Points at every five minutes (total of 12 data points) were used for the multiple contrast testing procedure (MCTP).

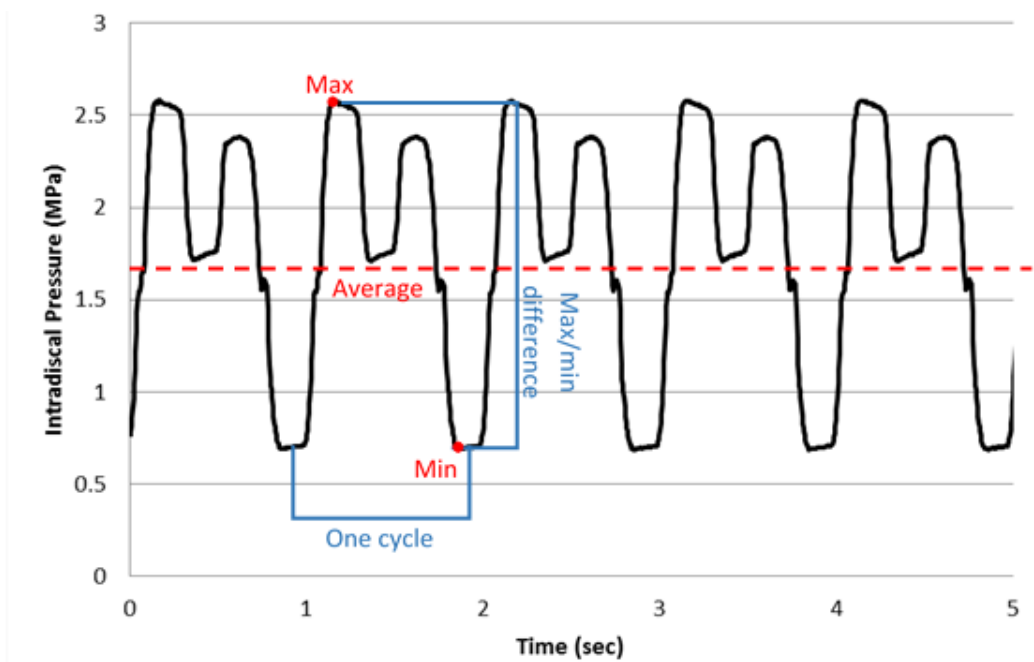


Figure 21: Dependent variables associated with intradiscal pressure: average, maximum, minimum, and the difference between maximum and minimum

There were seven variables compared to the injury classification: pressure trend, neutral zone (Section 4.2.4.3), cycle average moment, cycle average axial deformation, cycle average pressure, pressure difference, and angle at maximum pressure. Each variable, except pressure trend, was calculated by taking the difference between the baseline value (first minute) and the final value (58th minute) to represent the difference between pre and post FEC loading protocol. Pressure trend was classified in three categories: increase, decrease, and plateau. Initially, the pressure difference increased linearly; however, it began to deviate towards the end of the protocol. Therefore, a linear fit was applied to each pressure difference curve, and it was classified based on the correlation coefficient (increase = $r > 0.98$; decrease = $r < 0.90$; plateau = $0.90 < r < 0.98$). These criteria were in accordance with the visual observation.

4.2.9 Statistical analysis

A p-value of 0.05 was used to indicate significance. It was decided *a priori* that dependent measures considered for analysis were collapsed across cervical levels (i.e. C34, C56). All dependent variables were plotted and visually inspected to ensure that there was no apparent difference between the cervical levels.

4.2.9.1 Pearson correlation

Pearson correlation was conducted for the following pairs of datasets using 58 data points:

Table 9: Dependent variables used for Pearson correlation

Variables correlated	
Peak moment	Average axial deformation
Peak moment	Average pressure
Average axial deformation	Average pressure

To account for within subject bias, subject was added as a random effect to the mixed model. Statistical analyses were performed using SAS 9.3 (SAS Institute Inc., Cary, NC, USA).

4.2.9.2 Multiple contrast testing procedure (MCTP)

The statistical analyses were performed using R 3.0.1 (R Development Core Team 2013) using the MULTCOMP package (Bretz et al., 2001; Hothorn et al., 2008) for the following sixteen variables:

Table 10: Dependent variables used for multiple contrast testing procedures

Data sets compared	Pressure	Moment	Axial deformation	Angular displacement
Specific variables compared	Cycle average	Cycle average	Cycle average	At max pressure
	Max	Max	Max	
	Min	Min	Min	
	Difference	Difference	Difference	
	At flex. limit			
	At ext. limit			
	At neutral			

Comparisons for each time point relative to the baseline (Dunnett) as well as comparisons between sequential data points were performed. MCTP computes p-values for the overall hypothesis ($p < 0.05$) and simultaneous 95% confidence intervals at the same time, maintaining the family-wise error rate without using Bonferroni adjustment. Therefore, multiple comparisons, in this case 12 time points (0 – 55 minutes in five minute intervals), can be done without increasing the Type I error. It should be noted that confidence is 95% collectively and not for each interval. The advantage of MCTP is that there is no discrepancy between the overall hypothesis results (i.e. overall p-value) and simultaneous confidence intervals. For instance, if the overall result was significant, there is at least one confidence interval that does not contain zero indicating its significance. This concordance may not always occur for the traditional two-step procedures: testing the overall hypothesis and then performing the post-hoc pairwise

comparisons with p-value adjustments. Each confidence interval represents a range of mean difference between two data points. The range of the confidence interval indicates variance.

4.2.9.3 Spearman’s rank correlation

Spearman’s rank correlation was performed for the following pairs of dependent variables:

Table 11: Dependent variables used for Spearman's rank correlation

Variables correlated	
Injury type morphology	Pressure trend
	Neutral zone
	Cycle average pressure
	Pressure difference (max – min)
	Cycle average moment
	Cycle average axial deformation
	Angle at maximum pressure

The statistical analyses were performed using SAS 9.3 (SAS Institute Inc., Cary, NC, USA).

4.3 Results

4.3.1 Correlation between pressure, moments, and axial deformation

Strong correlations were observed for all cycle average comparisons ($r = 0.95 - 0.99$). There were negative correlations between peak moments and specimen height ($r = -0.99$; $p < 0.001$; $n = 14$) and between intradiscal pressure and moments ($r = -0.99$; $p < 0.001$; $n = 14$). The peak moments increased while the specimen height decreased. The intradiscal pressure decreased over time whereas the maximum moments increased over time. There was a positive correlation between intradiscal pressure and the specimen height ($r = 0.99$; $p < 0.001$; $n = 14$). Both pressure and specimen height decreased over time.

4.3.2 Intradiscal pressure, moments, axial deformation, and angular displacement change over time

All variables except axial deformation difference ($p = 0.07$) demonstrated overall significance, indicating that at least one comparison was significantly different from the baseline and from the preceding data point. The changes were seen as early as five minutes (300 cycles) from the start of the protocol. The overall trend indicated by the cycle average showed that intradiscal pressure ($p < 0.001$) and axial deformation ($p < 0.001$) decreased significantly while moment ($p < 0.001$) increased significantly from the baseline. Angular displacement at maximum pressure shifted significantly more towards flexion ($p < 0.01$) from the baseline.

Cycle average, maximum, and minimum intradiscal pressure decreased ($p < 0.001$) while pressure difference increased ($p < 0.001$) over time (Figure 22, Figure 23). Cycle average pressure demonstrated a significant decline from the baseline after 10 minutes (600 cycles), and all adjacent data points showed significant difference from each other, except for the first two data points (baseline and five minutes). On average, the cycle average pressure decreased from 2.68 (SD 0.68) MPa to 1.42 (SD 0.69) MPa, approximately a 45% reduction. Maximum pressure also decreased from the baseline after 10 minutes (600 cycles); however, no sequential decrease was significant after 45 minutes (2700 cycles). On the contrary, minimum pressure decreases were significant at every time point from the baseline and from the previous time point. On average, the maximum pressure decreased by 26.6% and the minimum pressure decreased by 75.5%. Pressure differences significantly increased at every time point from the baseline; however, the sequential changes were not significant after the 35 – 40 minutes comparison (2100 – 2400 cycles). Pressure difference increased by approximately 65% from the baseline. Generally, the confidence interval increased over time, particularly from the 40th minute, indicating that pressure variability had increased.

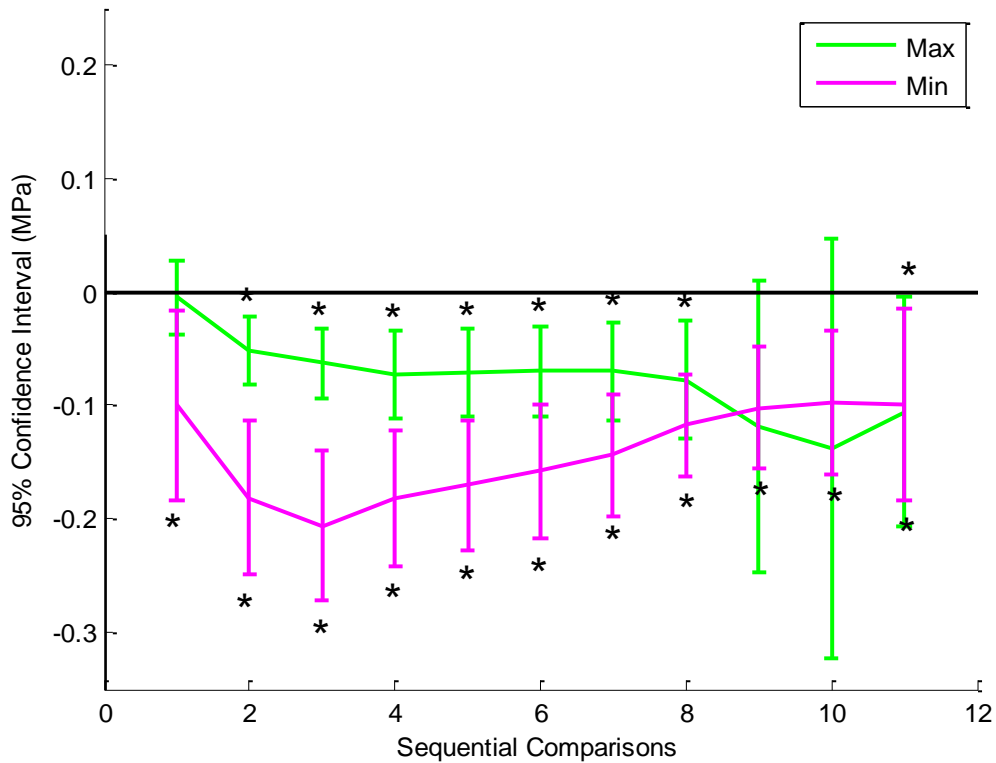
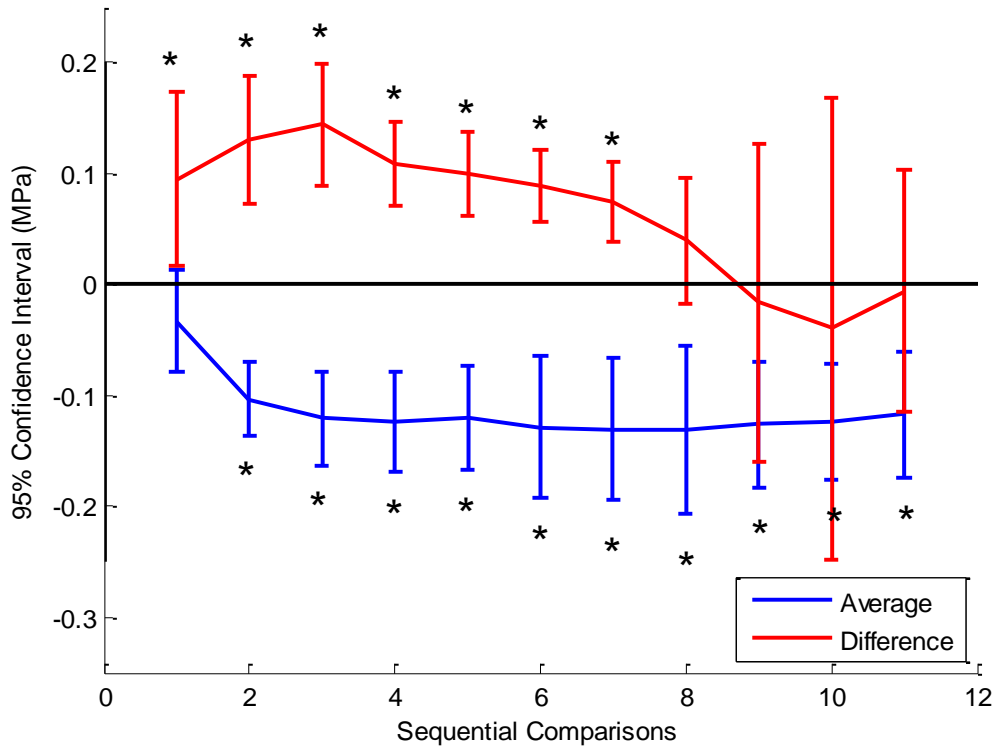


Figure 22: Confidence intervals for the sequential comparisons of the intradiscal pressure: on the x-axis, one represents the comparison between the baseline (0 min) and the 5th min, two represents the comparison between the 5th and 10th minutes, and so on up to the 55th min. An asterisk represents significance ($p < 0.05$).

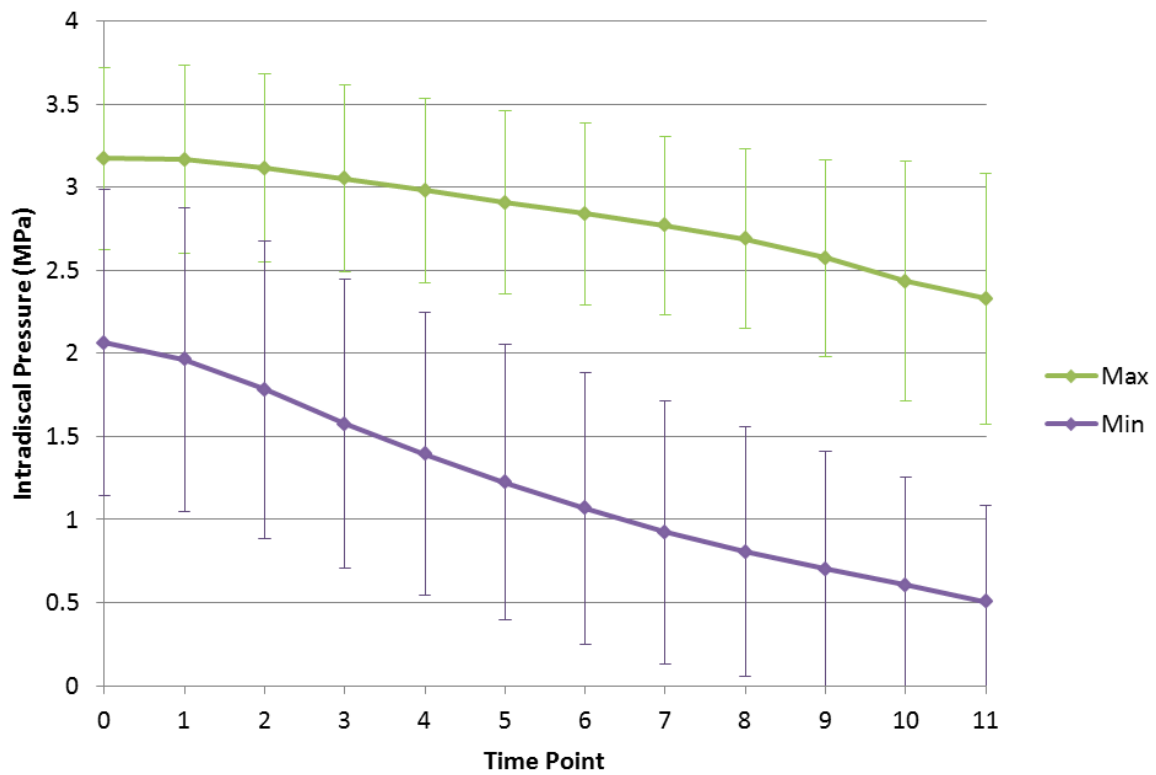
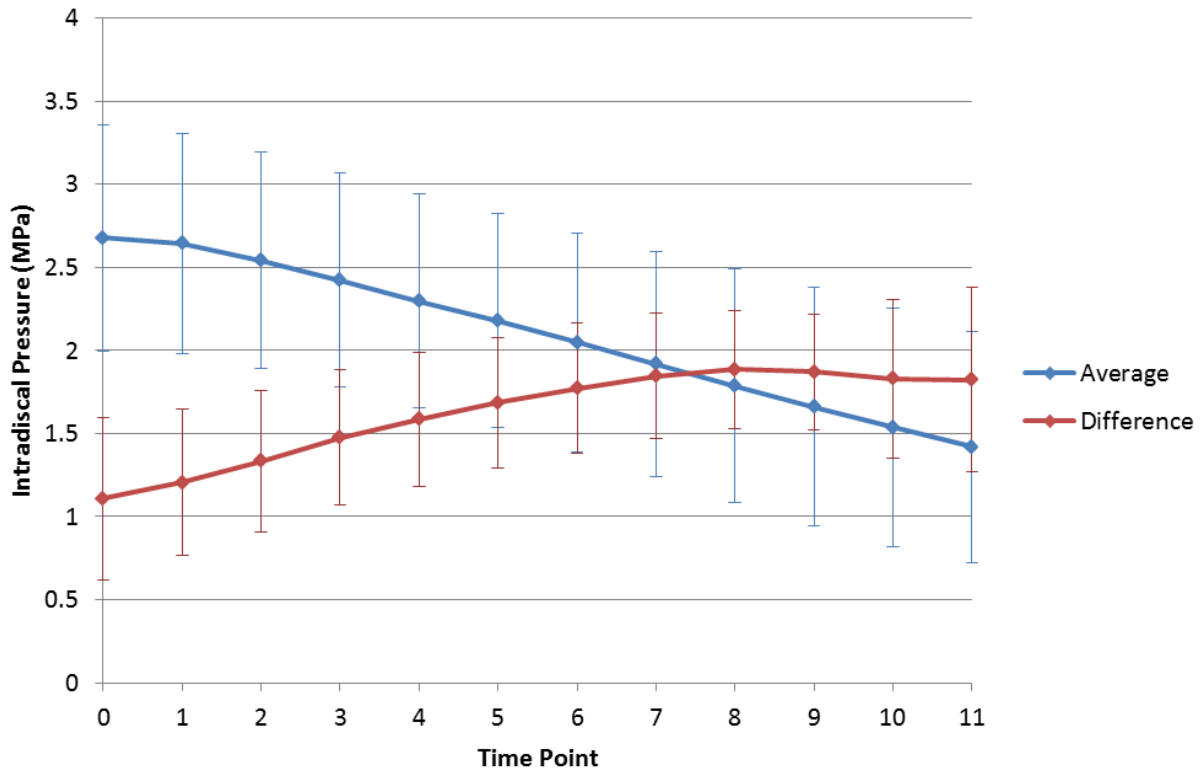


Figure 23: Averages and standard deviations of intradiscal pressure over time: on the x-axis, zero represents the baseline (0 min), and it goes up in an increment of five min, up to 55 min

Cycle average, maximum, and difference between maximum and minimum moment increased while minimum moment decreased significantly over time ($p < 0.001$) (Figure 24, Figure 25). At 55 minutes (3300 cycles), the maximum moment doubled and the minimum moment decreased by 43.3% (increased negative moment) compared to the baseline, resulting in moment difference in a cycle increasing from 18.5 Nm (SD 4.18) to 31.5 Nm (SD 5.92). All moment variables except average and minimum moments significantly changed at every time point from the baseline and from the preceding data point. Variability, indicated by confidence interval was consistent over time for each variable examined (Figure 24).

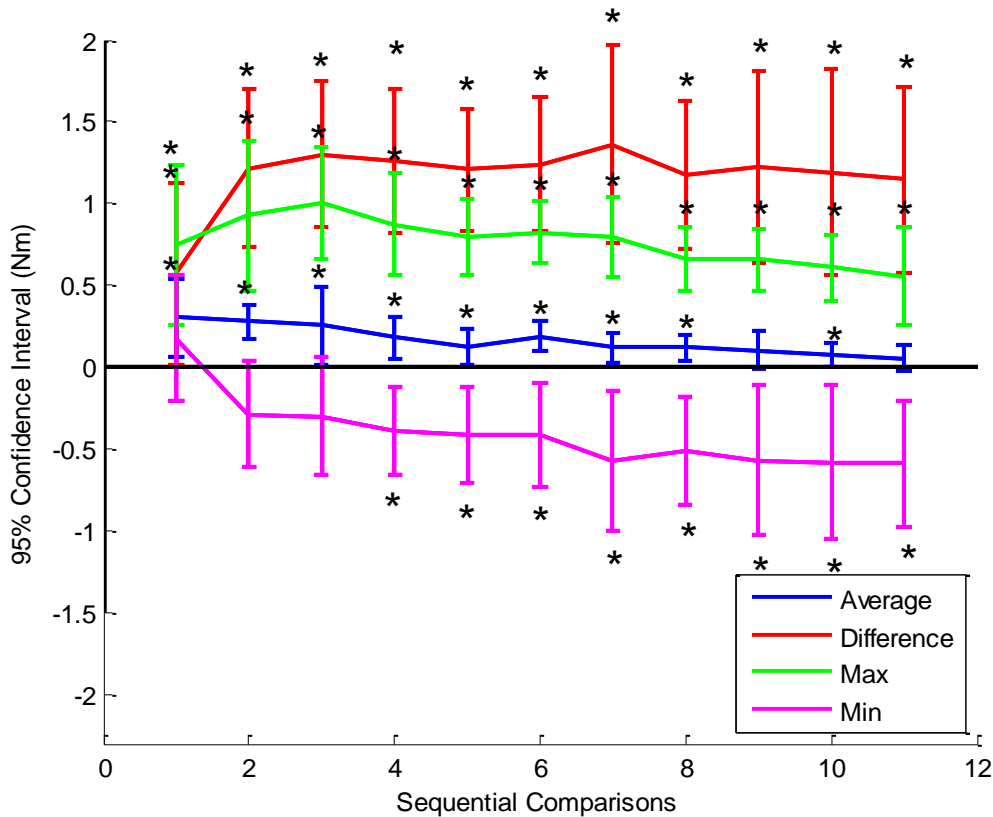


Figure 24: Confidence intervals for the sequential comparisons of the moments: on the x-axis, one represents the comparison between the baseline (0 min) and the 5th min, two represents the comparison between the 5th and 10th minutes, and so on up to the 55th min. An asterisk represents significance ($p < 0.05$).

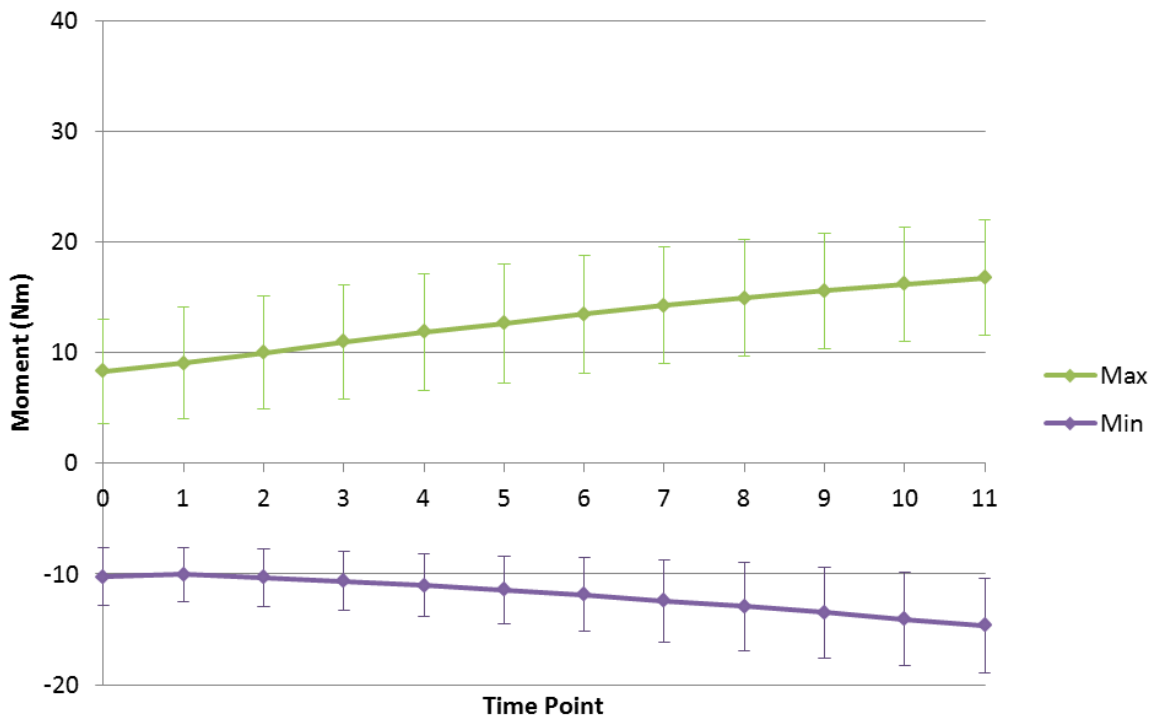
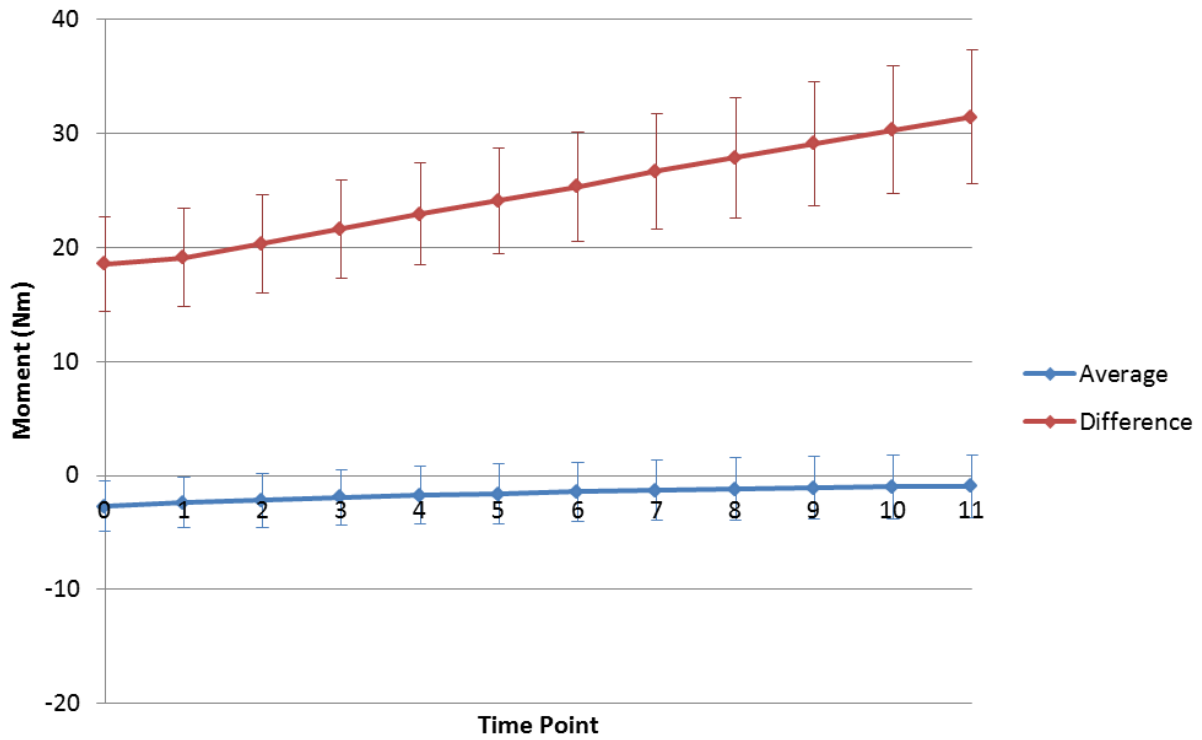


Figure 25: Averages and standard deviations of moments over time: on the x-axis, zero represents the baseline (0 min), and it goes up in an increment of five min, up to 55 min

Cycle average, maximum, and minimum axial deformation increased (decreased height of the specimen) significantly over time ($p < 0.001$) (Figure 26, Figure 27). Specimen height decreased by 2.27 (SD 0.51) mm. Average, maximum, and minimum axial deformation changed significantly from the baseline ($p < 0.001$) and from the preceding data point ($p < 0.001$). However, the difference between maximum and minimum deformation did not change from the baseline ($p = 0.07$), nor from the preceding data point ($p = 0.24$). The confidence interval range decreased or remained consistent over time (Figure 26).

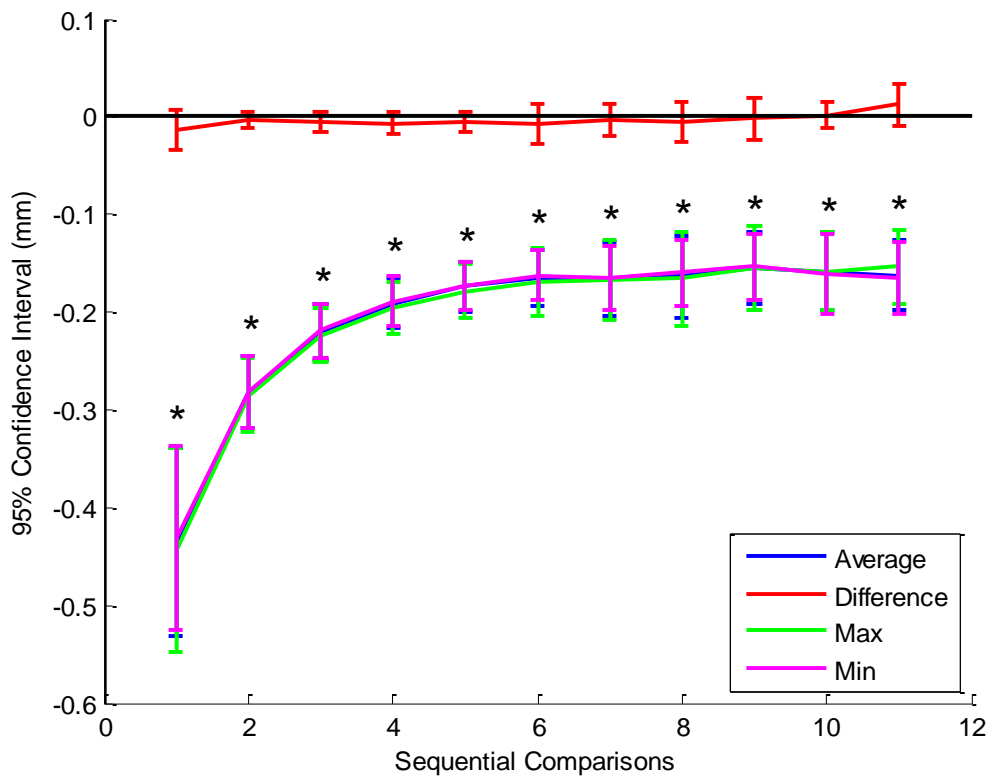


Figure 26: Confidence intervals for the sequential comparisons of the axial deformation (specimen height): on the x-axis, one represents the comparison between the baseline (0 min) and the 5th min, two represents the comparison between the 5th and 10th minutes, and so on up to the 55th min. An asterisk represents significance ($p < 0.05$).

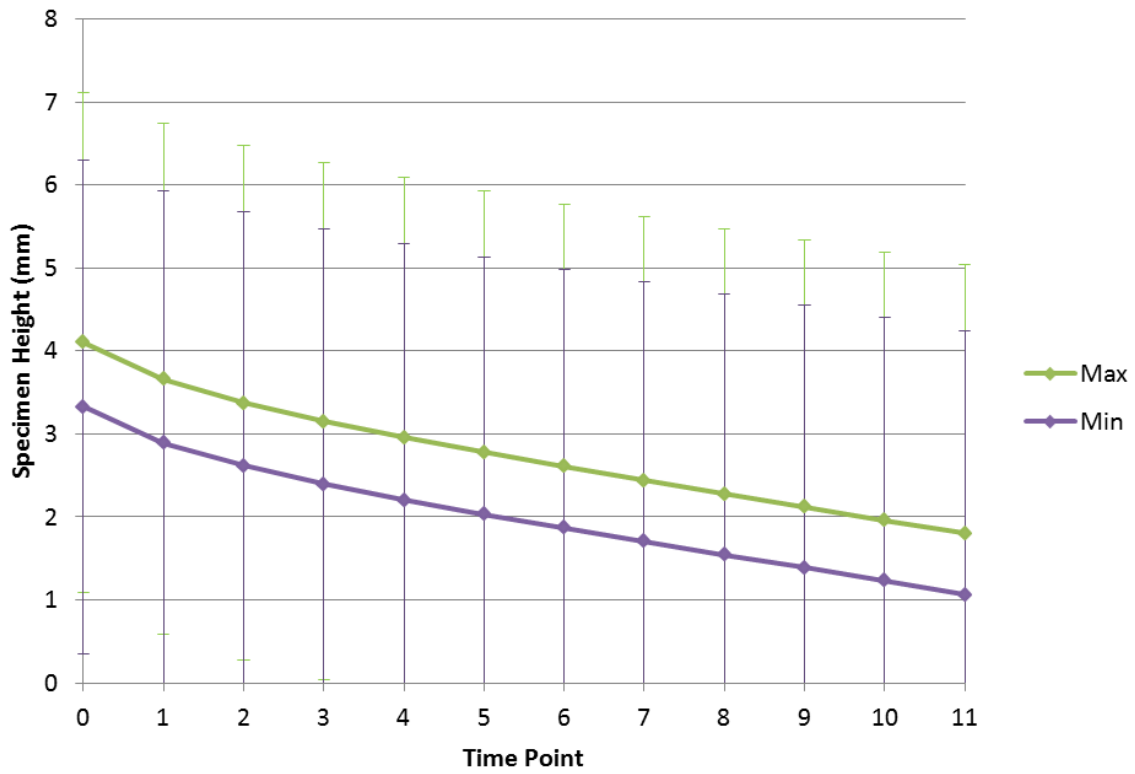
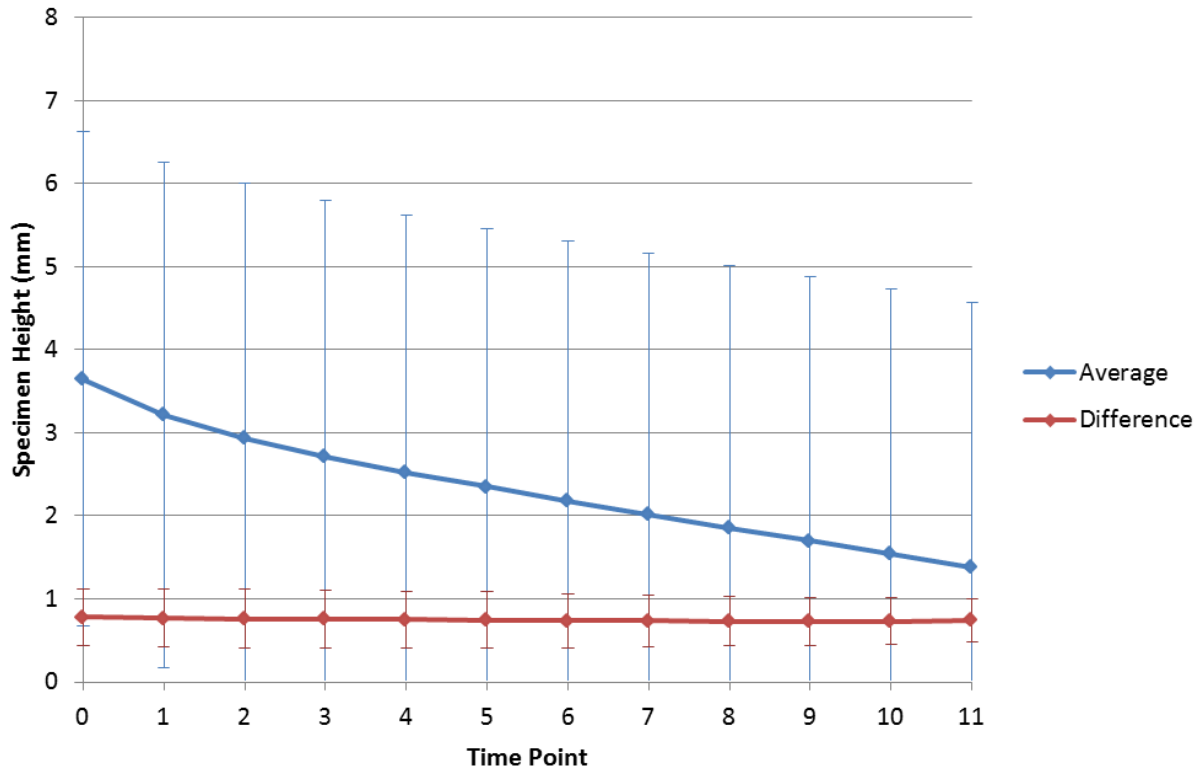


Figure 27: Averages and standard deviations of axial deformation over time: on the x-axis, zero represents the baseline (0 min), and it goes up in an increment of five min, up to 55 min

4.3.3 Pressure at flexion limit, extension limit, and neutral angle change over time

Pressure at flexion and extension limits and neutral angle decreased significantly over time ($p < 0.001$) (Figure 28, Figure 29). Pressure at flexion limit and at neutral angle significantly decreased from the baseline after 15 and 10 minutes (900 and 600 cycles), respectively. For both pressure at flexion limit and neutral angle, all sequential time points were different from each other except the first two (baseline and five minutes) and the last two (50 and 55 minutes) data points. Pressure at the extension limit significantly decreased at every time point from both the baseline and the preceding data point, except the last two (50 and 55 minutes) data points.

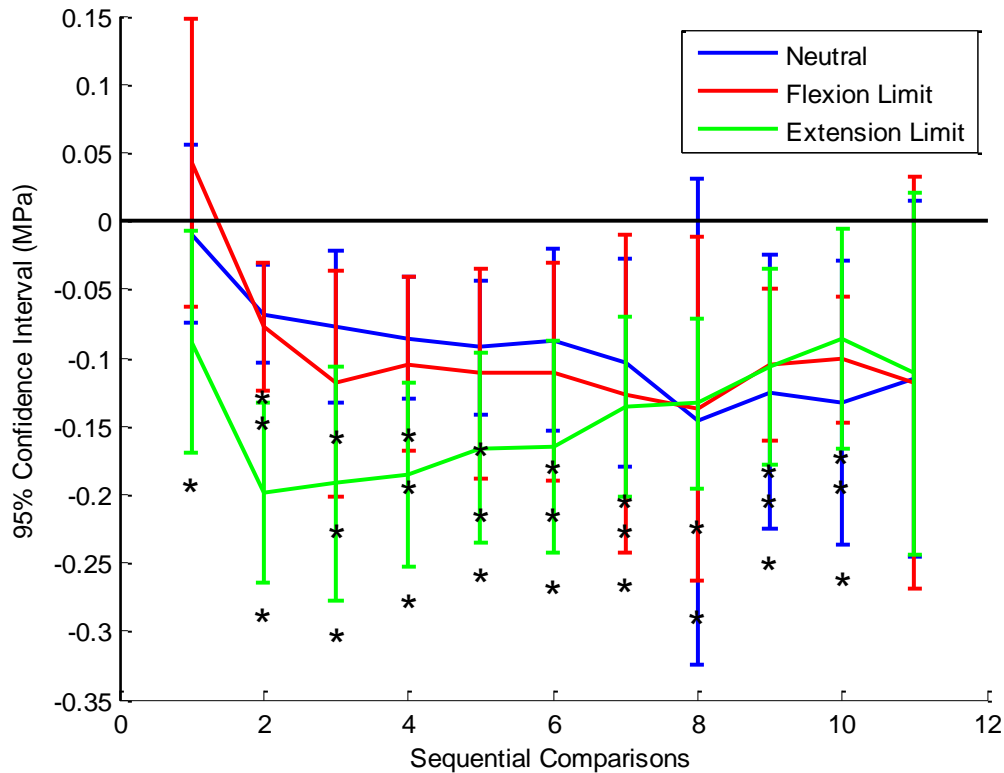


Figure 28: Confidence intervals for the sequential comparisons of the intradiscal pressure at specific angles: on the x-axis, one represents the comparison between the baseline (0 min) and the 5th min, two represents the comparison between the 5th and 10th minutes, and so on up to the 55th min. An asterisk represents significance ($p < 0.05$).

Pressure at neutral angle was the highest, and pressure at flexion limit was higher than at extension limit throughout the protocol. On average, pressure at neutral angle, flexion limit and extension limit decreased by 1.04 (SD 0.65) MPa, 1.07 (SD 0.57) MPa, and 1.57 (SD 0.57) MPa, respectively (Figure 29).

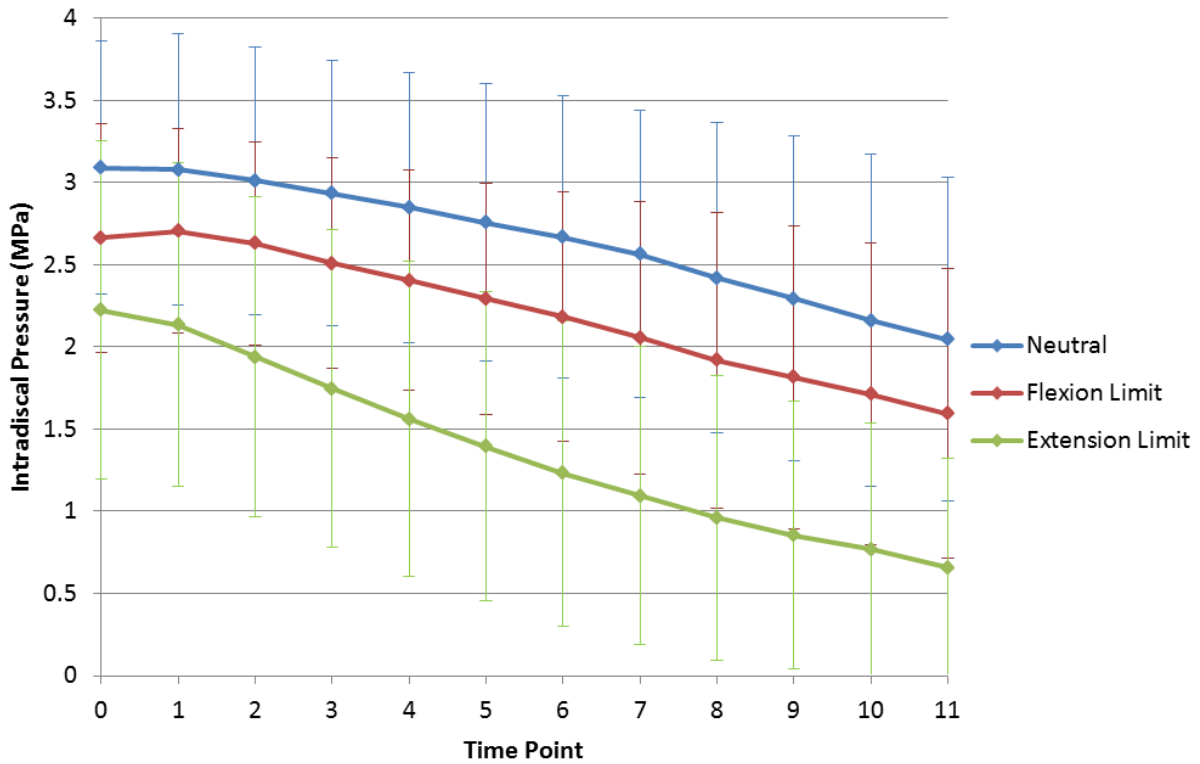


Figure 29: Averages and standard deviations of intradiscal pressure at specific angles over time: on the x-axis, zero represents the baseline (0 min), and it goes up in an increment of five min, up to 55 min

4.3.4 Angles at maximum pressure change over time

Angular displacement at maximum pressure shifted towards flexion limit over time compared to the baseline ($p < 0.01$); however, it was only significantly different after 45 minutes (2700 cycles) (Figure 30). On average, the angle changed by 3.64 (SD 2.12) degrees after 55 minutes (Figure 31). When compared sequentially, the only significant comparison was the difference between 45 minutes (2700 cycles) and 50 minutes (3000 cycles) ($p < 0.05$).

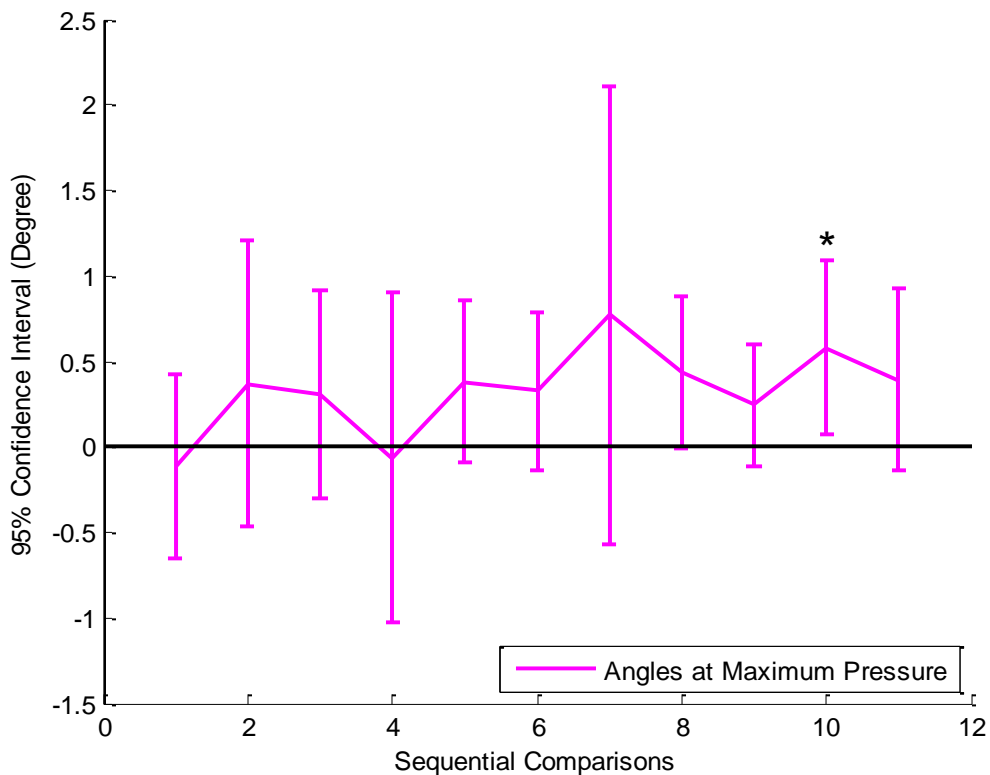


Figure 30: Confidence intervals for the sequential comparisons of the angles at maximum pressure: on the x-axis, one represents the comparison between the baseline (0 min) and the 5th min, two represents the comparison between the 5th and 10th minutes, and so on up to the 55th min. An asterisk represents significance ($p < 0.05$).

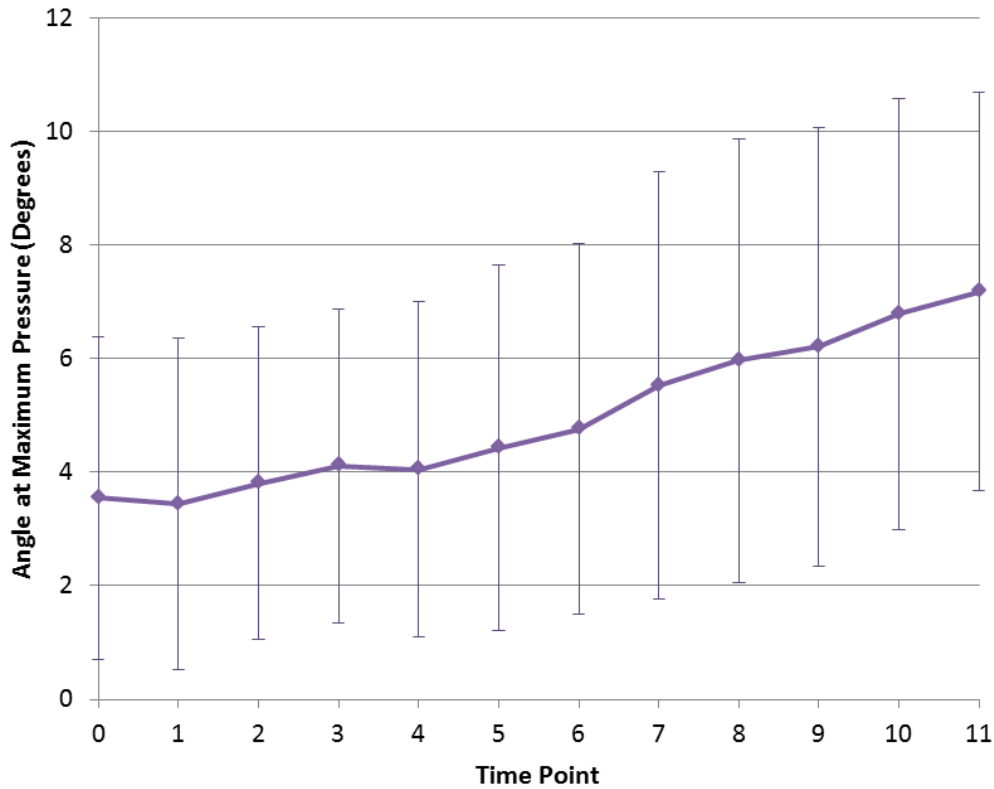


Figure 31: Averages and standard deviations of angles at maximum pressure over time: on the x-axis, zero represents the baseline (0 min), and it goes up in an increment of five min, up to 55 min

4.3.5 Correlation between injury type and other dependent variables

Spearman’s correlation demonstrated that there was no significant correlation between the injury type recorded during morphology observation and pressure trend ($r_s[14] = -0.16$, $p = 0.58$), neutral zone range ($r_s[13] = -0.18$, $p = 0.55$), pressure difference ($r_s[14] = 0.14$, $p = 0.64$), cycle average pressure ($r_s[14] = 0.26$, $p = 0.38$), cycle average moment ($r_s[14] = -0.05$, $p = 0.85$), and cycle average axial deformation ($r_s[14] = -0.29$, $p = 0.32$) (Figure 32). Of the fourteen specimens examined, there were two specimens without visible partial herniation (14.3%), nine specimens with posterior partial herniation (64.3%), and three specimens with ring-shaped partial herniation (21.4%) (Figure 33).

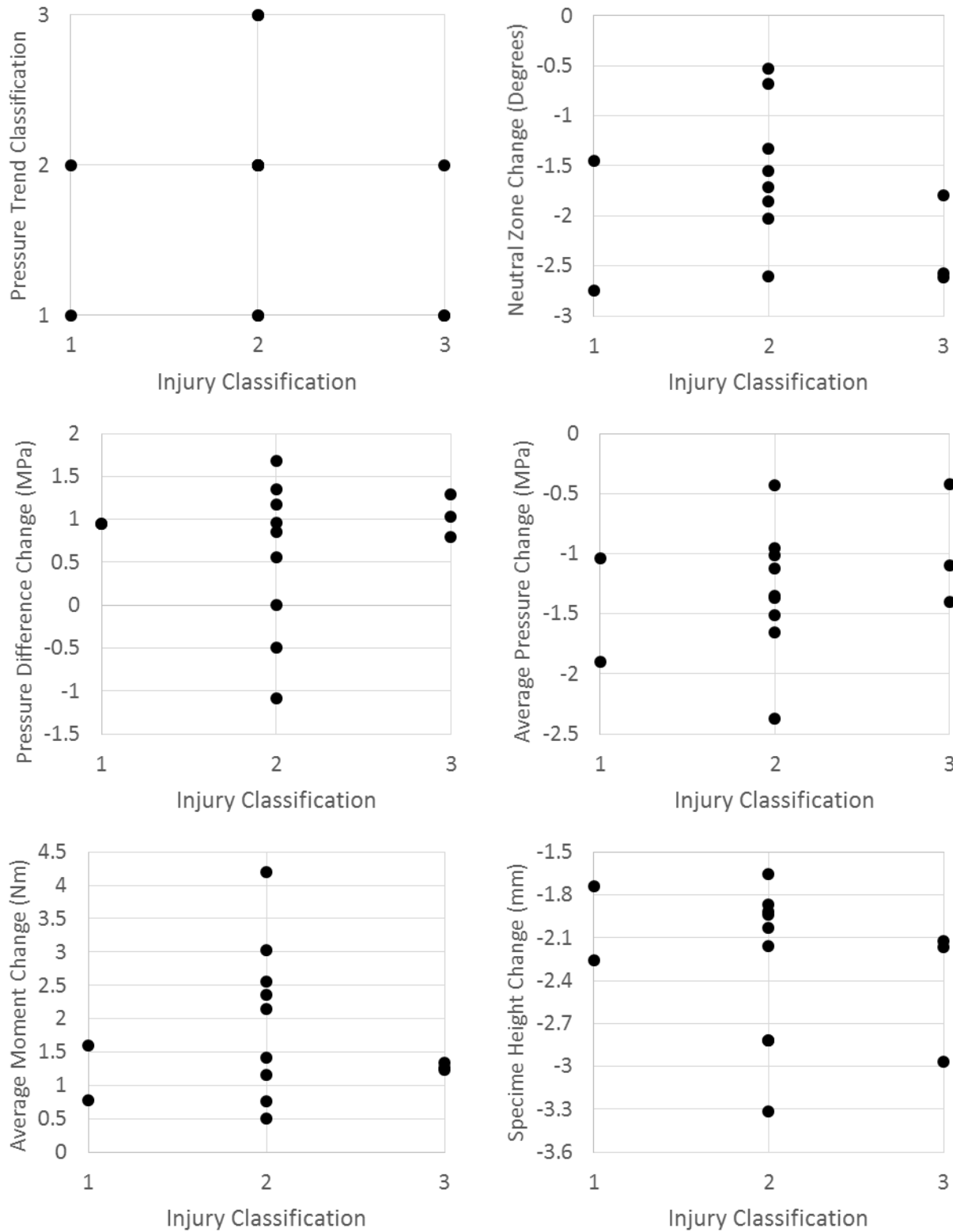


Figure 32: Scatter plots of six dependent variables examined using Spearman’s rank correlation - each specimen was classified into one of the three injury classifications

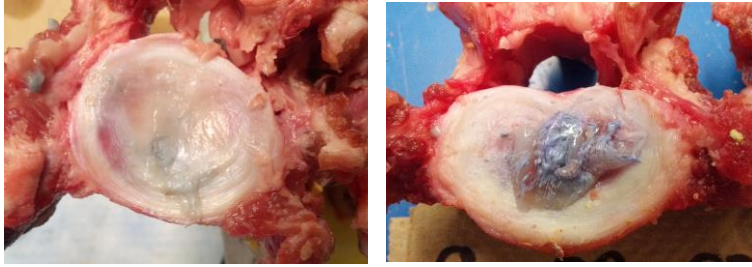
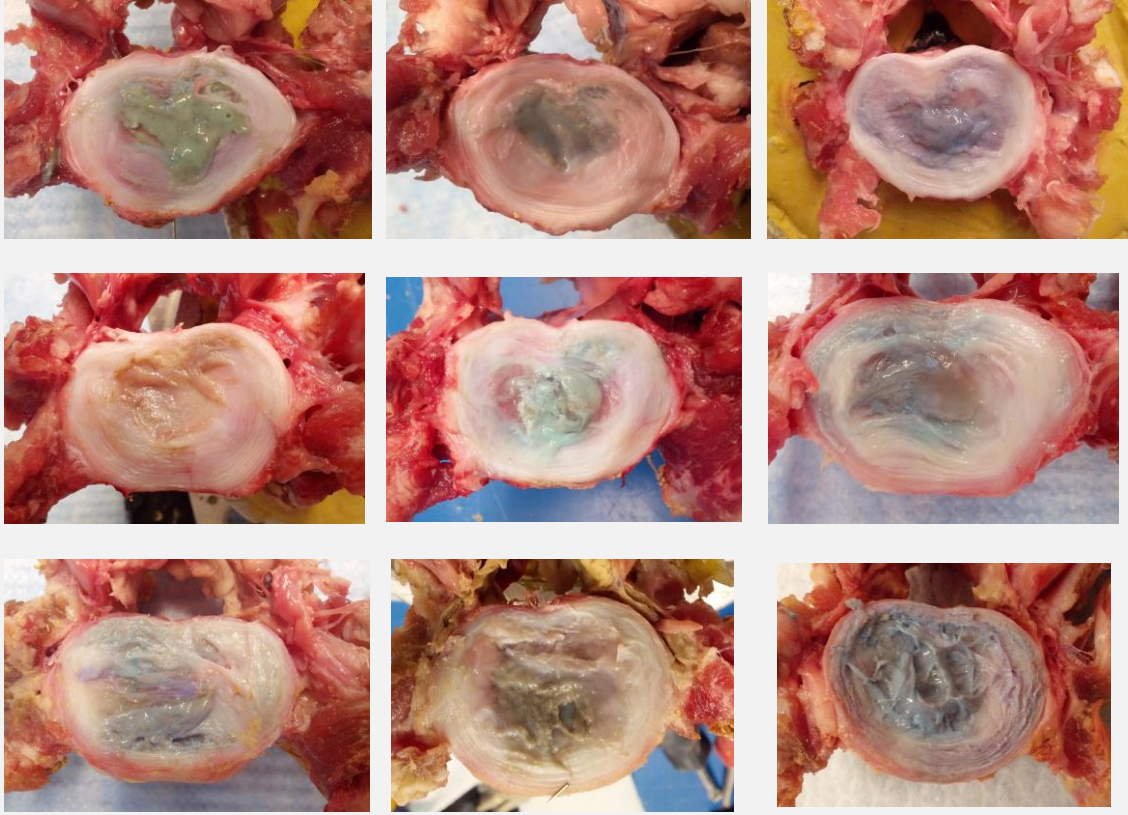
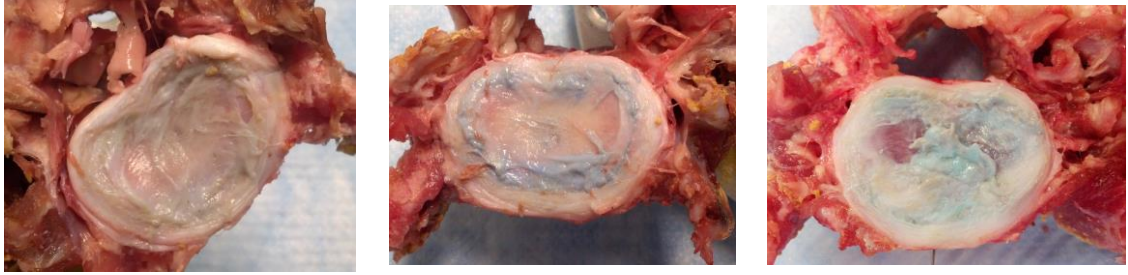
<p>Level 1: Minimal Disruption</p>			
<p>Level 2: Partial Herniation (Posterior)</p>			
<p>Level 3: Partial Herniation (Ring)</p>			

Figure 33: Injury morphology of 14 specimens classified into one of the three injury levels

4.4 Discussion

4.4.1 Correlation between pressure, moments, and axial deformation

As hypothesized, cycle average pressure highly correlated to maximum moments and average axial deformation. A cyclic or sustained creep load has been shown to decrease specimen height and intradiscal pressure (Adams et al., 1996a) and increase stiffness (Gordon et al., 1991; Callaghan and McGill, 2001; Drake et al., 2005). These changes occur due to a loss of fluid content from the nucleus and annulus fibrosus (Adams et al., 1996a; Adams et al., 1990) as well as due to damage to the endplate and annulus fibrosus (Adams et al., 2000). Therefore, in accordance with the previous studies, average pressure correlated highly ($|r| = 0.99$) to the specimen height and moment.

Although cycle average pressure seemed to correlate strongly with moments ($r = -0.99$) and specimen height ($r = 0.99$), the observations from failed trials (Figure 12) indicated that those variables were not sensitive to a drop in intradiscal pressure. When there was a non-linear response in pressure (e.g. a decline in pressure), there was no visible indication of change in moment or specimen height loss. This finding is powerful as it is the first to demonstrate that specimen height and moments are not sensitive to intradiscal pressure change, which is in accordance with the previous studies' inability to identify the initiation of disc disruption and eventual herniation from those measures (Gordon et al., 1991; Callaghan and McGill, 2001; Drake et al., 2005; Tampier et al., 2007). Adams et al. (1996) also noted that endplate fracture followed by cyclic loading did not always show noticeable radiographic signs of damage (Figure 34). Therefore, average pressure prediction from the magnitude of moment and axial deformation should be done cautiously.

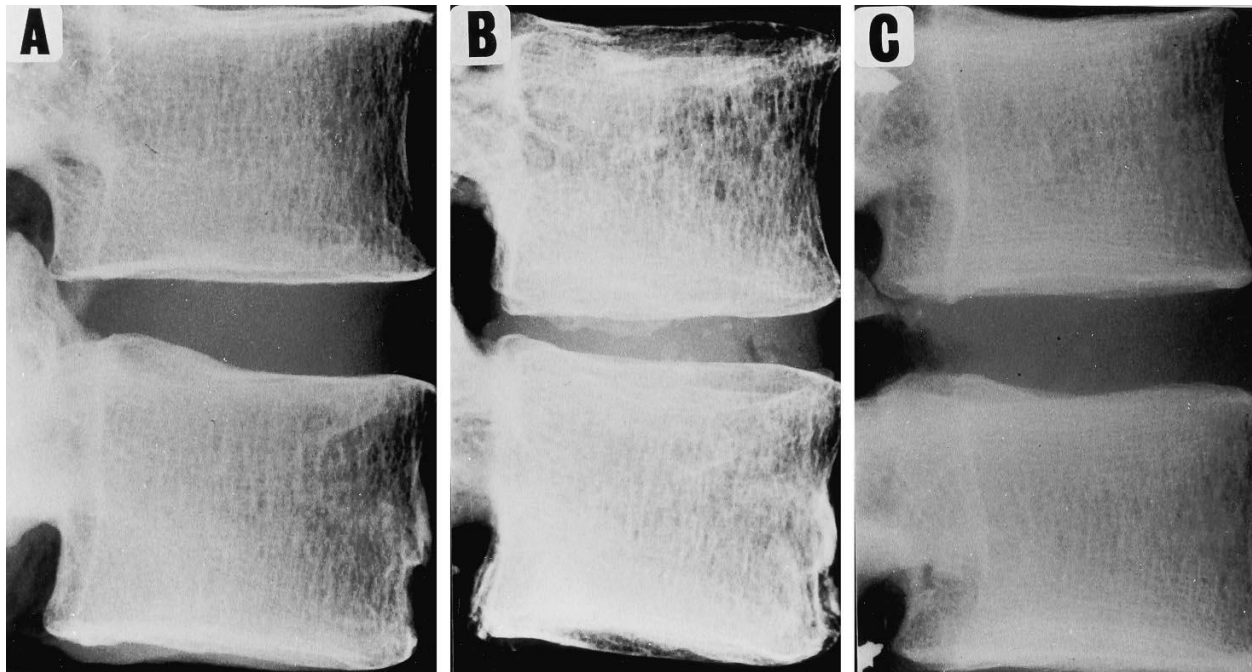


Figure 34: Radiographs of the specimens before (A) and after (B) endplate damage and cyclic loading (Male 61yrs old; L23). Younger specimen (Male 21yrs old; L23) after endplate fracture and cyclic loading (C) did not show noticeable radiographic signs of damage (Adams et al., 1996b).

4.4.2 Changes in pressure, moments, axial deformation, and angular displacement over time

As hypothesized, pressure decreased, moments increased, specimen height decreased, and angular displacement at maximum pressure moved towards flexion over time. The increase in peak moment was greater than 50% following the FEC loading protocol, which was similar to the finding of Callaghan and McGill (2001). The specimen height loss was 2.27 (SD 0.51) mm, comparable to the height loss of 2.83 (SD 0.91) mm following a partial herniation protocol consisting of applying a 1500N compressive load and moving through a range of motion at 1 Hz for 7000 cycles (Yates, 2009). This evidence suggests that instrumentation of the bore-screw pressure sensor system was successful and did not induce a different response from previous studies.

Different responses were observed when moment difference and axial deformation difference over time were examined. Cycle average moment and moment difference increased significantly over time. The moment difference increase was achieved by an increase in maximum moment and a decrease in minimum moment, which occurs as a result of an increase in stiffness (Callaghan and McGill, 2001; Drake et al., 2005; Gordon et al., 1991; Adams et al., 1990; Shum et al., 2010). On the other hand, specimen height difference across cycles did not change, indicating that maximum and minimum height changed at a similar rate over time (Yates, 2009). This result implies that specimen height may indicate the level of degeneration relative to a previously measured value (e.g. healthy disc height); however, if there is no baseline to compare to, the condition of the disc may not be apparent from a single dynamic range of motion test in a clinical setting. Therefore, both moment and axial deformation measures, except axial deformation difference, demonstrated time-varying changes as hypothesized; however, significant changes were seen at every time point (from the baseline and from the preceding time point), emphasizing that these measures would not be able to indicate when disc failure had initiated (Callaghan and McGill, 2001; Drake et al., 2005).

Intradiscal pressure decreased over time as hypothesized, but the rate that maximum and minimum pressure decreased were different, resulting in an increase in intradiscal pressure difference. Cycle average pressure decreased significantly from the 10th minute by 47.0%, while pressure difference increased by 64.5% from the baseline. A drop in average pressure occurred mainly due to minimum pressure decrease, which sequentially decreased from the baseline until the 55th minute, whereas the maximum pressure showed no significant decrease after the 45th minute. Decreases in maximum and minimum pressure were 26.6% and 75.5%, respectively. Minimum pressure typically occurred near the extension limit. Previous studies comparing intact

and damaged endplate specimens demonstrated that depressurization following a cyclic compressive load protocol was particularly greater in a lordotic (2 degrees of extension) posture compared to a flexed posture (Adams 1993; Adams 2000). A similar result was obtained in this experiment as the decrease in pressure at extension limit was 70.5% while decreases in pressure at neutral angle and flexion limit were 33.8% and 40.1%, respectively. Pressure at flexion limit and neutral angle did not show a significant decline from the baseline until 15 and 10 minutes into the protocol, respectively, suggesting that initial disruptive changes may not be related to pressure at those angles. This result may seem counterintuitive to what has been described and practiced in the field of low back pain – to avoid flexed postures and repetitive flexion (Vandergrift et al., 2012; Murtezani et al., 2011; Gallagher et al., 2005). Posture is still an important factor to consider for an injury mechanism; however, in terms of what factor may be contributing to the initiation of disc disruption, pressure at flexion limit alone cannot explain the phenomenon. A common mode of loading that has successfully induced herniation or partial herniation in previous studies (Adams et al., 1993; Gordon et al., 1991; Callaghan and McGill, 2001; Aultman et al., 2005; Drake et al., 2005; Tampier et al., 2007; Kuga and Kawabuchi, 2001; Adams et al., 2000) was cyclic in nature, which, we now know, induces large pressure fluctuations. Since the minimum pressure (occurring at the extension limit) has shown a greater decline over time, contributing to an increase in pressure difference, it may have a more damaging effect on the structural integrity of the inner annulus fibrosus.

A significant increase in pressure difference suggests that the inner annulus fibrosus failure mechanism may be related to fatigue (ASM International, 2008). Mechanical fatigue failure in materials occurs due to the application of fluctuating stresses; in this case, pressure. This variation in applied stresses combined with a large number of cycles could contribute to

fatigue failure. For instance, Paris' law (Paris and Erdogan, 1963) describes the relationship between stress intensity factor range and fatigue crack length under cyclic loading. This model has been used often in material science and fracture mechanics where prediction of temporal change in mechanical strength is essential for understanding the long-term effect. Paris' law is described as follows:

$$\frac{da}{dN} = C\Delta K^m$$

$$\Delta K = K_{max} - K_{min}$$

Equation 6: Paris' law

where a is the crack length, N is the number of load cycles, and ΔK is the range of stress intensity factor described by the difference between the stress intensity factors at maximum and minimum loading. C and m are material constants. In other words, the greater the difference between maximum and minimum stress intensity factors, the greater the crack length would be per load cycle. Paris' law can be used to quantify the residual life of a material given a particular crack size (ASM International, 2008). Assuming that there is inherent imperfection in the structure of annulus fibrosus (i.e. crack or rift in the structure), Paris' law may be able to describe how herniation propagates, at least within individual lamella. In previous studies, a decrease in pressure has been observed with aging, degeneration, and injuries to endplate (Adams et al., 1993; Sato et al., 1999; McNally et al., 1996; Nachemson, 1981; Adams et al., 1996b; Adams et al., 2000; McNally et al., 1993); however, the mechanism that causes damage to the inner annulus fibrosus was not clearly identified. In this study, a decrease in intradiscal pressure was also seen over time, while the compressive load and the range of motion remained the same. A decrease in pressure causes a decrease in specimen height and an increase in outward annular

deformation (Adams et al., 2000). Because of these changes, the stiffness at the end range of motion increases (i.e. increases in peak moments) (Gordon et al., 1991). The anterior disc of an intact specimen bulges outward in flexion and inward in extension, and the opposite effect is seen in the posterior part of the disc (Heuer et al., 2008), which may be occurring as a result of pressure fluctuation. In particular, the magnitude of inward bulging was increased by 40% (0.36 mm in flexion and 0.55 mm in extension) when the nucleus pulposus was removed (Heuer et al., 2008), suggesting that a decrease in average pressure seen in this study, in which an increase in pressure difference concurrently occurs, may have caused an increased fluctuation of the annular deformation towards the end of the protocol. Therefore, this fatigue failure mechanism could explain why inward buckling of the inner annulus fibrosus has been observed in LBP patients (Schwarzer et al. 1995; Dammers et al., 2002; DePalma et al., 2011; Tanaka et al., 1993; Adams et al., 2003; McNally et al., 1996; Adams et al., 1993; Adams et al., 2000).

The angle where maximum pressure occurred shifted significantly towards its flexion limit at the 45th minute, perhaps indicating a substantial structural change in passive tissues between the 40th and 45th minutes. With degeneration, anterior translation increases and the center of rotation can change significantly (Gertzbein et al., 1985; Zhao et al., 2005). During extension, the center of rotation has been shown to shift from the center of the disc towards the facet joints (Zhao et al., 2005). In addition, damage to the annulus fibrosus has been shown to decrease stiffness in the neutral zone (Panjabi, 1992) and increase facet joint contact due to axial deformation (Panjabi et al., 1977), which could explain the why the maximum pressure shifted towards the flexion limit. It may be important to note that there was no significant difference in pressure difference after 40 minutes, and the pressure angle significantly changed from the baseline at 45 minutes into the protocol. The relationship among pressure difference, maximum

pressure angle, and initiation of herniation still remains unclear; however, these measures should be monitored closely for future studies. Maximum pressure peaks typically occurred between neutral and maximum flexion angles (flexion limit), which is a very interesting observation since it has been reported that LBP patients who were instructed to move through a range of motion felt additional pain just before the maximum flexion angle they were able to perform (Shum et al., 2010). Again, it is not possible to conclude whether this observation is related to discogenic pain or not at this point; however, as Shum et al. (2010) addressed, future studies should examine a dynamic range of motion, as opposed to static postures, and variables associated with it (i.e. acceleration (deceleration), mass, and moment of inertia).

There was a difference between values obtained in this study and previous *in vivo* pressure studies when the pressure at flexion and extension limits and neutral angle were compared. Throughout the protocol, the pressure at the flexion limit (2.66 – 1.60 MPa) was higher than at the extension limit (2.22 – 0.66 MPa), similar to the results found in *in vivo* studies (Wilke et al., 1999; Sato et al., 1999). The pressure at neutral angle, however, was the highest (3.09 – 2.05 MPa) throughout the protocol. The pressure measured in previous *in vivo* studies showed that an upright standing posture had the lowest pressure, 0.50 – 0.54 MPa, compared to an extended posture, 0.60 MPa, or a flexed posture, 1.10 – 1.32 MPa (Wilke et al., 1999; Sato et al., 1999). The difference may have occurred due to the type of loading that was applied to the specimen in this study. For this *in vitro* study, a pure compressive load was applied throughout a range of motion. In other words, all of the force vector was compressive at the neutral posture; however, at the end range of motion, the force was divided into two components, compressive and shear, which resulted in a lower compressive force acting on the specimen. In *in vivo*, the compressive force on a joint consists of the upper body weight and the muscle forces. At a

neutral posture (upright standing), the compressive force on the lumbar spine is estimated to be between 500 and 800 N (Adams et al., 2003), whereas when lifting a 14 kg weight in a flexed posture, the contribution from the muscle forces and the upper body weight can amount to 4,000 N of compressive force (Potvin et al., 1996). Therefore, the difference in the application of forces explains why greater intradiscal pressure measurements were observed at the end range of motion in *in vivo* studies (Wilke et al., 1999; Sato et al., 1999).

4.4.3 Correlation between injury type and other dependent variables

There was no correlation between injury type and pressure trend, neutral zone range, pressure difference, cycle average pressure, moment, and axial deformation. Of the 14 specimens examined, 12 specimens showed partial herniation (85.7%). Previous studies using a similar protocol induced partial herniation in approximately 75% of the specimens after 3000 cycles (Drake et al., 2005), and up to 91% of the specimens after 7000 cycles (Yates, 2009; Aultman et al., 2005). Pressure trend and pressure difference were chosen in an attempt to explore whether there was any correlation with the injury type. Neutral zone range and moment were chosen since neutral zone has been shown to increase with disc degeneration (Panjabi, 1992; Mimura et al., 1994) and moment has been shown to increase with an increase in stiffness at the end range of motion (Mimura et al., 1994; Drake et al., 2005; Callaghan and McGill, 2001; Gordon et al., 1991). In this study, moment increased by 64.5% as expected, but neutral zone range did not. Neutral zone range decreased from 4.89 (SD 1.10) degrees to 2.93 (SD 1.29) degrees. Specimen height and average pressure have been shown to decrease with degeneration as well as due to dehydration and creep response (Adams et al., 1996a; Adams et al., 2000; Callaghan and McGill, 2001; Drake et al., 2005). As expected, specimen height decreased by 2.27 (SD 0.51) mm,

comparable to the loss of 2.97 (SD 1.05) mm shown by Yates (2009), and pressure decreased by 33.8% following the protocol, comparable to the loss in pressure seen in Grade 4 discs (Adams et al., 1996b). Attempts to correlate degenerative measures (neutral zone range, range of motion, bending stiffness, and height loss) to injury type have not been successful in a previous study as well (Zhao et al., 2005). Therefore, these results suggest that they may not be sensitive enough measures to correlate to injury types or perhaps the pre and post comparison method may not be a good indicator of injury types.

4.4.4 Limitations

There are several limitations that should be taken into account when considering the study results. The main limitation of this study was that the endplate needed to be punctured in order to implement the bore-screw pressure sensor system. Endplate damage has been shown to cause depressurization in the nucleus, which was considered to cause inward buckling of the annulus (Adams et al., 1993, Adams et al., 2000). It has been shown that approximately five minutes following endplate fracture, nucleus pressure decreased from 1.76 (SD 0.54) MPa to 1.41 (SD 0.67) MPa, which equals a total of 0.35 MPa (19.9%) decline (Adams et al., 2000). If endplate fracture was the main cause of pressure decrease in this study, an equal or a greater amount of pressure decrease should have been seen. In this study, five minutes of cyclic loading led to a pressure loss of only 0.03 (SD 0.06) MPa. Furthermore, previous studies have shown that herniation or partial herniation could occur without any damage to the endplate (Drake et al., 2005; Tampier et al., 2007; Aultman et al., 2005). Considering that a similar proportion of partial herniation was induced in this study using the bore-screw pressure sensor system, any confounding effect on pressure due to endplate fracture was deemed minimal.

As mentioned in the discussion, the load type used in this study may not represent valid physiological loading. The types of loading used in spine *in vitro* studies depend on the constraints (or lack of constraints) and the direction of load application (e.g. follower-load vs. pure compressive load). The pressure at neutral angle was higher than in a flexed posture in this study, which was opposite from the *in vivo* intradiscal measurements recorded previously (McNally et al., 1996; Sato et al., 1999). The type of loading used in this study, a compressive load with sagittal motion, simulated the passive loading experienced *in vivo*, which neglects additional compressive load contribution from the surrounding muscles at the end range of motion. Although the purpose of the study was achieved with this current setting, future studies may need to explore different loading types in order to simulate *in vivo* loading conditions.

4.4.5 Conclusions and future directions

This study was the first to examine time-domain pressure changes in a dynamic range of motion protocol. Intradiscal pressure is an important factor to measure since it changes depending on the load, posture, and the number of repetition – and because of this time-varying response, it cannot be easily predicted from moment or specimen height. Intradiscal pressure and angular displacement showed meaningful changes towards the end of the protocol where disruptive changes were expected; however, injury types were not correlated to the magnitude of change in intradiscal pressure. There were several other key findings:

- Average intradiscal pressure was correlated to peak moments and axial deformation; however, predicting pressure from those variables should be done cautiously as demonstrated by failed trials.

- Even with the implementation of the bore-screw pressure sensor system, flexion and extension moments increased and specimen height decreased over time as shown in previous studies.
- Intradiscal pressure decreased over time during an FEC loading protocol, whereas the difference between maximum and minimum pressure difference increased.
- A significant shift in the maximum pressure angle occurred (45th minute) after which there was no significant change in intradiscal pressure difference from the preceding time point (40th minute).
- FEC loading protocol induced partial herniation in the posterolateral region in 12 out of 14 specimens (85.7%).

With the given results, conclusive evidence was not found in terms of variables that can be used to diagnose or predict the level of IVD degeneration; however, they also provided insight into other variables to be considered for the future studies:

- Are there any morphology changes between 30, 40, and 50 minutes into the FEC loading protocol (1800, 2400, and 3000 cycles, respectively)?
- Is crack (or rift) length correlated to pressure difference?
- Does speed of movement affect pressure difference?
- Does type of loading change the pressure at specific angles?

Pilot tests using the hematoxylin and eosin stain (H&E stain) have been done to examine the morphology of the annulus fibrosus in detail, which would enable us to quantify the length or the number of cracks/rifts in the lamellae. The following figure (Figure 35) clearly shows the

difference in the morphology of the lamella between an hour static loading at 1500 N (control) and an FEC loading protocol. Therefore, more research needs to be done in order to understand the mechanism of annulus failure that ultimately leads to herniation.

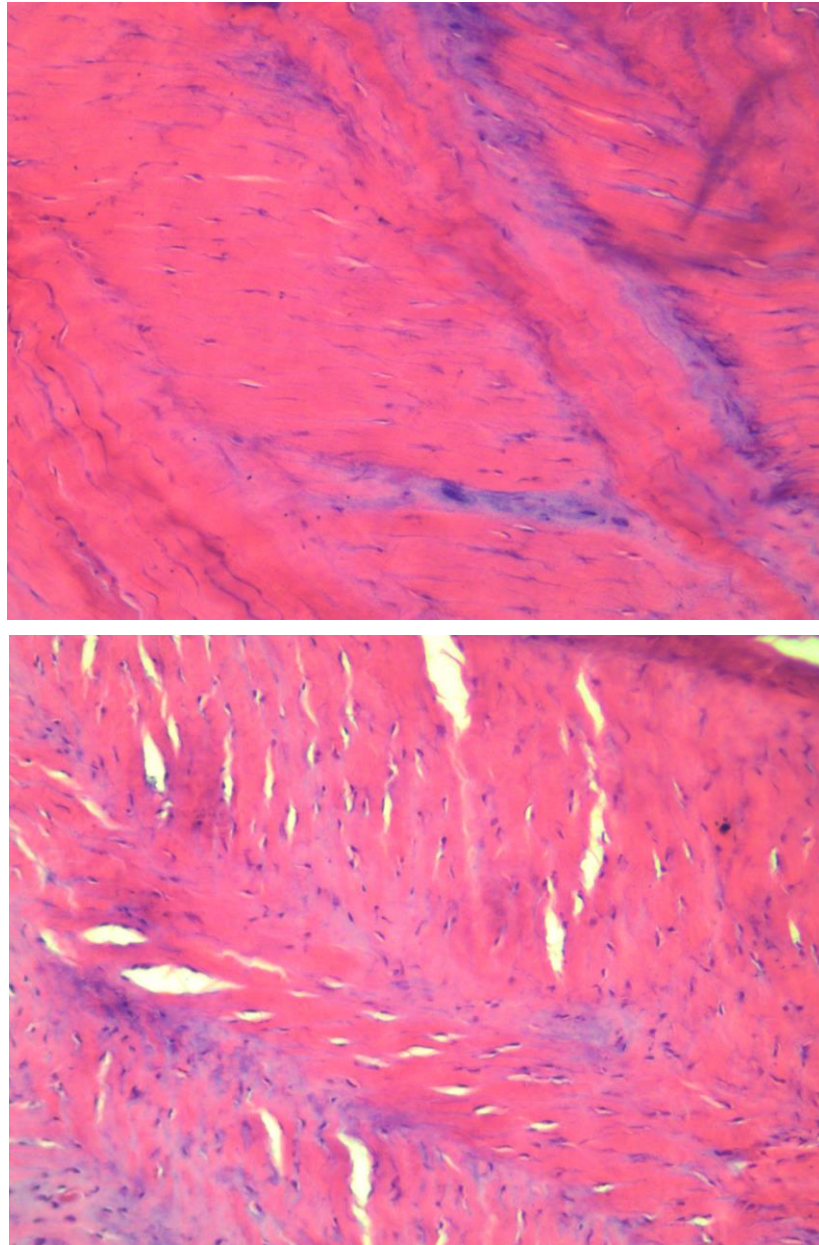


Figure 35: H&E staining of control (top) and FEC loading protocol (bottom) specimens. Posterior region of annulus fibrosus was dissected following each protocol and immediately fixed in the OCT (optimal cutting temperature). The fixed annulus was cut horizontally (along the layers of lamellae) into 10 μ m slices using a cyrotome. Following the H&E staining procedure, above images were taken using a PixeLINK PL-B623CU microscope camera (B700; magnification 10x/0.03; PixeLINK, Ottawa, ON). Specimens that underwent FEC loading protocol showed multiple clefts along the orientation of fibres, whereas the control group showed minimal gap between fibres.

Chapter 5

Summary of Contributions

In this thesis, the intradiscal pressure was characterized over time using a protocol known to induce internal disc disruption. In the first part of the thesis, the bore-screw pressure sensor system was designed and validated in order to allow for pressure measurement during a dynamic protocol. The system without specimen had an error of less than 1% with temperature correction, and the system when inserted into a specimen did not show significant changes in the neutral zone, peak moment and specimen height following the FEC loading protocol. The bore-screw pressure sensor output compared to a needle pressure sensor was highly correlated and there was no lag in response to changes in pressure. Instrumentation was successful in 50% of the specimens used, suggesting that pressure is difficult to measure, particularly during a dynamic protocol. However, since there is no direct measure that can accurately estimate the pressure, this first study contributes greatly in providing an alternative means to monitor how pressure changes over time during IVD herniation.

The second part of the thesis conclusively demonstrated that intradiscal pressure changes during a dynamic flexion-extension protocol. The pressure fluctuated within a cycle, in which pressure at the flexion limit angle was always higher than pressure at the extension limit angle. The average pressure decreased by 47%, while pressure difference between maximum and minimum pressure in each cycle increased by 64% over time. Although the injury type was not correlated to pressure changes, indicating that a reliable method for diagnosing or predicting macro-damages still remains unclear. Further investigation is necessary in order to characterize the relationship between micro-damages (i.e. cleft number and sizes) and the pressure change,

which may provide better understanding of the discogenic pain mechanism and IVD injury initiation and progression.

References

- Adams, M. A., Bogduk, N., Burton, K., & Dolan, K. (2003). *The biomechanics of back pain*. Edinburgh ; New York: Churchill Livingstone.
- Adams, M. A., Dolan, P., Hutton, W. C., & Porter, R. W. (1990). Diurnal changes in spinal mechanics and their clinical significance. *J Bone Joint Surg Br*, 72(2), 266-270.
- Adams, M. A., Freeman, B. J., Morrison, H. P., Nelson, I. W., & Dolan, P. (2000). Mechanical initiation of intervertebral disc degeneration. *Spine (Phila Pa 1976)*, 25(13), 1625-1636.
- Adams, M. A., & Hutton, W. C. (1982). Prolapsed intervertebral disc. A hyperflexion injury 1981 Volvo Award in Basic Science. *Spine (Phila Pa 1976)*, 7(3), 184-191.
- Adams, M. A., & Hutton, W. C. (1983). The effect of fatigue on the lumbar intervertebral disc. *J Bone Joint Surg Br*, 65(2), 199-203.
- Adams, M. A., & Hutton, W. C. (1985). Gradual disc prolapse. *Spine (Phila Pa 1976)*, 10(6), 524-531.
- Adams, M. A., McMillan, W... (1996 a)
- Adams, M. A., McNally, D. S., & Dolan, P. (1996 b). 'Stress' distributions inside intervertebral discs. The effects of age and degeneration. *J Bone Joint Surg Br*, 78(6), 965-972.
- Adams, M. A., McNally, D. S., Wagstaff, J., & Goodship, A. E. (1993). Abnormal stress concentrations in lumbar intervertebral discs following damage to the vertebral bodies: a cause of disc failure? *Eur Spine J*, 1(4), 214-221.
- Alqarni, A. M., Schneiders, A. G., & Hendrick, P. A. (2011). Clinical tests to diagnose lumbar segmental instability: a systematic review. *J Orthop Sports Phys Ther*, 41(3), 130-140.
- Arun, R., Freeman, B. J. C., Scammell, B. E., McNally, D. S., Cox, E., & Gowland, P. (2009). 2009 ISSLS Prize Winner: What Influence Does Sustained Mechanical Load Have on Diffusion in the Human Intervertebral Disc? An In Vivo Study Using Serial Postcontrast Magnetic Resonance Imaging. *Spine (Phila Pa 1976)*, 34(21), 2324-2337.
- Aultman, C. D., Scannell, J., & McGill, S. M. (2005). The direction of progressive herniation in porcine spine motion segments is influenced by the orientation of the bending axis. *Clin Biomech (Bristol, Avon)*, 20(2), 126-129.
- Ayturk, U. M., Garcia, J. J., & Puttlitz, C. M. (2010). The micromechanical role of the annulus fibrosus components under physiological loading of the lumbar spine. *J Biomech Eng*, 132(6), 061007.
- Bass, E. C., Duncan, N. A., Hariharan, J. S., Dusick, J., Bueff, H. U., & Lotz, J. C. (1997). Frozen storage affects the compressive creep behavior of the porcine intervertebral disc. *Spine (Phila Pa 1976)*, 22(24), 2867-2876.
- Battie, M. C., Videman, T., & Parent, E. (2004). Lumbar disc degeneration: epidemiology and genetic influences. *Spine (Phila Pa 1976)*, 29(23), 2679-2690.

- Bogduk, N. (1991). The lumbar disc and low back pain. *Neurosurg Clin N Am*, 2(4), 791-806.
- Bogduk, N., & Twomey, L.T. (1991). Clinical anatomy of the lumbar spine. Churchill Livingstone. New York.
- Bretz, F., Genz, A., & Hothorn, L. A. (2001). On the numerical variability of multiple comparison procedures. *Biometrical J*, 43(5), 645-656.
- Burke, J. G., Watson, R. W., McCormack, D., Dowling, F. E., Walsh, M. G., & Fitzpatrick, J. M. (2002). Intervertebral discs which cause low back pain secrete high levels of proinflammatory mediators. *J Bone Joint Surg Br*, 84(2), 196-201.
- Callaghan, J. P., & McGill, S. M. (1995). Frozen storage increases the ultimate compressive load of porcine vertebrae. *J Orthop Res*, 13(5), 809-812. doi: 10.1002/jor.1100130522
- Callaghan, J. P., & McGill, S. M. (1995). Muscle activity and low back loads under external shear and compressive loading. *Spine (Phila Pa 1976)*, 20(9), 992-998.
- Callaghan, J. P., & McGill, S. M. (2001). Intervertebral disc herniation: studies on a porcine model exposed to highly repetitive flexion/extension motion with compressive force *Clin Biomech (Bristol, Avon)*, 16(1), 28-37.
- Cannella, M., Arthur, A., Allen, S., Keane, M., Joshi, A., Vresilovic, E., & Marcolongo, M. (2008). The role of the nucleus pulposus in neutral zone human lumbar intervertebral disc mechanics. *J Biomech*, 41(10), 2104-2111.
- Carragee, E. J., Don, A. S., Hurwitz, E. L., Cuellar, J. M., Carrino, J. A., & Herzog, R. (2009). 2009 ISSLS Prize Winner: Does discography cause accelerated progression of degeneration changes in the lumbar disc: a ten-year matched cohort study. *Spine (Phila Pa 1976)*, 34(21), 2338-2345.
- Cuellar, J. M., Golish, S. R., Reuter, M. W., Cuellar, V. G., Angst, M. S., Carragee, E. J., . . . Scuderi, G. J. (2010). Cytokine evaluation in individuals with low back pain using discographic lavage. *Spine J*, 10(3), 212-218.
- Dammers, R., & Koehler, P. J. (2002). Lumbar disc herniation: level increases with age. *Surg Neurol*, 58(3-4), 209-212; discussion 212-203.
- Drake, J. D., Aultman, C. D., McGill, S. M., & Callaghan, J. P. (2005). The influence of static axial torque in combined loading on intervertebral joint failure mechanics using a porcine model. *Clin Biomech (Bristol, Avon)*, 20(10), 1038-1045.
- Ekstrom, L., Holm, S., Holm, A. K., & Hansson, T. (2004). In vivo porcine intradiscal pressure as a function of external loading. *J Spinal Disord Tech*, 17(4), 312-316.
- Endean, A., Palmer, K. T., & Coggon, D. (2010). Potential of magnetic resonance imaging findings to refine case definition for mechanical LBP in epidemiological studies. *Spine (Phila Pa 1976)*, 36(2), 160-169.
- Ferguson, S. J., Ito, K., & Nolte, L. P. (2004). Fluid flow and convective transport of solutes within the intervertebral disc. *J Biomech*, 37(2), 213-221.
- Fujita, Y., Duncan, N. A., & Lotz, J. C. (1997). Radial tensile properties of the lumbar annulus fibrosus are site and degeneration dependent. *J Orthop Res*, 15(6), 814-819.

- Galante, J. O. (1967). Tensile properties of the human lumbar annulus fibrosus. *Acta Orthop Scand*, Suppl 100:101-191.
- Gallagher, S., Marras, W. S., Litsky, A. S., & Burr, D. (2005). Torso flexion loads and the fatigue failure of human lumbosacral motion segments. *Spine (Phila Pa 1976)*, 30(20), 2265-2273.
- Geiger, G. (2008). Principles of Leak Detection. 1st Edition. Krohne Oil & Gas, Breda.
- Gertzbein, S. D., Seligman, J., Holtby, R., Chan, K. H., Kapasouri, A., Tile, M., & Cruickshank, B. (1985). Centrode patterns and segmental instability in degenerative disc disease. *Spine (Phila Pa 1976)*, 10(3), 257-261.
- Gooyers, C. E., McMillan, R. D., Howarth, S. J., & Callaghan, J. P. (2012). The impact of posture and prolonged cyclic compressive loading on vertebral joint mechanics. *Spine (Phila Pa 1976)*, 37(17), E1023-1029.
- Gordon, S. J., Yang, K. H., Mayer, P. J., Mace, A. H., Jr., Kish, V. L., & Radin, E. L. (1991). Mechanism of disc rupture. A preliminary report. *Spine (Phila Pa 1976)*, 16(4), 450-456.
- Green, T. P., Adams, M. A., & Dolan, P. (1993). Tensile properties of the annulus fibrosus II. Ultimate tensile strength and fatigue life. *Eur Spine J*, 2(4), 209-214.
- Gregory, D.E. (2009). The influence of the tensile material properties of single annulus fibrosus lamellae and the interlamellar matrix strength on disc herniation and progression. *Unpublished PhD dissertation*. University of Waterloo.
- Gregory, D. E., Veldhuis, J. H., Horst, C., Wayne Brodland, G., & Callaghan, J. P. (2011). Novel lap test determines the mechanics of delamination between annular lamellae of the intervertebral disc. *J Biomech*, 44(1), 97-102.
- Gunzburg, R., Parkinson, R., Moore, R., Cantraine, F., Hutton, W., Vernon-Roberts, B., & Fraser, R. (1992). A cadaveric study comparing discography, magnetic resonance imaging, histology, and mechanical behavior of the human lumbar disc. *Spine (Phila Pa 1976)*, 17(4), 417-426.
- Hadler, N. M. (1986). Work disability and musculoskeletal disease. *Arthritis Rheum*, 29(11), 1410-1411.
- Handa, T., Ishihara, H., Ohshima, H., Osada, R., Tsuji, H., & Obata, K. (1997). Effects of hydrostatic pressure on matrix synthesis and matrix metalloproteinase production in the human lumbar intervertebral disc. *Spine (Phila Pa 1976)*, 22(10), 1085-1091.
- Heuer, F., Schmidt, H., & Wilke, H. J. (2008). Stepwise reduction of functional spinal structures increase disc bulge and surface strains. *J Biomech*, 41(9), 1953-1960.
- Holm, S., Holm, A. K., Ekstrom, L., Karladani, A., & Hansson, T. (2004). Experimental disc degeneration due to endplate injury. *J Spinal Disord Tech*, 17(1), 64-71.
- Hothorn, T., Bretz, F., & Westfall, P. (2008). Simultaneous Inference in General Parametric Models. *Biometrical J*, 50(3), 346-363.
- Howarth, S. J., Gallagher, K. M., & Callaghan, J. P. (2013). Postural influence on the neutral zone of the porcine cervical spine under anterior-posterior shear load. *Med Eng Phys*, 35(7), 910-918.

- Hunter, C. J., Matyas, J. R., & Duncan, N. A. (2003). The notochordal cell in the nucleus pulposus: a review in the context of tissue engineering. *Tissue Eng*, 9(4), 667-677.
- Human Resources and Skills Development Canada. (2013). Work – Employment Rate: *Employment rate, by age, 2012*. Retrieved July 20, 2013, from http://www4.hrsdc.gc.ca/3ndic.1t.4r@-eng.jsp?iid=13#M_3.
- Hutton, W. C., Toribatake, Y., Elmer, W. A., Ganey, T. M., Tomita, K., & Whitesides, T. E. (1998). The effect of compressive force applied to the intervertebral disc in vivo. A study of proteoglycans and collagen. *Spine (Phila Pa 1976)*, 23(23), 2524-2537.
- Igarashi, T., Kikuchi, S., Shubayev, V., & Myers, R. R. (2000). 2000 Volvo Award winner in basic science studies: Exogenous tumor necrosis factor-alpha mimics nucleus pulposus-induced neuropathology. Molecular, histologic, and behavioral comparisons in rats. *Spine (Phila Pa 1976)*, 25(23), 2975-2980.
- Ishihara, H., McNally, D. S., Urban, J. P., & Hall, A. C. (1996). Effects of hydrostatic pressure on matrix synthesis in different regions of the intervertebral disk. *J Appl Physiol*, 80(3), 839-846.
- Ito, M., Incurvaia, K. M., Yu, S. F., Fredrickson, B. E., Yuan, H. A., & Rosenbaum, A. E. (1998). Predictive signs of discogenic lumbar pain on magnetic resonance imaging with discography correlation. *Spine (Phila Pa 1976)*, 23(11), 1252-1258; discussion 1259-1260.
- Jarvik, J. J., Hollingworth, W., Heagerty, P., Haynor, D. R., & Deyo, R. A. (2001). The longitudinal assessment of imaging and disability of the back (LAIDBack) study: baseline data. *Spine (Phila Pa 1976)*, 26(10), 1158-1166.
- Jensen, M. C., Brant-Zawadzki, M. N., Obuchowski, N., Modic, M. T., Malkasian, D., & Ross, J. S. (1994). Magnetic resonance imaging of the lumbar spine in people without back pain. *N Engl J Med*, 331, 69-73.
- Kelsey, J. L., Githens, P. B., White, A. A., 3rd, Holford, T. R., Walter, S. D., O'Connor, T., . . . Calogero, J. A. (1984). An epidemiologic study of lifting and twisting on the job and risk for acute prolapsed lumbar intervertebral disc. *J Orthop Res*, 2(1), 61-66.
- Kuga, N., & Kawabuchi, M. (2001). Histology of intervertebral disc protrusion: an experimental study using an aged rat model. *Spine (Phila Pa 1976)*, 26(17), E379-384.
- Marchand, F., & Ahmed, A. M. (1989). Mechanical properties and failure mechanisms of the lumbar disc annulus. *35th Annual Meeting, Orthopaedic Research Society*.
- McMillan, D. W., Garbutt, G., & Adams, M. A. (1996). Effect of sustained loading on the water content of intervertebral discs: implications for disc metabolism. *Ann Rheum Dis*, 55(12), 880-887.
- McNally, D. S., Adams, M. A., & Goodship, A. E. (1993). Can intervertebral disc prolapse be predicted by disc mechanics? *Spine (Phila Pa 1976)*, 18(11), 1525-1530.
- McNally, D. S., Shackelford, I. M., Goodship, A. E., & Mulholland, R. C. (1996). In vivo stress measurement can predict pain on discography. *Spine (Phila Pa 1976)*, 21(22), 2580-2587.

- Melrose, J., Smith, S. M., Appleyard, R. C., & Little, C. B. (2008). Aggrecan, versican and type VI collagen are components of annular translamellar crossbridges in the intervertebral disc. *Eur Spine J*, 17(2), 314-324.
- Mimura, M., Panjabi, M. M., Oxland, T. R., Crisco, J. J., Yamamoto, I., & Vasavada, A. (1994). Disc degeneration affects the multidirectional flexibility of the lumbar spine. *Spine (Phila Pa 1976)*, 19(12), 1371-1380.
- Ministry of Labor. (2009). Ergonomics. In *Prevent Workplace Pains & Strains! It's time to take action!*. Retrieved July 28, 2012, from http://www.labour.gov.on.ca/english/hs/pubs/ergonomics/is_ergonomics.php.
- Murtezani, A., Ibraimi, Z., Sllamniku, S., Osmani, T., & Sherifi, S. (2011). Prevalence and risk factors for low back pain in industrial workers. *Folia Med*, 53(3), 68-74.
- Nachemson, A. (1966). The load on lumbar disks in different positions of the body. *Clin Orthop Relat Res*, 45, 107-122.
- Nachemson, A., & Elfstrom, G. (1970). Intravital dynamic pressure measurements in lumbar discs. A study of common movements, maneuvers and exercises. *Scand J Rehabil Med Suppl*, 1, 1-40.
- Nachemson, A. L. (1981). Disc pressure measurements. *Spine (Phila Pa 1976)*, 6(1), 93-97.
- National Institute for Occupational Safety and Health (NIOSH). (1997). *Musculoskeletal Disorders and Workplace Factors* (Pub. no. 97 141). Cincinnati, OH: NIOSH.
- Noguchi, M., Gooyers C. E., Holms, M. W., & Callaghan, J. P. *In Press*. The impact of compressive force magnitude on the in vitro neutral zone range and passive stiffness during a flexion-extension range of motion test.
- Olmarker, K. (2011). Combination of two cytokine inhibitors reduces nucleus pulposus-induced nerve injury more than using each inhibitor separately. *Open Orthop J*, 5, 151-153.
- Olmarker, K., & Larsson, K. (1998). Tumor necrosis factor alpha and nucleus-pulposus-induced nerve root injury. *Spine (Phila Pa 1976)*, 23(23), 2538-2544.
- Olmarker, K., & Rydevik, B. (2001). Selective inhibition of tumor necrosis factor-alpha prevents nucleus pulposus-induced thrombus formation, intraneural edema, and reduction of nerve conduction velocity: possible implications for future pharmacologic treatment strategies of sciatica. *Spine (Phila Pa 1976)*, 26(8), 863-869.
- Osvolder, A. L., Neumann, P., Lovsund, P., & Nordwall, A. (1990). Ultimate strength of the lumbar spine in flexion--an in vitro study. *J Biomech*, 23(5), 453-460.
- Oxland, T. R., Panjabi, M. M., Southern, E. P., & Duranceau, J. S. (1991). An anatomic basis for spinal instability: a porcine trauma model. *J Orthop Res*, 9(3), 452-462.
- Panjabi, M. M. (1992). The stabilizing system of the spine. Part II. Neutral zone and instability hypothesis. *J Spinal Disord*, 5(4), 390-396; discussion 397.

- Panjabi, M., Brown, M., Lindahl, S., Irstam, L., & Hermens, M. (1988). Intrinsic disc pressure as a measure of integrity of the lumbar spine. *Spine (Phila Pa 1976)*, 13(8), 913-917.
- Panjabi, M. M., Krag, M. H., White, A. A., & Southwick, W.O. (1977). Effects of preload on load displacement curves of the lumbar spine. *Orthop Clin N Am*, 8(1), 181-192.
- Paris, P., & Erdogan, F. (1963). A critical analysis of crack propagation laws. *J Basic Eng-T ASME*, 528-534.
- Park, C., Kim, Y. J., Lee, C. S., An, K., Shin, H. J., Lee, C. H., . . . Shin, J. W. (2005). An in vitro animal study of the biomechanical responses of anulus fibrosus with aging. *Spine (Phila Pa 1976)*, 30(10), E259-265.
- Parkinson, R. J., & Callaghan, J. P. (2009). The role of dynamic flexion in spine injury is altered by increasing dynamic load magnitude. *Clin Biomech*, 24(2), 148-154.
- Potvin, J. R., McGill, S. M., & Norman, R. W. (1991). Trunk muscle and lumbar ligament contributions to dynamic lifts with varying degrees of trunk flexion. *Spine (Phila Pa 1976)*, 16(9), 1099-1107.
- R Core Team. (2013). R: A language and environment for statistical computing. R Foundation for Statistical Computing, Vienna, Austria. URL <http://www.R-project.org/>.
- Roughley, P. J. (2004). Biology of intervertebral disc aging and degeneration: involvement of the extracellular matrix. *Spine (Phila Pa 1976)*, 29(23), 2691-2699.
- Sambrook, P. N., MacGregor, A. J., & Spector, T. D. (1999). Genetic influences on cervical and lumbar disc degeneration: a magnetic resonance imaging study in twins. *Arthritis Rheum*, 42(2), 366-372.
- Schechtman, H., Robertson, P. A., & Broom, N. D. (2006). Failure strength of the bovine caudal disc under internal hydrostatic pressure. *J Biomech*, 39(8), 1401-1409.
- Schendel, M. J., Wood, K. B., Buttermann, G. R., Lewis, J. L., & Ogilvie, J. W. (1993). Experimental measurement of ligament force, facet force, and segment motion in the human lumbar spine. *J Biomech*, 26(4-5), 427-438.
- Schollum, M. L., Robertson, P. A., & Broom, N. D. (2008). ISSLS prize winner: microstructure and mechanical disruption of the lumbar disc annulus: part I: a microscopic investigation of the translamellar bridging network. *Spine (Phila Pa 1976)*, 33(25), 2702-2710.
- Schwarzer, A. C., Aprill, C. N., Derby, R., Fortin, J., Kine, G., & Bogduk, N. (1995). The prevalence and clinical features of internal disc disruption in patients with chronic low back pain. *Spine (Phila Pa 1976)*, 20(17), 1878-1883.
- Simunic, D. I., Robertson, P. A., & Broom, N. D. (2004). Mechanically induced disruption of the healthy bovine intervertebral disc. *Spine (Phila Pa 1976)*, 29(9), 972-978.
- Skaggs, D. L., Weidenbaum, M., Iatridis, J. C., Ratcliffe, A., & Mow, V. C. (1994). Regional variation in tensile properties and biochemical composition of the human lumbar anulus fibrosus. *Spine (Phila Pa 1976)*, 19(12), 1310-1319.

- StatsCanada. (2011). 2011 Analytical Product. In *The Canadian Population in 2011: Age and Sex*. Retrieved July 28, 2012, from <http://www12.statcan.gc.ca/census-recensement/2011/as-sa/98-311-x/98-311-x2011001-eng.cfm>.
- Tampier, C. (2006). Progressive disc herniation: An investigation of the mechanism using histochemical and microscopic techniques. *Unpublished MSc thesis*. University of Waterloo.
- Tampier, C., Drake, J. D., Callaghan, J. P., & McGill, S. M. (2007). Progressive disc herniation: an investigation of the mechanism using radiologic, histochemical, and microscopic dissection techniques on a porcine model. *Spine (Phila Pa 1976)*, *32*(25), 2869-2874.
- Tanaka, M., Nakahara, S., & Inoue, H. (1993). A pathologic study of discs in the elderly. Separation between the cartilaginous endplate and the vertebral body. *Spine (Phila Pa 1976)*, *18*(11), 1456-1462.
- Thompson, R. E., Barker, T. M., & Percy, M. J. (2003). Defining the Neutral Zone of sheep intervertebral joints during dynamic motions: an in vitro study. *Clin Biomech (Bristol, Avon)*, *18*(2), 89-98.
- Tobinick, E. L., & Britschgi-Davoodifar, S. (2003). Perispinal TNF-alpha inhibition for discogenic pain. *Swiss Med Wkly*, *133*(11-12), 170-177.
- Urban, J. P., Smith, S., & Fairbank, J. C. (2004). Nutrition of the intervertebral disc. *Spine (Phila Pa 1976)*, *29*(23), 2700-2709.
- Vandergrift, J. L., Gold, J. E., Hanlon, A., & Punnett, L. (2012). Physical and psychosocial ergonomic risk factors for low back pain in automobile manufacturing workers. *Occup Environ Med*, *69*(1), 29-34.
- Veres, S. P., Robertson, P. A., & Broom, N. D. (2008). ISSLS prize winner: microstructure and mechanical disruption of the lumbar disc annulus: part II: how the annulus fails under hydrostatic pressure. *Spine (Phila Pa 1976)*, *33*(25), 2711-2720.
- Veres, S. P., Robertson, P. A., & Broom, N. D. (2009). The morphology of acute disc herniation: a clinically relevant model defining the role of flexion. *Spine (Phila Pa 1976)*, *34*(21), 2288-2296.
- Wade, K. R., Robertson, P. A., & Broom, N. D. (2012). On the Extent and Nature of Nucleus-Annulus Integration. *Spine (Phila Pa 1976)*.
- Walsh, A. J., & Lotz, J. C. (2004). Biological response of the intervertebral disc to dynamic loading. *J Biomech*, *37*(3), 329-337.
- Wilke, H. J., Geppert, J., & Kienle, A. (2011). Biomechanical in vitro evaluation of the complete porcine spine in comparison with data of the human spine. *Eur Spine J*, *20*(11), 1859-1868.
- Wilke, H. J., Neef, P., Caimi, M., Hoogland, T., & Claes, L. E. (1999). New in vivo measurements of pressures in the intervertebral disc in daily life. *Spine (Phila Pa 1976)*, *24*(8), 755-762.
- Yates, J. P. (2009). Establishing the effect of vibration and postural constraint loading on the progression of intervertebral disc herniation. *Unpublished MSc thesis*. University of Waterloo.
- Yates, J. P., Giangregorio, L., & McGill, S. M. (2010). The influence of intervertebral disc shape on the pathway of posterior/posterolateral partial herniation. *Spine*, *35*(7), 734-739.

Yingling, V. R., Callaghan, J. P., & McGill, S. M. (1999). The porcine cervical spine as a model of the human lumbar spine: an anatomical, geometric, and functional comparison. *J Spinal Disord*, 12(5), 415-423.

Zhao, F., Pollintine, P., Hole, B. D., Dolan, P., & Adams, M. A. (2005). Discogenic origins of spinal instability. *Spine (Phila Pa 1976)*, 30(23), 2621-2630.